UNIVERSITY
OF OSLO

Evdokiia Potolitsyna

LncRNA *HOTAIR* in adipogenesis: transcriptomic and functional characterization

Thesis submitted for the degree of Philosophiae Doctor

Department of Molecular Medicine
Institute of Basic Medical Sciences

Faculty of Medicine
University of Oslo

2022

Series of dissertations submitted to the
Faculty of Medicine, University of Oslo

ISBN 978-82-348-0125-9

Cover: UiO.
Print production: Graphics Center, University of Oslo.

Acknowledgement

The work presented in this thesis was conducted from 2018 to 2022 at the Department of Molecular Medicine, Institute of Basic Medical Sciences, and funded by the Research Council of Norway and the University of Oslo. Nolwenn Briand and Philippe Collas supervised this work.

First, I would like to thank my supervisors Philippe Collas and Nolwenn Briand, for giving me a chance to work in a lively scientific environment. Specifically, I would like to thank Nolwenn for guidance, patience, and for sharing many exciting scientific discussions. I want to thank Philippe for his support, constructive criticism, and his ability to encourage me during difficult times.

I would also like to thank all the members of the Collas lab for their support throughout the years. I want to thank Erwan Delbarre and Thomas Germier for their immense contribution to my microscopy skills. Anita and Kristin, with whom I have shared the office - for their daily help and great expertise. I want to thank Sarah for all the shared and much-needed tea breaks. Aurelie, Natalia, and our little group for the parties, beer-brewing, and a lovely road trip we did together.

I want to thank my friends, especially those who travel the Ph.D. journey themselves, for their understanding and humor. I also would like to thank my family for being supportive during the ups and downs of my PhD times. Last but not least, I would like to thank my partner for his help with so many things and his great support.

Evdokiia Potolitsyna
Oslo, September 2022

List of Papers

Paper I

Evdokiia Potolitsyna*, Sarah Hazell Pickering*, Ave Tooming-Klunderud, Philippe Collas and Nolwenn Briand "*De novo* annotation of lncRNA *HOTAIR* transcripts by long-read RNA capture-seq reveals a differentiation-driven isoform switch". *BMC Genomics, under revision.*

Paper II

Evdokiia Potolitsyna, Sarah Hazell Pickering, Thomas Germier, Philippe Collas, Nolwenn Briand "Long non-coding RNA *HOTAIR* regulates cytoskeleton remodeling and lipid storage capacity during adipogenesis". In: *Scientific reports 12, 10157 (2022).* DOI: 10.1038/s41598-022-14296-6

Paper III

Evdokiia Potolitsyna, Sarah Hazell Pickering, Thomas Germier, Philippe Collas, Nolwenn Briand "Cytoskeletal remodeling defines nucleolar architecture in adipogenesis". *Manuscript.*

Summary

Human adipose tissue depots are physiologically different, with distinct metabolic properties and contributions to disease. The underlying mechanisms for these differences are yet to be uncovered. Large-scale transcriptomic studies of human adipose tissues have identified HOX genes, particularly the lncRNA *HOTAIR*, as the most differentially expressed gene between upper and lower body adipose depots. However, the role of *HOTAIR* and its regulation during adipogenesis are not fully elucidated.

To gain a deeper understanding of *HOTAIR* regulation during adipogenic differentiation of adipose stem cells (ASCs), we have performed a *de novo* annotation of *HOTAIR* transcripts. Using long-read PacBio sequencing, we uncover a tightly regulated shift in isoform composition upon induction of adipogenesis. Our results highlight the complexity and cell type-specificity of *HOTAIR* isoforms and open perspectives on the functional implications of these variants and their balance to key cellular processes.

We further explored the function of *HOTAIR* during adipogenesis by performing stable knockdown. We find that upon adipogenic commitment, *HOTAIR* regulates protein synthesis and cytoskeleton remodeling pathways, later impacting mature adipocyte lipid storage capacity. Our results support novel and important functions of *HOTAIR* in the physiological context of adipogenesis.

The emerging link between translation regulation and cytoskeleton prompted us to investigate the nucleolar dynamics during adipogenesis, a system where cytoskeletal remodeling is crucial. Altogether, our results point to nucleolar remodeling as an active, mechano-regulated mechanism during adipogenic differentiation and demonstrate a key role of the actin cytoskeleton in defining nuclear and nucleolar architecture in differentiating ASCs.

This thesis includes three research articles, two of which are dedicated to lncRNA *HOTAIR* and one to nucleolar dynamics during differentiation. Although primarily relevant in an adipose tissue context, the results presented in this thesis will be of interest to researchers working with other cellular models where cells transit from state to state.

Sammendrag (Norwegian)

Menneskekroppens ulike fettvevsdepoter er fysiologisk forskjellige, med distinkte metabolske egenskaper og ulikt potensiale for bidrag til sykdomsutvikling. De underliggende molekylære mekanismene for disse forskjellene er ennå ikke avdekket. Storskala transkriptomikk-studier av humant fettvev har identifisert HOX-gener, spesielt lncRNA *HOTAIR*, som det mest differensielt uttrykte genet når man sammenlikner fettdepoter fra over- og underkroppen. Hvilken rolle *HOTAIR* spiller, og hvordan dette genet er regulert under adipogenesen, er derimot ikke godt undersøkt.

For å få en dypere forståelse av hvordan *HOTAIR* reguleres gjennom adipogen differensiering av fettstamceller (ASC), har vi gjennomført en ny-annotering av *HOTAIR*s ulike transkripter. Ved bruk av såkalt PacBio-sekvensering som leser av lange RNA-sekvenser, har vi avdekket en nøye regulert endring i isoformsammensetning ved induksjon av adipogenese. Resultatene våre viser noe av kompleksiteten og celletypespesifisiteten til ulike *HOTAIR*-isoformer og åpner nye perspektiver rundt de funksjonelle implikasjonene av disse variantene og deres balanse i sentrale cellulære prosesser.

Videre undersøkte vi funksjonen til *HOTAIR* under adipogenese, blant annet ved å slå ut uttrykket fra genet gjennom såkalt stabil knockdown. Vi ser at *HOTAIR* regulerer proteinsyntese og remodelering av cytoskjelettet når cellene forplikter seg til adipogen differensiering. Dette påvirker senere lagringskapasiteten for de modne adipocyttene. Resultatene våre peker på nye og viktige funksjoner for *HOTAIR* i den fysiologiske konteksten som adipogenesen er en del av.

Denne nye koblingen mellom translasjonsregulering og cytoskjelettet inspirerte oss til å undersøke nukleolusdynamikk under adipogenesen, et system der remodelering av cytoskjelettet er avgjørende. Samlet sett peker resultatene våre på nukleolær remodelering som en aktiv, mekanoregulert mekanisme under adipogen differensiering, og avdekker en nøkkelrolle for aktincytoskjelettet med hensyn til å definere cellekjernearkitektur og nukleolær arkitektur under differensiering av ASC'er.

Denne doktorgradsavhandlingen er bygd opp rundt tre forskningsartikler, hvorav to fokuserer på lncRNA *HOTAIR* og en på nukleolær dynamikk under adipogen differensiering. Selv om de primært er relevante i fettvevssammenheng, bør resultatene som presenteres være av interesse for forskere som arbeider med andre cellulære modeller der fokuset er differensiering.

List of Abbreviations

4EBP1	eukaryotic translation initiation factor 4E-binding protein 1.
Akt	akt serine/threonine kinase.
ASAT	abdominal subcutaneous adipose tissue.
ASCs	adipose stem cells.
BAT	brown adipose tissue.
BMI	body mass index.
bp	base pair.
C/EBP	CCAAT-enhancer-binding protein.
cAMP	cyclic adenosine monophosphate.
cDNA	complementary DNA.
ChIP	chromatin immunoprecipitation.
ChIP-Seq	chromatin immunoprecipitation sequencing.
ChREBP	carbohydrate response element binding protein.
DFC	dense fibrillar component.
DNA	deoxyribonucleic acid.
ECM	extracellular matrix.
eIF4E	eukaryotic translation initiation factor 4E.
EMT	epithelial-to-mesenchymal transition.
ESCs	embryonic stem cells.
F-actin	fibrillar actin.
FC	fibrillar component.
FSM	full splice match.
GC	granular component.
GLUT4	glucose transporter type 4.
GSAT	gluteal subcutaneous adipose tissue.
H3K9me2	histone H3 lysine 9 dimethylation.
H3K9me3	histone H3 lysine 9 trimethylation.
hnRNP	heterogeneous nuclear ribonucleoproteins.
IBMX	3-isobutyl-1-methylxanthine.
IR	insulin receptor.
ISM	incomplete splice match.
KD	knockdown.
KLF	kruppel-like factor.
LAD	lamina-associated domain.
LINC	linker of nucleoskeleton and cytoskeleton.
LMNA	lamin A.
lncRNA	long non-coding RNA.
LR	long-read.
LSD1	lysine-specific demethylase 1.

miRNA	micro RNA.
MMP	matrix metalloproteinases.
mRNA	messenger RNA.
MSCs	mesenchymal stem cells.
mTOR	mammalian target of rapamycin.
mTORC1	mammalian target of rapamycin complex 1.
NAD	nucleolus associated domain.
ncRNA	non-coding RNA.
NIC	novel in catalog.
NF-kB	nuclear factor kappa B.
NNC	novel not in catalog.
NOR	nucleolus organizing region.
OE	overexpression.
pAs	polyadenylation signals.
PCR	polymerase chain reaction.
PI3K	phosphoinositide 3-kinase.
PKA	protein kinase A.
POSTN	periostin.
PPAR	peroxisome proliferator-activated receptor.
PRC2	polycomb repressive complex 2.
qRT-PCR	quantitative real-time PCR.
RACE	rapid amplification of cDNA ends.
RNA	ribonucleic acid.
RNA-Seq	RNA sequencing.
rRNA	ribosomal RNA.
S6K	ribosomal protein S6 kinase.
snoRNA	small nucleolar RNA.
SQANTI	structural and quality annotation of novel transcript isoforms.
SR	short read.
SREBP	sterol regulatory element-binding protein.
SRRF	super resolution radicval fluctuations.
SVF	stromal vascular fraction.
TGFb	transforming growth factor beta.
TNFalpha	tumor necrosis factor alpha.
TSS	transcription start sire.
UPR	unfolded protein response.
UTR	untranslated region.
WAT	white adipose tissue.
Zc3h10	zinc finger CCCH-type containing 10.

Contents

Chapter 1

Introduction

1.1 Overview of adipose tissue in humans

Adipose tissue is responsible for lipid storage and energy homeostasis. Adipose tissues are broadly classified into energy-storing white adipose tissue (WAT) and energy-dissipating brown adipose tissue (BAT). This classification is however simplified as beige adipocytes, functionaly close to brown adipocytes, can reside in small proportions within WAT (Giralt and Villarroya, 2013; Wang and Seale, 2016). White, brown, and beige adipocytes differ in their ability to generate heat (Giralt and Villarroya, 2013; Wang and Seale, 2016).

Anatomically, adipose tissues are divided into subcutaneous and visceral (Fig1.1) (Rosen and MacDougald, 2006; Tchkonia et al., 2013). Visceral adipose tissue is located in the intra-abdominal area (Shen et al., 2003). The main subcutaneous WAT depots are located in the abdominal, gluteal, and femoral areas (Fig1.1). Several smaller subcutaneous white adipose depots serve a mechanical function in providing support and cushioning to surrounding organs. For example, in the heel pad, adipocytes surrounded by a dense network of collagen fibers provide mechanical support (Hepler and Gupta, 2017; Zwick et al., 2018). The subcutaneous fat functions as a layer of thermal insulation.

Here, we will focus on white adipose tissue of subcutaneous origin. Historically, adipose tissue was considered an inert storage of fat. Currently, WAT is recognized as a metabolically dynamic organ of the human body with a turnover rate of 10% per year (Spalding et al., 2008). The main function of WAT is to store lipids and regulate their release and uptake from the blood (Kershaw and Flier, 2004; Ottaviani et al., 2011). On the hormonal level, insulin is the key regulator of the balance between lipid release and uptake. Insulin is produced in the pancreas upon food intake and sends an antilipolytic signal to adipocytes, preventing lipid release into the blood, and stimulates glucose uptake and *de novo* lipid synthesis. In a healthy organism, adipose tissue and liver coordinate the level of glucose and lipids in the blood.

Histologically, adipose tissue is a loose connective tissue. It is comprised of unilocular mature adipocytes surrounded by a thin layer of extracellular matrix (ECM) and a stromavascular fraction. The extracellular matrix is made mainly of collagen type I and collagen type III, and in healthy adipose tissue, a balance is maintained between the degradation and the production of ECM (Tordjman, 2013). This balance is necessary for adipose tissue to adapt to the changing size of adipocytes. The stromavascular fraction (SVF) includes adipose stem cells (ASCs), endothelial cells, fibroblasts, and various immune cells including, macrophages, T cells, mast cells, and NK cells (Coelho et al., 2013).

Another important role for adipose tissue is hormonal regulation. In fact,

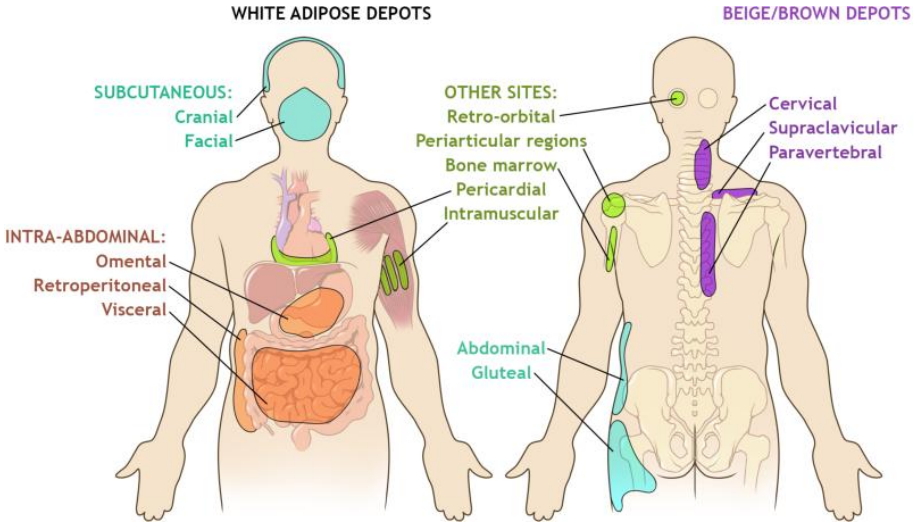

Figure 1.1: White and brown adipose depots in human body. The major subcutaneous WAT includes the abdominal, gluteal, and femoral depots. Intra-abdominal adipose tissue is located within the peritoneum and includes the omental, retroperitoneal, and visceral (mesenteric) fat. White adipocytes also accumulate in other locations, including behind the eye (retro-orbital), around joints (periarticular), in bone marrow, surrounding the heart (pericardial), and within the skeletal muscle (intramuscular). From (Hepler and Gupta, 2017).

adipose tissue is the largest endocrine organ in the body. Adipocytes secrete various hormones and adipokines, including leptin, adiponectin, and resistin (Ouchi et al., 2011; Pereira and Alvarez-Leite, 2014). Sex steroids are converted from inactive to active forms in adipose tissue (Ackerman et al., 1981; Killinger et al., 1987).

The importance of adipose tissue for the human body is illustrated by pathologies such as obesity and lipodystrophies, where an excess or a lack of adipose tissue are both detrimental for whole body metabolism (Chehab, 2008; Garg, 2006). Obesity is associated with insulin resistance, hypertension, and metabolic syndrome. Interestingly, lipodystrophies are also associated with insulin resistance (Hegele et al., 2007; Mann and Savage, 2019). When adipose tissue is insulin-resistant, lipolysis cannot be suppressed even in presence of high insulin levels. Both obesity and lipodystrophy can lead to an increased level of circulating lipids in blood and abnormal fat deposition in other tissues such as skeletal muscles or liver, a phenomenon called lipid spillover (Hegele et al., 2007; Mann and Savage, 2019)).

1.1.1 Good and bad fat

Subcutaneous white adipose depots are not identical throughout the body. Depots differ at multiple levels, such as the production of inflammatory and anti-inflammatory cytokines, mechanical properties, and metabolic responses (Estève et al., 2019; Karpe and Pinnick, 2015). Thus, individual depots have even been characterized as individual endocrine organs (Tchkonia et al., 2013).

Due to these differences, the distribution of adipose depots in the human body is highly significant for metabolic health (Festa et al., 2001; Kissebah et al., 1982; Stranges et al., 2004; Zaadstra et al., 1993). Lower body fat, mainly represented by gluteofemoral subcutaneous adipose tissue (GSAT), is a metabolically protective energy storage depot (Lemieux, 2004; Snijder et al., 2003; Yim et al., 2008). In contrast, excess upper body fat, such as abdominal subcutaneous adipose tissue (ASAT), is associated with metabolic disorders (Karastergiou et al., 2012). The different physiological properties of these adipose depots may be linked to distinct embryonic origins as adipose tissues develop simultaneously in multiple locations (Poissonnet et al., 1984). At the gene expression level, the difference between depots is determined by distinct expression patterns of developmental *HOX* genes (Karastergiou et al., 2013), including *HOTAIR*, a long noncoding RNA from *HOXC* gene locus (see Section 1.3.3). In addition, stem cells isolated from different depots maintain these intrinsic properties after isolation when cultured *in vitro* (Tchkonia et al., 2013).

One of the major functional differences between GSAT and ASAT is the mechanism of their expansion. Lower body adipose tissue expands by differentiating new adipocytes (hyperplasia), while the upper body adipose tissue expands by hypertrophy, that is, increased size of individual adipocytes (Hepler and Gupta, 2017; Tchoukalova et al., 2010). Mechanisms of tissue expansion are important, since larger adipocytes are considered less metabolically favorable (Lundgren et al., 2007; Salans et al., 1968; Weyer et al., 2000). *In vivo*, adipocyte size and insulin sensitivity are negatively correlated. Therefore, while smaller adipocytes are beneficial, larger adipocytes are deleterious to whole body metabolism. In line with this, lower body fat is known to be more insulin sensitive. Overall, due to the sum of physiological differences between upper and lower body fat, healthy obesity is associated with a pear-shaped body type in which lower body fat is dominant (Karpe and Pinnick, 2015; Pinnick et al., 2012; Tchkonia et al., 2013).

1.1.2 Models to study adipogenesis

Investigating the mechanisms of adipose tissue function *in vitro* requires the use of cell line models, with each model having advantages and disadvantages. Widely known models to study adipogenesis include murine cell lines such as 3T3L-1, C3H10T1/2, OP9, and human ASCs.

3T3L-1 cells originate from a mouse embryo and have a fibroblast-like morphology (Green and Meuth, 1974a). These cells have been extensively studied to uncover the mechanisms of adipocyte differentiation, insulin signaling, and

glucose transport. 3T3L-1 model has certain limitations: Differentiation efficiency decreases with passage number and cells lose the differentiation potential if maintained at high confluence. They present the advantage to be easy to culture, and constitute a homogeneous population with a homogeneous response to stimuli (Poulos et al., 2010). However, the relevance of the 3T3L-1 data to human research is questionable. First, clonal cell lines do not represent the heterogeneity of a stromal fraction of adipose tissue. Second, adipogenesis of mouse and human cells is fundamentally different. For example, 3T3L-1 cells undergo mitotic clonal expansion upon induction of differentiation (Tang et al., 2003), while human ASCs do not (Madsen-Østerbye et al., 2022).

Human ASCs are cells obtained from adipose tissue of adult donors and are essentially mesenchymal stem cells of adipose origin (Bunnell et al., 2008; K.-H. Cheng et al., 2011; De Francesco et al., 2015). ASCs can differentiate into osteogenic, chondrogenic, and adipogenic mesodermal lineages. The main advantage of human ASCs is that they are the closest model to *in vivo* human adipogenic differentiation. The main disadvantages are those of a primary human cell model - ASCs age quickly in culture (differentiation efficiency is reduced after passage ten) and are difficult to transfect. Another feature of ASCs is heterogeneity: ASCs are obtained by plating the SVF of adipose tissue (Prieto González, 2019). When plated and passaged *in vitro*, cell population becomes more homogenous and expresses mesenchymal markers (CD90, CD73, CD105 and, CD44), but loses hematopoietic markers expression (CD45, CD34). The level of heterogeneity in ASCs is still much higher than in clonal cell lines due to interindividual variation between donors, leading to heterogenous responses to stimuli. The health status of the donors must also be considered, along with the age, body mass index, and sex (Gruber et al., 2012; Pérez et al., 2015; Silva et al., 2015). ASCs are widely used in pathological studies, such as studies of obesity, diabetes, and heart disease (Jeffery et al., 2015; Tchoukalova et al., 2010).

During the adipose differentiation procedure, cells grow confluent, create a surrounding collagen network, and accumulate lipids (Boquest et al., 2005; Bunnell et al., 2008; Hoefner et al., 2020. ASCs must be maintained in culture at subconfluent densities as cell contacts inhibits cell division. Differentiation protocols differ slightly between groups; I will describe the one we use, as it is key to understanding our results later in the thesis.

1.1.3 Adipogenesis *in vitro*

To differentiate ASCs, cells are seeded at high confluence, grown to full confluence and kept confluent for up to 72 hours prior to induction (D0). Confluence is essential for successful differentiation, as in our experience inducing subconfluent cells lowers differentiation efficiency. Differentiation media is renewed every three days for nine days (D9). Proliferating cells are fibroblast-like and heterogeneous in shape and size, while at D0, a monolayer of cells aligns in wave-like structures (Figure 1.2). D9 cells are larger, rounder in shape, and harbor multiple lipid droplets (Figure 1.2). For some experiments, we further let the cells mature in

media supplemented with insulin for six additional days (D15), promoting lipid droplet growth.

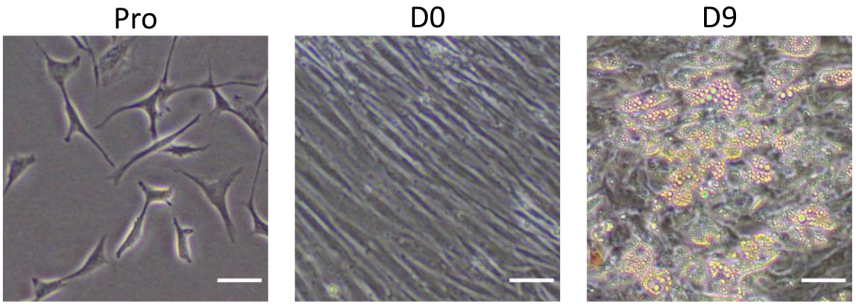

Figure 1.2: Human ASCs cultivated *in vitro*. Pro - actively proliferating cells, D0 - confluent cells prior to induction of differentiation, D9 - adipocytes nine days after induction, scale bar, 100 µm.

In our differentiation system, four compounds are used to induce adipogenesis: 3-isobutyl-1-methylxanthine, indomethacin, dexamethasone, and insulin. These were empirically selected and initially developed for the 3T3L-1 cell line, the first described adipogenesis model Green and Meuth, 1974b; Hwang et al., 1997.

1.1.4 Transcriptional regulation of adipogenesis

The differentiation of ASCs into adipocytes is controlled by a complex network of transcription factors (Figure 1.3A) that coordinate the expression of hundreds of genes responsible for the acquisition of the fat cell phenotype. During differentiation, waves of transcritpional activity include large groups of up-regulated, down-regulated, and transiently expressed genes (Figure 1.3B). The main regulators of adipogenesis are peroxisome proliferator-activated receptor gamma (PPARγ) and CCAAT-enhancer binding protein alpha (C/EBPα). Both are essential for adipose differentiation in culture and *in vivo* (Lefterova et al., 2014; Lowell, 1999; Rosen et al., 2002; Rosen et al., 2000). C/EBPs are a group of 6 transcription factors named from C/EBPα to C/EBPζ. Three C/EBPs are important in adipogenesis and are expressed in different transcriptional waves. C/EBPβ and C/EBPδ are expressed in early differentiation and are needed to induce C/EBPα and PPARγ (Z. Cao et al., 1991; Guo et al., 2015; Yeh et al., 1995). PPARγ and C/EBPα positively regulate each other (J.-E. Lee et al., 2019; Rosen et al., 2002). PPARγ and C/EBPs induce the expression of multiple target genes responsible for lipid accumulation and storage, such as lipoprotein lipase, GLUT4 (glucose transporter) and adiponectin (Payne et al., 2009). The loss of C/EBPs or PPARγ leads to an absence of adipose tissue or decreased fat tissue mass in murine models and decreased adipogenesis (Barak et al., 1999; Linhart, Ishimura-Oka, et al., 2001; Tanaka et al., 1997).

In addition, multiple transcription factors from the Kruppel-like factor family (KLF) have pro-adipogenic or anti-adipogenic effects (Wu et al., 2013). Some KLFs are induced early in the first hours of adipogenesis, such as KLF4 and KLF5. These factors can transactivate C/EBPβ or interact with C/EBPβ and δ (Birsoy et al., 2008; Oishi et al., 2005). The pro-adipogenic and anti-adipogenic effects of KLFs are summarized in Figure 1.3A.

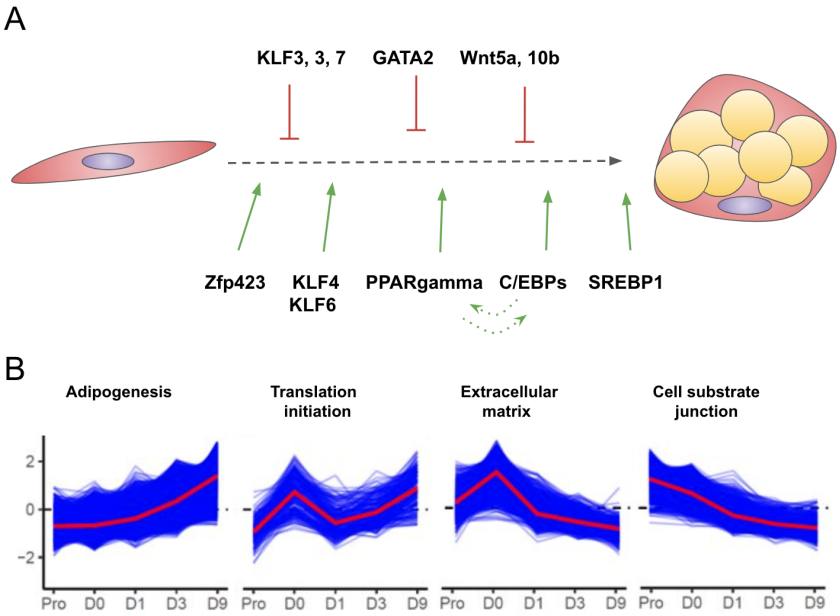

Figure 1.3: A - Schematic representation of main transcription factors positively and negatively regulating adipogenesis; B - gene clusters with corresponding GO terms in Illumina RNA-Seq differentiation timecourse (own data).

Sterol-regulatory element binding protein 1c (SREBP1c) is another essential transcription factor that regulates the expression of multiple genes involved in lipid metabolism (Ferré and Foufelle, 2007; J. B. Kim and Spiegelman, 1996). SREBPs are a family of helix-loop-helix transcription factors that consists of SREBP1a, SREBP1c, and SREBP2 (Eberlé et al., 2004). SREBP1a and SREBP1c promote fatty acid synthesis, while SREBP2 promotes cholesterol synthesis. SREBP1c is particularly important in adipose tissue and postitively regulates PPARγ (Eberlé et al., 2004). SREBP1c activation requires the cleavage of inactive SREBP1c, located in the endoplasmic reticulum, and its translocation to the nucleus (Eberlé et al., 2004). Importantly, the mechanistic target of rapamycin complex 1 (mTORC1) is a crucial positive regulator of SREBP1 mRNA transcription and SREBP1 processing downstream of the insulin/AKT pathway (Crewe et al., 2019). Hence, SREBP1c is insulin sensitive and integrates

information about nutritional and metabolic status in adipocytes (Payne et al., 2009). SREBP1c regulates *de novo* lipogenesis and the expression the adipokines leptin and adiponectin in adipocytes (Crewe et al., 2019).

Another transcription factor that regulates lipid biosynthesis genes is the carbohydrate response element binding protein (ChREBP). The capacity for *de novo* lipogenesis depends on the availability of glucose and fructose, intermediates of which activate ChREBP (Iizuka et al., 2004; Yamashita et al., 2001). Mice lacking ChREBP do not have carbohydrate-stimulated lipogenesis (Herman et al., 2012; Iizuka et al., 2004). It should be noted that ChREBP exists in the form of two isoforms transcribed from different promoters. ChREBPα was discovered first and was considered canonical. The expression of ChREBPα is not regulated by glucose flux, but is necessary for glucose-sensitive expression of ChREBPβ (Herman et al., 2012).

1.1.5 *De novo* lipogenesis

In differentiated adipocytes, the transcription factors described in Section1.1.4 regulate lipid synthesis, uptake, and storage. *In vivo*, *de novo* lipogenesis is not a major pathway, as adipocytes uptake fatty acids from blood (Björntorp and Sjöström, 1978; Letexier et al., 2003; Strawford et al., 2004). However, *de novo* lipogenesis is affected by obesity and is correlated with insulin sensitivity (Ameer et al., 2014; Roberts et al., 2009; Strable and Ntambi, 2010). *In vitro*, the main source of energy is carbohydrates, since there are few lipids in fetal bovine serum used as a supplement. Therefore, lipids in differentiating cells *in vitro* are synthesized by *de novo* lipogenesis (Collins et al., 2011). Adipocytes uptake simple sugars from the medium through GLUT4, a glucose transporter that localizes at the plasma membrane in the presence of insulin (Figure 1.4) (Shepherd and Kahn, 1999). Glucose metabolites activate ChREBPα, which in turn activates ChREBPβ and the downstream expression of multiple enzymes that synthesize fatty acid (Figure 1.4) (Herman et al., 2012). The final product of *de novo* lipogenesis is the triglycerides stored in the lipid droplets by adipocytes (Ameer et al., 2014; Song et al., 2018) (Figure 1.4).

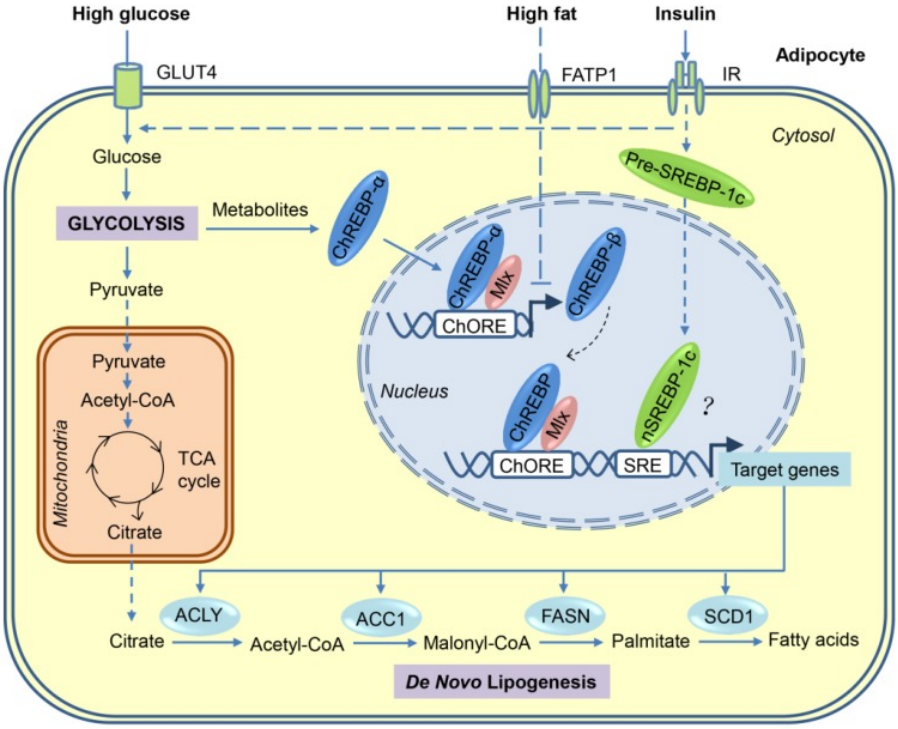

Figure 1.4: Schematic representation of *de novo* lipogenesis with key enzymes and transcription factors. Cells uptake glucose, convert it to pyruvate, which then turns into citrate as an intermediate product of the tricarboxylic acid cycle (TCA) in the mitochondria. Citrate is transported back to the cytosol and used as a substrate for *de novo* lipogenesis catalyzed be multiple enzymes, including ATP-citrate lyase (ACLY), acetyl-CoA carboxylases 1 (ACC1), fatty acid synthase (FASN), and stearoyl-CoA desaturase-1 (SCD1). Glucose metabolites generated during glycolysis activate ChREBPα, which binds to the carbohydrate response elements (ChoRE) in the promoters of target genes required for lipogenesis. From (Song et al., 2018).

1.2 Remodeling of the cell

During adipogenesis, ASCs undergo a drastic remodeling of the cell morphology to harbor large lipid droplets that occupy most of the cell's volume. *In vivo*, white adipocytes are filled with one large LD, while all other organelles are located at the periphery (W. Yang et al., 2013).

1.2.1 Extracellular matrix

In vivo, differentiated adipocytes are surrounded by a thin layer of extracellular matrix (ECM) (Mariman and Wang, 2010). During 3T3L-1 adipogenesis, the expression of specific collagens (*Col6a1*, *Col4a1*, *Col5a1*) and laminins is upregulated, while fibronectin, *Col1a1* and *Col3a1* expression is downregulated (Mori et al., 2014). Adipose differentiation of ASCs isolated from newborn mice also leads to a gradual extracellular matrix accumulation (Yasuaki Kubo et al., 2000). The fibronectin network appears first, while the type I collagen network develops in the later stage of differentiation (Yasuaki Kubo et al., 2000). As mentioned above, a healthy balance between ECM deposition and degradation is important for adipose tissue homeostasis (Tordjman, 2013). In pathological conditions of fibrosis, increased collagen deposition and increased expression of matrix metalloproteases results in abnormal ECM accumulation. Fibrosis has an impact on tissue expandability by limiting adipocyte hypertrophy and *de novo* differentiation of adipose progenitors (Carver and Goldsmith, 2013; K. Sun et al., 2013).

The effects of ECM modulation are perceived by the cell through mechanosensing focal adhesions, multiprotein complexes that transmit the mechanical cues from ECM to the cytoskeleton (Geiger et al., 2009; Martino et al., 2018). Cells respond to mechanical cues by transcriptional changes or by modifying the cytoskeletal architecture and cell elasticity (Webster et al., 2014). In adipogenesis, an artificially stiffer matrix leads to increased actin stress fibers in adipocytes, a global decrease in differentiation efficiency and an increase in collagen deposition (Di Caprio and Bellas, 2020). Conversely, plating cells on a softer matrix promotes adipogenesis (Szabo et al., 2009).

1.2.2 Cytoskeleton

The cytoskeleton is a dynamic structure made of actin fibers, microtubules, and intermediate filaments. Together, they form a highly organized network that is essential for organelle integrity and maintenance (Fletcher and Mullins, 2010; Toivola et al., 2005). The cytoskeleton is responsible for the mechanical properties of the cell and controls its shape and motility (Fletcher and Mullins, 2010). These properties are largely dependent on the dynamics and polarity of all cytoskeletal components. Cells respond to changes in the organization of the cytoskeleton by modulating gene expression (Dupont et al., 2011; Iyer et al., 2012; Lammerding et al., 2006).

Reorganization of the cytoskeleton is required for the morphological transition from fibroblast-like ASCs to a mature spherical adipocyte. A defined actin filaments cytoskeleton in undifferentiated cells is replaced with diffuse cortical actin at the plasma membrane of adipocytes (Kanzaki and Pessin, 2001, 2002). Furthermore, adipocytes have a cell-type specific cytoskeleton where lipid droplets are surrounded by vimentin and actin networks (Nobusue et al., 2014). Inhibition of actin polymerization in ASCs, MSCs, and embryonic stem cells (ESCs) improves adipogenesis (Chen et al., 2018; Feng et al., 2010). Treatment with CytochalasinD (an inhibitor of actin polymerization) can also increase the expression of *PPARG* even without adipogenic induction (Chen et al., 2018). Modulation of the cytoskeleton is relevant for adipose tissue pathology, such as fibrosis and obesity (Jones et al., 2020). For example, a high-fat diet in mice induces a drastic increase in polymerized actin (F-actin) levels in adipocytes and correlates with impaired insulin signaling (Hansson et al., 2019). Recent findings link lipid storage and the cytoskeleton through the Zc3h10 protein (Audano et al., 2021). Zc3h10 is a transcription factor that regulates adipogenesis by controlling translation and F-actin interactions with mitochondria. Upon Zc3h10 knockdown, fewer cells engage in adipogenesis, the actin cytoskeleton has fewer branches and is less prominent, while differentiated cells harbor larger lipid droplets. The finding further confirms that a less-defined actin cytoskeleton favors adipogenesis and lipid droplet growth (Audano et al., 2021).

1.2.3 Nuclear morphology

Inside the cell, the Linker of Nucleoskeleton and Cytoskeleton (LINC) complex connects the nucleus to the cytoskeleton via the nuclear envelope. The nucleus integrates signals from the cytoskeleton through the LINC complex and responds by changes in gene expression (Bouzid et al., 2019; Khilan et al., 2021). 3T3-L1 adipogenesis is accompanied by a decrease in nuclei size which is correlated with lipid accumulation (McColloch et al., 2019). The authors of the study suggest that as the actin cytoskeleton is disassembled during adipogenesis, the stretching force of the actin fibers decreases, thus releasing the nucleus and allowing it to shrink (McColloch et al., 2019). In agreement, treatment with actin stabilizer jasplakinolide increases the nuclear size (McColloch et al., 2019). During differentiation, the decrease in nuclear volume precedes the deposition of lipids, suggesting that nuclear remodeling could be a prerequisite for differentiation (McColloch et al., 2019).

The nucleus is the stiffest organelle in the cell (Caille et al., 2002; Ofek et al., 2009) but changes in shape and size during differentiation require some degree of plasticity. The nucleus is surrounded by a double nuclear membrane underlined by the nuclear lamina, a network of type-V intermediate filaments (Gruenbaum et al., 2005). The nuclear lamina consists of lamins present in several forms - lamin A, lamin C, lamin B1, and lamin B2. Lamin A and lamin C are splice isoforms encoded by the *LMNA* gene, while lamin B1 and B2 are encoded by the *LMNB1* and *LMNB2* genes (Burke and Stewart, 2013). The relative protein level of the lamins is a key factor that defines the stiffness of

the nuclear lamina and, therefore, plasticity of the nuclear shape (Broers et al., 2004; Dechat et al., 2010; Lammerding et al., 2006; Pajerowski et al., 2007; Swift et al., 2013). A high lamin A/C to lamin B1 ratio is characteristic of stiffer tissues, such as bone and cartilage (Swift et al., 2013). Accordingly, high levels of lamin A and C are correlated with a stiffer nucleus and a stiffer cell environment. Stiff environments favors osteogenesis, while the softer matrix favors adipogenesis (Swift et al., 2013; Szabo et al., 2009). The expression of lamins, in particular lamin A, is regulated during adipogenic differentiation. According to (McColloch et al., 2019), in 3T3L-1 cells the lamin A protein level increases during adipogenic differentiation. However, another study reports that the lamin A protein level is significantly lower in differentiated adipocytes obtained from human preadipocytes (Verstraeten et al., 2011).

Lamins are responsible not only for nuclear shape, but also for chromosome positioning (Malhas et al., 2007; Mewborn et al., 2010). Condensed heterochromatin can attach to the nuclear lamina and form repressive lamina-associated domains (LADs). LADs have been implicated in many nuclear functions, including higher order genome organization, chromatin regulation, transcription, DNA replication, and DNA repair (Briand and Collas, 2020; Dittmer and Misteli, 2011; van Steensel and Belmont, 2017). Nuclear organization depends on lamins both via control of biophysical parameters such as nuclear lamina stiffness and via gene expression regulation and chromosome localization through dynamic LADs.

1.2.4 Genome organization

The human genome is highly organized in 3 dimensions, with chromosomes occupying distinct territories (Branco and Pombo, 2006; Cremer and Cremer, 2010). High-order arrangements of the genome influence gene expression (Branco and Pombo, 2006; Cremer and Cremer, 2010). Spatial localization of genes is likely related to the state of gene activity (Egecioglu and Brickner, 2011; Stachecka et al., 2018). In adipogenesis, changes in nuclear shape, volume, and stiffness related to changes in lamin levels trigger large-scale genome rearrangements. For example, chromosomes 12 and 16 change their localization during adipose differentiation in a non-random manner (Kuroda et al., 2004). LADs also undergo significant remodeling in adipogenesis with multiple genes associating or dissociating from the nuclear lamina upon differentiation induction (Madsen-Østerbye et al., 2022; Paulsen et al., 2019; Rønningen et al., 2015). At the gene expression level, adipogenesis invokes massive rewiring of transcriptional networks to activate the lineage-specific gene expression program (Figure1.3B). The program is regulated by the spatial localization of regulatory elements, such as promoters and enhancers, and by epigenetic regulation by histone modifications (Rauch et al., 2019; Sarusi Portuguez et al., 2017; Siersbæk et al., 2017). Posttranslational modifications of histones can regulate gene expression by directly modulating the chromatin structure or providing binding platforms for activators or repressors of gene transcription (Q. Zhang et al., 2012). Histone acetylation is generally considered an active marker among the

different forms of histone modifications (Kimura, 2013). In contrast, histone H3 lysine 9 dimethylation and trimethylation (H3K9me2, H3K9me3) and lysine 27 trimethylation (H3K27me3) have been defined as repressive markers. (Bártová, Krejcıé, Harnicarová, Galiová, et al., 2008; R. Cao et al., 2002; Jacobs et al., 2001; Kimura, 2013).

Overall, genome organization is usually studied in early adipogenesis, whereas a stronger effect on the nuclear organization can be expected with lipid accumulation in late differentiation.

1.2.5 The nucleolus

Inside the nucleus, the largest subcompartment is the nucleolus. The nucleolus is a dense membraneless condensate formed by liquid-liquid phase separation (Lafontaine et al., 2021), a process where components of similar properties form fluid droplets (Hyman et al., 2014). Functionally, the nucleolus is the central hub regulating global protein translation levels. Structurally, the nucleolus consists of dense fibrillar components (DFC), fibrillar centers (FC), and of the granular component (GC) (Boisvert et al., 2007; Schwarzacher and Wachtler, 1993). The DNA component of the nucleolus is the nucleolar organizing regions (NORs); in humans, these are located on five acrocentric chromosomes, namely chromosomes 13, 14, 15, 21, and 22. Ribosomal DNA genes are present in a high number of copies - 90-300 in humans (McStay and Grummt, 2008). Active decondensed chromatin from NORs containing rDNA genes loops into the nucleolus and is transcribed at the border of FC and DFC by RNA PolI. The first product of transcription, the 47S pre-rRNA, is processed to 18S, 28S, and 5.8S rRNA molecules. These are concomitantly assembled with ribosomal proteins in the nucleolus to form pre-40S and pre-60S subunits of the ribosome (Pelletier et al., 2018) (Figure 1.5).

As the primary regulator of ribosome biogenesis, the nucleolus controls protein synthesis, thus affecting fundamental cell processes such as proliferation, survival, and differentiation. In addition to orchestrating ribosome biogenesis, the nucleolus is a key stress hub, integrating the stress response for different types of physiological stressors, including hypoxia, UV-damaged DNA, and redox stress (Weeks et al., 2019). Although the size and shape of nucleoli change in cellular senescence and in response to stress such as DNA damage, the implications are unclear.

Importantly, nucleolus assembly depends on the biophysical properties of the surrounding chromatin (Lafontaine et al., 2021). Interactions between the nucleolus and rDNA can influence local chromatin organization and gene expression. Structural changes in the nucleolus could have an impact on ribosome biogenesis and have implications for genome organization (Bersaglieri et al., 2022; Gupta et al., 2010).

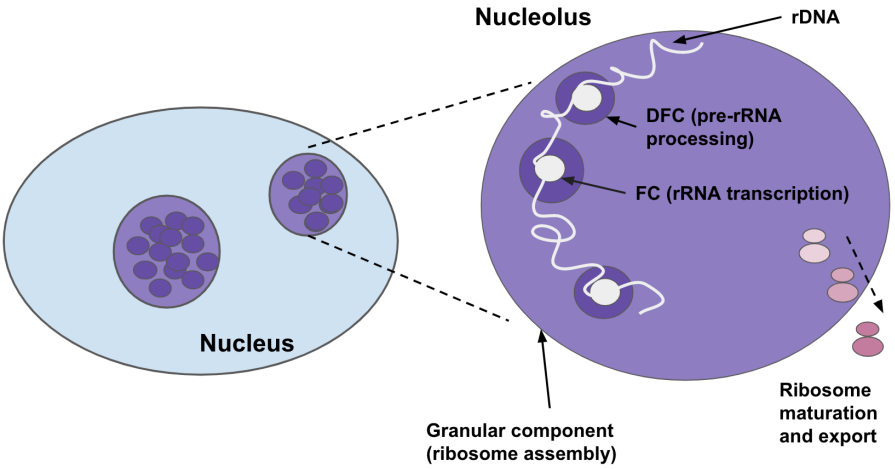

Figure 1.5: Nucleolar structure and function. FC - fibrillar center, DFC - dense fibrillar component, GC - granular component, rDNA - ribosomal DNA, rRNA - ribosomal RNA.

Nucleolar dynamics during differentiation

Although significant remodeling of multiple cell compartments is described in differentiation systems, surprisingly little is known about the behavior of the nucleolus in cell differentiation, and there are no data for the adipogenic lineage. Therefore, I will summarize the findings from other model systems.

In vivo, as keratinocytes progress through the layers of the epidermis, the nuclei and nucleoli undergo multiple changes (Gdula et al., 2013). The nuclear volume decreases, the number of nucleoli per cell decreases, and they move to the center of the nucleus. Furthermore, the frequency of contact between pericentromeric clusters and nucleoli increases. These observations suggest a role for nucleoli as a heterochromatin microenvironment that supports appropriate gene expression programs (Gdula et al., 2013). In the eye of Drosophila melanogaster, nucleolar size is reduced during specification of stem cell fate (Baker, 2013). These changes are associated with cell cycle arrest that precedes differentiation (Baker, 2013). In mouse ESCs, upon exit from pluripotency, 30-40% of the rRNA genes gain heterochromatin marking by increasing CpG methylation and H3K9me2 and H3K9me3 histone marks (Savić et al.,

2014). Downregulation of rRNA transcription during mouse and human ESC differentiation is a well-described functional phenomenon (Savić et al., 2014; Watanabe-Susaki et al., 2014; Woolnough et al., 2016). In contradiction to the study carried out in keratinocytes (Gdula et al., 2013), active pluripotent mESCs have one prominent active nucleolus (Meshorer and Misteli, 2006). Upon differentiation, the number of nucleoli increases and the nuclei become smaller as cellular activity drops.

Changes in nucleolar morphology and structure are perhaps better characterized outside of the differentiation context. A characteristic feature of senescence is one large nucleolus (Dillinger et al., 2017). Fibroblasts from patients with Hutchinson-Gilford progeria syndrome have larger nucleoli, enhanced ribosome biogenesis, and increased global protein synthesis (Buchwalter and Hetzer, 2017). Interestingly, Hutchinson-Gilford progeria syndrome is caused by a mutation in the *LMNA* gene, encoding Lamin A and C, and induction of mutant *LMNA* expression is sufficient to drive nucleolar expansion (Buchwalter and Hetzer, 2017). Another determinant of nucleolar size and number, namely matrix stiffness, was recently described (Pundel et al., 2022). A recent study using *in vitro* keratinocytes links stiffness of the ECM to nucleolar morphology and function (Pundel et al., 2022). Essentially, a softer matrix promotes nucleolar fusion with an overall reduction in nuclear volume and an increase in heterochromatin formation. In contrast, plating cells on a stiffer matrix leads to a higher number of nucleoli per cell and larger elongated nuclei (Pundel et al., 2022).

Changes in nucleolar morphology are not random and are associated with cells transitioning from one state to another. Overall, the morphology of the nucleoli is highly variable and depends on cell type - nucleoli can differ in size, shape, and number in different systems. However, there is no consensus on whether and how nucleolar morphology and numbers are linked to its function.

1.2.6 Translation machinery

Differentiation leads to significant changes in the cell transcriptome (Brunmeir et al., 2016; Casado-Dıéaz et al., 2017; Jääger et al., 2012; Menssen et al., 2011) and consequently to a different proteome (DeLany et al., 2005; Welsh et al., 2004), but the underlying regulation of translation is not extensively studied. However, there are indications that the correlation between mRNA levels and protein synthesis in eukaryotes is not high (Tebaldi et al., 2012).

A study reports that in human ASCs, induction of adipogenesis leads to the downregulation of *de novo* protein synthesis and decreased translational activity (Marcon et al., 2017). Accordingly, the expression of ribosomal protein genes decreases (Marcon et al., 2017). Negative regulation of ribosomal proteins (at the translational level) has also been reported in mouse ESCs after embryoid body formation and in the C2C12 cell line as a result of myogenesis (de Klerk et al., 2015; Ingolia et al., 2014). Protein synthesis in differentiation appears to be regulated at both the transcriptional and translational levels. However, more studies are needed to characterize the regulation of global protein synthesis in differentiation *in vitro*.

Main signalling pathways regulating translation

Marcon et al. describe a downregulation of protein synthesis in human adipogenesis (Marcon et al., 2017). An important translation regulator mentioned in this study is eIF4E - eukaryotic translation initiation factor 4E. eIF4E is required to successfully recruit a 40S ribosomal subunit to the 5' cap of mRNA. The activity of eIF4Fe is mainly regulated by 4E-BP1, which binds to eIF4E and inhibits translation when phosphorylated (Jackson et al., 2010). Two main signaling pathways, PI3K/Akt/mTOR and Ras/MAPK/Mnk, regulate the activity of eIF4E by phosphorylating 4E-BP (Siddiqui and Sonenberg, 2015). Another important mTOR downstream pathway is mediated by the S6 kinase (S6K), which regulates protein translation and ribosome biogenesis. PI3K/Akt/mTOR and the downstream pathways are the main signaling pathways that regulate cell growth, cell proliferation, and stress response. Multiple studies have established the importance of mTOR, eIF4E, and S6K in adipose tissue homeostasis and adipogenesis (Carnevalli et al., 2010; Conn et al., 2021; Lamming et al., 2013; P. L. Lee et al., 2017). Interestingly, another member of the initiation factors, eIF2A, is important for lipid metabolism and insulin sensitivity in mice (Anderson et al., 2021; Oyadomari et al., 2008).

A recent study has identified a novel transcription factor that impacts adipogenesis via a global effect on translation, cytoskeleton, and mitochondria independently of the canonical 4E-BP1 pathway (see Section 1.2.2) (Audano et al., 2021). The connection between cytoskeleton, translation, and lipid synthesis is discussed in Chapter 4 in relation to our findings.

1.3 LncRNA in mammalian genomes

Before next-generation sequencing technologies, the human genome was thought to consist of approximately 20,000 genes encoding proteins, interspersed with largely repetitive and silent non-coding elements with no function (or "junk DNA"). The only recognized non-coding elements were then promoters and enhancers. The first non-coding RNAs (ncRNAs) were discovered in the early 1990s in the genomes of Mus musculus and Caenorhabditis elegans. These were the first members of the later established microRNA (*lin-4*) and long non-coding RNA (*H19*, *Xist*) classes. (Brannan et al., 1990; Brockdorff et al., 1992; Brown et al., 1992; R. C. Lee et al., 1993).

In the last 20 years, high throughput sequencing revealed pervasive transcription of mammalian genomes. In contrast to previous assumptions, up to 80% of the human genome is transcribed (Carninci et al., 2005; Derrien et al., 2012) (Figure 1.6). These findings have changed the general concept of "junk DNA", yet the noncoding genome was and still is often referred to as "the dark matter" of the genome (Lusic and Mhlanga, 2022; Martin and Chang, 2012; Mefford, 2014).

Surprisingly, the number of non-coding genes in the human genome turned out to be higher than that of coding genes. Currently, the GENCODE database (version v35) counts 60,656 genes, of which only 19,954 are protein-coding genes, and 229,580 transcripts, of which only 84,485 are protein-coding transcripts (Frankish et al., 2019, https://www.gencodegenes.org). In quantity, mRNAs represent approximately 3% of cell RNA (Squillaro et al., 2020) (Figure 1.6). Of note, ribosomal RNA (rRNA) and transfer RNA (tRNA) are non-coding and account for 90% of all RNA expressed in the cell. rRNA and tRNA are not included in the ncRNAs discussed here because they have separate specific functions.

Initially, ncRNAs have been separated into categories depending on their length: those below 200 bp, such as microRNAs (miRNAs) and small nucleolar RNAs (snoRNAs), and those above 200 bp called long non-coding RNAs (lncRNAs) (Figure 1.6). Among these, lncRNAs are the most similar to protein-coding mRNAs.

Generally, lncRNAs have a spatially restricted expression pattern throughout the body and are, on average, expressed at lower levels than coding genes (Derrien et al., 2012; Hangauer et al., 2013). However, and although estimations of expression levels are very relative, specific lncRNAs can be highly expressed in brain cells (Q. Ma and Chang, 2016).

The expression of lncRNAs is more tissue-specific than protein-coding genes, with only 11% of lncRNA genes versus 65% of protein-coding genes ubiquitously expressed (Derrien et al., 2012).

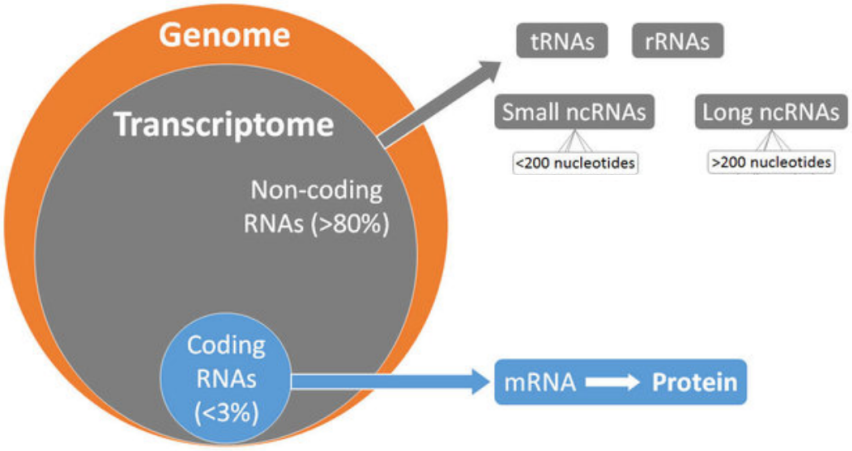

Figure 1.6: The proportions of coding and non-coding RNAs in the human genome. Adapted from (Gomes et al., 2019).

1.3.1 Genomic loci, structures, isoforms

Various types of transcripts are included in the lncRNA class. One parameter distinguishing lncRNAs is their genomic location and orientation: lncRNAs genes can be intergenic or intronic, with a sense or antisense direction. Moreover, lncRNAs can be expressed from regulatory elements of protein-coding genes such as enhancers, promoters or 3'-UTRs, and even from telomeres (Qureshi and Mehler, 2012). Depending on their origin, lncRNAs can be classified into enhancer ncRNAs, promoter ncRNAs, long intergenic ncRNAs, or intronic ncRNAs (Bonasio and Shiekhattar, 2014). Depending on the directionality of the gene, they can also be categorized as sense and antisense. Finally, based on their mode of action, they are defined as cis- or trans-acting (Ulitsky and Bartel, 2013). The processing of lncRNA can also vary; many are capped at the 5' end, spliced at canonical sites, and polyadenylated at the 3' end (Cabili et al., 2011; Chew et al., 2013; Guttman et al., 2009). Essentially, lncRNAs that have their gene transcribed by PolII and are polyadenylated and 5'capped are not much different from mRNAs. An example of fully processed and multiexonic long intergenic noncoding RNA is *HOTAIR*, the subject of my

research. Unfortunately, no systematic classification of lncRNAs exists, making the class of lncRNAs large and highly varied.

As mRNAs of protein-coding genes, lncRNAs can have multiple isoforms. One of the sources of isoform variability is alternative polyadenylation, which happens when a gene sequence harbors more than one polyadenylation signal sequence (pAs). In the mouse genome, approximately 70% of mRNAs and 66% of lncRNAs have more than one pAs (Hoque et al., 2013). Interestingly, lncRNA genes show more variability in the localization of pAs than mRNA. A larger proportion of lncRNA genes have pAs upstream of the last 3'-end exon, suggesting more variation in the expressed exons. Around 45% of the conserved regions in lncRNA genes lie downstream of the first pAs, which means that alternative polyadenylation can have a functional effect if important conserved regions are included or excluded depending on the pAs used (Hoque et al., 2013). In the human genome, two functionally different isoforms of CCAT1 lncRNAs have been reported; the main difference between the isoforms lies in the use of alternative pAs (Xiang et al., 2014). Similarly to mRNAs, lncRNAs can undergo alternative splicing, and seemingly all exons of lncRNAs can be spliced, thus creating the possibility of an enormous number of isoforms (Deveson et al., 2018).

Conservation levels of lncRNAs are lower than those of protein-coding mRNAs, and on average lncRNAs have fewer exons (Derrien et al., 2012; Haerty and Ponting, 2013; Pang et al., 2006). The low level of genomic conservation could result from a lower evolutionary pressure on the sequence compared to a coding sequence. Interestingly, in the human genome, exonic splicing enhancers for multiexonic lncRNAs (6 nt DNA motifs that direct splicing) are conserved to the level of protein-coding genes across mammals (Haerty and Ponting, 2015). Furthermore, conserved splicing patterns were confirmed in another study using human and mouse transcriptomes (Deveson et al., 2018). Such conservation of splicing patterns suggests that correct processing and exon composition are essential for multiexonic lncRNAs.

1.3.2 Are lncRNAs functional?

There are multiple opinions on whether lncRNAs are functional, whether all of them are functional, and whether some of them are transcriptional "noise" (Pang et al., 2006; Ponjavic et al., 2007). LncRNAs genes are epigenetically regulated and can be marked with H3K4me3 and H3K6me3 histone modicifcations (Mikkelsen et al., 2007). These histone marks are found at active promoters and gene bodies of actively transcribed

genes. Active epigenetic marking contradicts the notion that lncRNAs are transcriptional "noise" arising from spurious transcription by RNA Pol II (Derrien et al., 2012; Hangauer et al., 2013).

Probably due to their variability as a class, lncRNAs have functions in many cellular processes, including proliferation, differentiation, apoptosis, and migration. Mechanistically, lncRNAs can act as protein decoys, scaffolds, or guides (Rinn and Chang, 2012). LncRNAs can also sponge miRNAs, preventing them from acting and positively regulating downstream mRNAs (López-Urrutia et al., 2019).

While proteins regulating adipogenesis have been studied extensively, regulation of adipogenesis by non-coding RNAs has not been investigated to the same extent. A transcriptomic study carried out in mouse tissues and isolated cells reports that expression levels of up to 175 lncRNAs are tightly regulated in adipogenesis (L. Sun et al., 2013). There are no such estimates for the human transcriptome, but a similar magnitude of regulation can be expected. A recent report summarizes 14 lncRNAs that have been studied in adipose biology and adipogenesis. These 14 lncRNAs include potential regulators of the white and beige adipose lineages (Squillaro et al., 2020). It should be noted that some of the lncRNAs related to adipose tissue homeostasis in mice have been shown to regulate the cell cycle in 3T3-L1 cells (Rey et al., 2021). One of the 14 lncRNAs is *HOTAIR*, the gene of interest in this thesis.

Tight transcriptional control of lncRNAs and evolutionary conservation, together with multiple studies proposing distinct (though very diverse) functions for lncRNAs, strongly suggest that lncRNAs as a class are functional and represent a complex layer of genome regulation rather than "transcriptional noise".

1.3.3 LncRNA *HOTAIR* from the *HOXC* locus

HOX genes are an ancient group of genes involved in anterior-posterior specialization during development. *HOX* genes are found in evolution as early as in Cnidaria and are present in all animals with an anterior-posterior axis (Lewis, 1992). *HOX* clusters were duplicated throughout evolution and initially all arose from one *HOX* gene (Carroll, 1995; Kappen et al., 1993). There are 4 *HOX* loci in the mammalian genome. In humans, these are called *HOXA*, *HOXB*, *HOXC*, and *HOXD* and are located on chromosomes 7p14, 17q21, 12q13, and 2q31 respectively. (Lappin et al., 2006). All protein-coding genes in *HOX* loci encode transcription factor proteins with a homeobox domain - a highly conserved motif. Mutations in the *HOX* genes lead to malformations of organs and many skeletal bones

(Quinonez and Innis, 2014). *HOX* genes share biologically important features, one of which being spatial colinearity. During development, *HOX* genes are expressed from the 3' end to the 5' end of the locus in a gradient manner, with the gene numbers starting from 1 (for example, *HOXA1*) at the 3'-end (McGinnis and Krumlauf, 1992). The pattern of expression of *HOX* genes according to the anterior-posterior axis is preserved in the adult organism (Ackema and Charité, 2008; Picchi et al., 2013; Rinn et al., 2007). Although the role of *HOX* genes in the development and spatial organization of the embryo is well known (Iimura and Pourquié, 2007; Krumlauf, 1994), the functions of *HOX* genes in an adult organism are less clear. One hypothesis is that the expression of *HOX* genes supports developmental plasticity in tissues that continue to undergo rapid developmental changes in the adult organism and have high turnover (Daftary and Taylor, 2006).

LncRNAs from *HOX* loci

For a few decades, the research has mainly focused on protein-coding genes of the *HOX* loci. However, multiple antisense transcripts embedded in *HOX* loci were later discovered. Of note, noncoding *HOX* transcripts are present both in human and mouse, suggesting a preserved function. These transcripts have been attributed to various functions in the cis and trans regulation of gene expression (De Kumar and Krumlauf, 2016). In my research, I have focused on lncRNA *HOTAIR*, an antisense transcript located directly downstream of the *HOXC11* gene. *HOTAIR* was first identified by Rinn et al. in a study focusing on the lncRNAs in *HOX* clusters (Rinn et al., 2007). In this study, the authors identify in human cells 231 spatially expressed *HOX* ncRNAs and demonstrate that their genomic location often demarkates large epigenetic domains (Rinn et al., 2007). Overall, early findings on *HOTAIR* led to an understanding that *HOX* genes have a non-coding level of regulation (Mainguy et al., 2007; Rinn et al., 2007).

HOTAIR

HOTAIR gene starts inside the *HOXC11* gene, is located on the antisense strand, and contains 11 canonical GT-AG introns and a total of 7 exons, although these estimates and the numeration vary (Hajjari and Rahnama, 2017; Mozdarani et al., 2020). RefSeq and Ensembl report a different number of alternative transcripts for *HOTAIR* with their lengths varying

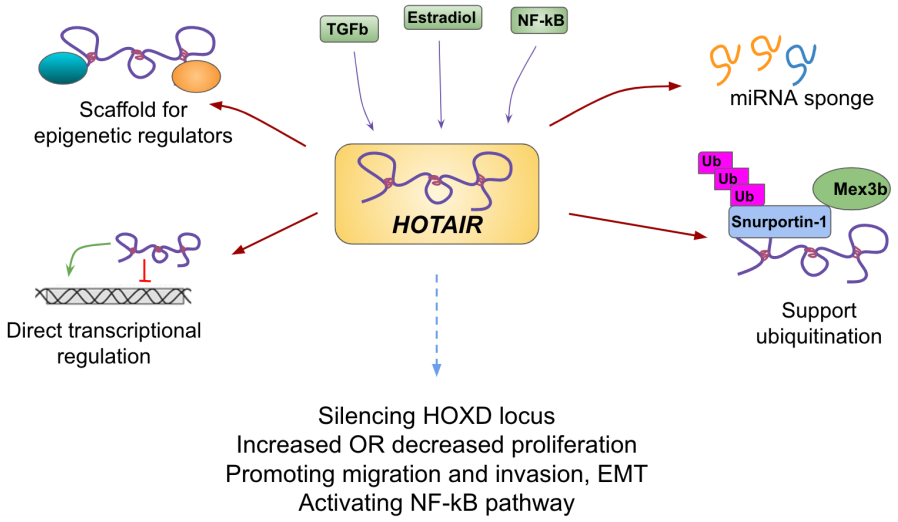

Figure 1.7: Multiple functions attributed to *HOTAIR*. TGFb - transforming growth factor beta, Ub - ubiquitination, NF-kB - nuclear factor kappa B.

from 500 to 2000 bp. Two active promoters were identified in the *HOTAIR* gene, one upstream of the first exon and another encompassing exons E3 to E5. *HOTAIR* gene also display alternative TSSs and multiple polyadenylation signals (Hajjari and Rahnama, 2017). *HOTAIR* is transcribed by PolII, spliced, and processed like an mRNA, has a 5'-cap and a polyA tail. In transcriptomic studies using adipose tissue biopsies from healthy donors, *HOTAIR* was identified as the most differentially expressed gene between subcutaneous fat in the upper and lower body (Divoux et al., 2014; Pinnick et al., 2014). This is in agreement with the anterior-posterior gradient of the overall expression pattern of *HOX* genes. However, across all four *HOX* loci *HOTAIR* is the most significantly upregulated gene in the lower body adipose tissue.

1.3.4 *HOTAIR* as an epigenetic scaffold

HOTAIR was shown to interact with the polycomb repressive complex (PRC2) and to downregulate the *HOXD* locus in trans through trimethylation of H3K27me3 (Khalil et al., 2009). *HOTAIR* was then shown to interact with the LSD1/CoREST complex, an epigenetic complex with robust demethylase activity (Tsai et al., 2010). The PRC2-binding domain is located closer to the 5'-end of *HOTAIR*, while LSD1/CoREST is

located at the 3'-end (Tsai et al., 2010). The ability to bind two chromatin modifiers at different ends of *HOTAIR* allows the construction of a large epigenetic complex (Tsai et al., 2010). A study focused on the secondary structure of *HOTAIR* found that 50% of the sequence is involved in base pairing, making it a highly structured lncRNA (Somarowthu et al., 2015). *In vitro*, *HOTAIR* reproducibly folds into four independent domains (Somarowthu et al., 2015), all of which show sequences of high evolutionary covariation, suggesting their functional importance. Two of these domains include the predicted binding regions of PRC2 and LSD1 (Somarowthu et al., 2015). However, *HOTAIR* has also be reported to directly silence genes independent of PRC2 (Portoso et al., 2017). This could be conceivibly relate to its hability to form a DNA-DNA-RNA triple helix structure (Kalwa et al., 2016). Furthermore, *HOTAIR* can act as a sponge for various miRNAs (Cantile et al., 2021) and can silence specific miRNA genes at the epigenetic level (D. Cheng et al., 2018; Y.-W. Liu et al., 2015). Hence, *HOTAIR* can regulate gene expression both via epigenetic complexes and independently of them (Figure 1.7).

1.3.5 The pathological and physiological roles of *HOTAIR*

HOTAIR has been extensively studied in the context of cancer. However, reviewing the role of *HOTAIR* in cancer is beyond the scope of this thesis; therefore, I will only briefly summarize the main concepts in the field.

The high expression of *HOTAIR* is a feature of multiple types of cancer where it associates with metastasis and a poor prognosis (Bhan and Mandal, 2015; Gupta et al., 2010; L. Lu et al., 2012; Sørensen et al., 2013). In the cancer context, *HOTAIR* expression can be regulated by multiple stimuli, such as estradiol, specific miRNAs, c-Myc, Collagen-1, and TGF-b (Bhan et al., 2013; M.-Z. Ma et al., 2014; Z. Zhang et al., 2018; Zhuang et al., 2013) (Figure 1.7). In breast cancer cell lines, overexpression of *HOTAIR* promotes cancer invasiveness, while the knockdown of *HOTAIR* does the opposite (Gupta et al., 2010). In summary, *HOTAIR* is associated with aggressive migratory cancers and regulates genes involved in cell migration, epithelial-to-mesenchymal transition, and tumorogenesis.

On the contrary, little is known about the physiological role of *HOTAIR*. Functional studies of *HOTAIR* in a physiological context are scarce and often controversial. In the first report of *HOTAIR* differential expression between the upper and lower body adipose tissue, it was shown that *HOTAIR* overexpression promotes adipogenesis of abdominal ASCs (Divoux et al., 2014). However, a recent paper reports that overexpression of *HOTAIR* in abdominal ASCs impairs adipogenesis (Kuo, Huang, et al.,

Model	Method	Effect on gene expression	Phenotype	Reference
Bone-marrow MSCs	Retroviral OE, siRNA KD	No significant effect	OE: Proliferation not affected Osteogenesis not affected Adipogenesis ↓ KD: Proliferation ↓ Both adipogenesis and osteogenesis ↑	Kalwa et al., 2016
Abdominal ASCs	Retroviral OE	Adipogenic markers, *HOXD3* and *HOXD4* ↑	Proliferation not affected Adipogenesis ↑	Divoux et al., 2014
Immortalized abdominal ASCs	Retroviral OE	GO terms: Rho-signaling, actin cytoskeleton, cell motility ↑ Cell cycle ↓	Adipogenesis ↓	Kuo H et al., 2022
Gluteofemoral ASC, Abdominal ASCs	siRNA KD, Retroviral OE	Upregulated in KD and downregulated in OE GO terms: TNF-α signaling, EMT, G2M checkpoint	Proliferation not evaluated	Erdos et al, 2022
Immortalized abdominal and gluteal ASCs	shRNA retroviral	*HOXD8*, *HOXD9*, *HOXD10* ↑ *CEBPA*, *PPARG* ↓	Adipogenesis ↓ Proliferation ↑	Kuo FC et al., 2022
Aortic Valve Interstitial Cells	siRNA KD	Valve calcification genes ↑	Wnt-signaling suppresses *HOTAIR*	Carrion et al., 2014
Bone-marrow MSCs	siRNA KD Adenoviral OE	Both directions - *RUNX2*, *COL1A1*	KD osteogenesis ↑ OE osteogenesis ↓	Wei et al., 2017

Figure 1.8: Summary of *HOTAIR* functional studies in human non-malignant cells. KD - knockdown, OE - overexpression. ↑ - increased, ↓ - decreased.

2022). In bone-marrow MSCs, overexpression of *HOTAIR* also inhibits adipogenesis (Kalwa et al., 2016). Figure 1.8 summarizes functional studies of *HOTAIR* performed in a non-cancerous context in human cell lines. Of note, not all functional studies of *HOTAIR* report changes in gene expression (Figure 1.8), and gene regulation mediated by *HOTAIR*-PRC2 is often not considered or not significantly affected.

Similarly to human research, knockout studies in mice report controversial findings. One study reports homeotic transformation and skeletal malformations after *HOTAIR* knockout, as expected from distal deletion of the *HOX* gene (L. Li et al., 2013). The phenotype is supported by derepression of hundreds of genes and, more importantly, derepression of *HOXD* genes (L. Li et al., 2013). However, a second knockout study did not confirm these findings (Amândio et al., 2016). Notably, the structure and sequence of the *HOTAIR* gene are poorly conserved between mouse and human, with the LSD1 binding domain having only a general conservation of 50%-70% and the EZH2 binding sites absent from mouse *HOTAIR* (Schorderet and Duboule, 2011). Little sequence similarity and controversial results from mouse knockout models make it challenging to speculate on a similar role of *HOTAIR* in mice and in humans.

The discrepancy between functional studies of *HOTAIR* might stem from the differences between models and approaches used to overexpress or deplete *HOTAIR*. The reasons likely leading to inconsistent and controversial findings of functional studies are discussed in Chapter 4.

1.4 Long-read sequencing to decipher lncRNA structure

LncRNA genes give rise to multiple isoforms (Deveson et al., 2018), however, identifying these and verifying their structure is technically challenging. Initially, rapid amplification of cDNA ends (RACE) techniques were used to study gene isoforms (Birman et al., 1994; Pischedda et al., 1995; Sekelsky et al., 1999). RACE allows one to "scan" the transcript either from the 3'-end or 5'-end. However, the RACE methods are very tedious and require sequential steps of PCR and cloning. In addition, RACE is not always capable of correctly detecting isoforms from the 3'-end to the 5'-end, as the method requires a known sequence anchor to place primers (Ozawa et al., 2004).

Although high-throughput short-read RNA sequencing (SR RNA-seq) technology made it easy to quantitatively assess gene expression levels, SR RNA-seq fails to accurately recapitulate isoform structures due to a very short read length (up to 600 bp, but usually between 50-150 bp per read) (De Paoli-Iseppi et al., 2021; Soneson et al., 2016; Steijger et al., 2013). Moreover, SR RNA-Seq requires a high depth of sequencing to detect and characterize isoforms. As previously mentioned, one of the features of lncRNAs is a low level of expression compared to many protein-coding genes. Therefore, discovery of lncRNA isoform pools is biased, since more lncRNA isoforms are below the detection threshold (Derrien et al., 2012). Another common feature of lncRNA is tissue specificity, which means that annotations made in one tissue or cell type might not apply in other contexts.

1.4.1 Advantages and limitations of long-read sequencing

A few years after SR RNA-seq became a standard method, long-read sequencing technology (LR) was developed to allow isoform annotation. With LR PacBio SMRT sequencing technologies, the read length can reach 20 kb, and while the raw error rate is up to 15%, the post-processing error rate is <1% (Hon et al., 2020; Tardaguila et al., 2018). The main advantage of LR RNA-seq is that a full-length transcript is sequenced from beginning to end in one read. Thus, LR RNA-seq alleviates the issue of reconstructing possible isoforms from short overlapping reads. The data obtained by LR RNA-seq led to the discovery of many novel isoforms and revealed complex splicing patterns (Clark et al., 2019). PacBio LR sequencing for RNA is called Iso-Seq and is used to detect and quantify isoforms (Ambardar et al., 2016).

The limitation of LR RNA-seq lies in the depth of sequencing, as the

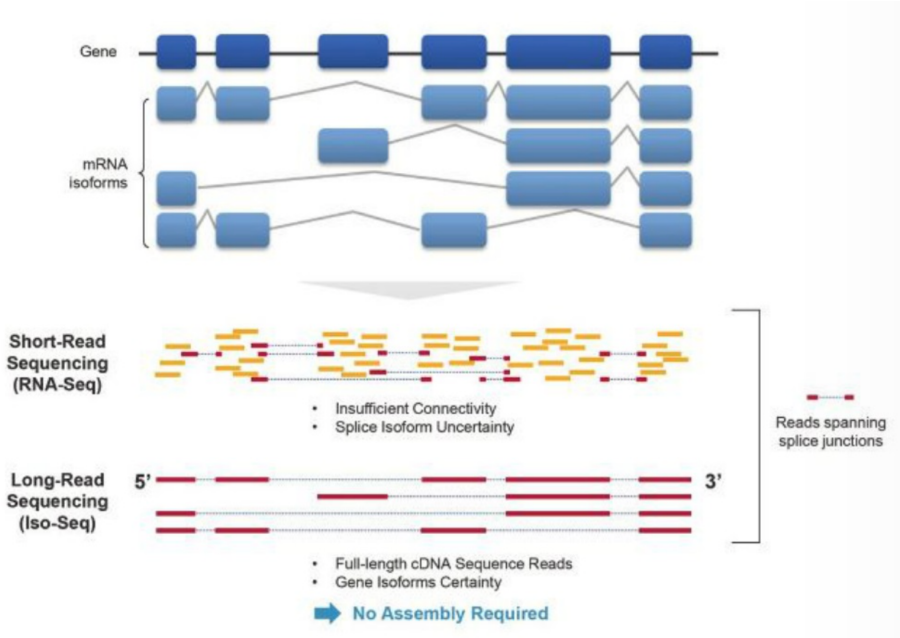

Figure 1.9: Comparison of SR and LR RNA-Seq for identifying isoforms. Modified from (https://www.ddw-online.com/full-length-isoform-sequencing-iso-seq-yields-a-more-comprehensive-view-of-gene-activity-1586-201608/)

average number of reads is much lower than in SR RNA-seq. Sequencing the whole transcriptome with PacBio technology is very expensive, and the lowly expressed transcripts might not have enough sequencing coverage for isoform detection. To overcome this challenge, the Capture-Seq method uses oligonucleotide probes to enrich the target transcript (Clark et al., 2015; Mercer et al., 2014). We have used the Capture-Seq method to enrich *HOTAIR* transcripts from the full-length cDNA library in our **Paper I**.

1.4.2 Library generation

LR RNA-seq requires the construction of a full-length cDNA library where transcripts are amplified from both ends. An oligo-dT primer with an adaptor sequence is annealed to the 3'-end polyA tail, while the 5'-end anneals with a template-switching oligo (TSO). Essentially, full-length cDNA can be generated from a polyadenylated mRNA without prior knowledge of the transcript sequence. Sequencing can then be performed on either unamplified or PCR-amplified cDNA, depending on

the expression level and amount of material available. Since longer transcripts will be underrepresented after PCR amplification, some protocols include cDNA size fractionation to enrich the longer fraction, a step that is considered necessary for transcripts above 4000 base pair (bp) . For long-read sequencing of *HOTAIR*, we have performed PCR amplification but we did not use size fractionation as *HOTAIR* transcripts only range from 500 to 2000 bp.

Importantly, repeated rounds of PCR amplification necessary to obtain full-length enriched libraries make quantitative comparisons between different samples impossible. In the cDNA library, transcripts of 500 bp are amplified in the same PCR reaction together with transcripts of 5000 bp. Length variation between fragments will inevitably lead to over-representation of shorter sequences. Capture-Seq data are thus qualitative and isoform abundance can only be quantified inside one sample, but not between samples.

1.4.3 Data analysis

From LR RNA-seq data, the isoform composition can be identified with high precision. Multiple programs can be used to collapse identical transcripts into a high-confidence set of unique isoforms. We have used SQANTI (for Structural and Quality Annotation of Novel Transcript Isoforms), a tool used to create a detailed and reference-corrected characterization of transcripts and splice junctions (Tardaguila et al., 2018). SQANTI has an internal set of quality controls preventing false positive detection of isoforms, which could potentially arise from poly-dT primer annealing to adenine-rich sequences, or from template switching of the reverse transcriptase on a secondary structure pin of the RNA. In SQANTI, transcripts that are perfectly, or partially matching splice junctions from an annotated isoform are respectively labeled Full Splice Match (FSM) or Incomplete Splice Match (ISM) of this annotated transcript (Tardaguila et al., 2018). Novel isoforms resulting from a novel combination of previously known splicing events are labeled Novel in Catalog (NIC), while isoforms including at least one unknown splicing junctions are labeled Novel Not in Catalog (NNC). In general, SQANTI uses more quality controls and a larger panel of descriptors to categorize isoforms than previous softwares.

Chapter 2

Aim of the study

Human adipose tissue depots are physiologically different, with distinct metabolic properties and contributions to disease. The underlying reasons for these differences are yet to be investigated in detail. Large-scale transcriptomic studies of human adipose tissues have identified *HOX* genes and, in particular, the lncRNA *HOTAIR* to be the most differentially expressed between upper and lower body adipose depots. The role of *HOTAIR* and its regulation in adipogenesis are not well studied. Previous studies performed in human ASCs and MSCs report at times controversial results. In this context, the aims of this study were to:

- Explore the epigenetic regulation of *HOTAIR* in gluteal and abdominal adipose stem cells, characterize the expression and regulation of *HOTAIR* during adipose differentiation **(Paper I)**
- Assess the function of *HOTAIR* during adipogenic differentiation of ASCs by performing knockdown experiments to identify the affected pathways **(Paper II)**
- Characterize nucleolar and cytoskeletal remodeling in adipogenic differentiation **(Paper III)**

While **Paper I** and **Paper II** focus on *HOTAIR*, **Paper III** is not related to *HOTAIR* but rather to the general process of adipogenesis. **Paper III** is presented in the form of manuscript and does not study lncRNA *HOTAIR*, but further explores processes affected by *HOTAIR* knockdown in **Paper II**. Results and conclusions of **Paper II** led us to characterize nucleolar dynamics upon cytoskeletal remodeling during in adipose differentiation.

Own contribution:

My contributions to this thesis work include conceptual planning, generating and analyzing data, and writing manuscripts. For all three papers presented here I have carried out a large part of cell culture experiments. I have generated and analyzed all the microscopy data in both **Paper II** and **Paper III**. Additionally, I have optimized full-length cDNA library generation and designed capture probes for PacBio sequencing of *HOTAIR*. For **Paper II** I have designed shRNA sequences, cloned them, and generated stable cell lines using a lentiviral system.

Capture and PacBio sequencing for **Paper I** was performed by Ave Tooming-Klingerud from the Norwegian Sequencing Centre (NSC) (CEES node). Anita Løvstad Sørensen from our group contributed to cell culture experiments and performed chromatin immunoprecipitation for **Paper I**. Bioinformatics analysis of the short-read RNA-Seq and the long-read sequencing data for all three papers included in this thesis was carried out in the lab by Sarah Hazell Pickering. Thomas Germier, a former member of Collas lab, contributed to microscopy analysis.

Chapter 3

Summary of the papers

3.1 Paper I

De novo annotation of lncRNA *HOTAIR* transcripts by long-read RNA capture-seq reveals a differentiation-driven isoform switch

Evdokiia Potolitsyna, Sarah Hazell Pickering, Ave Tooming-Klunderud, Philippe Collas[$] § Nolwenn Briand[$]. 2022. *BMC Genomics, under revision.*
[$]Corresponding author.

Background: LncRNAs are tissue-specific and emerge as important regulators of various biological processes and as disease biomarkers. *HOTAIR* is a well-established pro-oncogenic lncRNA which has been attributed a variety of functions in cancer and native contexts. However, a lack of an exhaustive, cell type-specific annotation questions whether *HOTAIR* functions are supported by the expression of multiple isoforms. Results: Using a capture long-read sequencing approach, we characterize *HOTAIR* isoforms expressed in human primary adipose stem cells. We find *HOTAIR* isoforms population displays varied splicing patterns, frequently leading to the exclusion or truncation of canonical LSD1 and PRC2 binding domains. We identify a highly cell type-specific *HOTAIR* isoform pool regulated by distinct promoter usage, and uncover a shift in the *HOTAIR* TSS usage that modulates the balance of *HOTAIR* isoforms at differentiation onset. Conclusion: Our results highlight the complexity and cell type-specificity of *HOTAIR* isoforms and processes.

3.2 Paper II

Long non-coding RNA *HOTAIR* regulates cytoskeleton remodeling and lipid storage capacity during adipogenesis
Evdokiia Potolitsyna, Sarah Hazell Pickering, Thomas Germier, Philippe Collas[$] & Nolwenn Briand[$]. 2022. *Scientific reports* 12, 10157
[$]Corresponding author.

The long non-coding RNA *HOTAIR* is the most differentially expressed gene between upper- and lower-body adipose tissue, yet its functional significance in adipogenesis is unclear. We report that *HOTAIR* expression is transiently induced during early adipogenic differentiation of gluteofemoral adipose progenitors and repressed in mature adipocytes. Upon adipogenic commitment, *HOTAIR* regulates protein synthesis pathways and cytoskeleton remodeling with a later impact on mature adipocyte lipid storage capacity. Our results support novel and important functions of *HOTAIR* in the physiological context of adipogenesis.

3.3 Paper III

Cytoskeletal remodeling defines nucleolar architecture during adipogenesis

Evdokiia Potolitsyna, Thomas Germier, Sarah Hazell Pickering, Philippe Collas,[$] and Nolwenn Briand,[$]. 2022. *Manuscript*
[$]Corresponding author.

The differentiation of adipose progenitor cells into mature adipocytes entails dramatic reorganization of the cellular architecture to accommodate lipid storage into cytoplasmic lipid droplets, which occupy the quasi totality of the cell volume in vivo, compressing the nucleus beneath the plasma membrane. Yet, how this cellular remodeling affects nucleus substructure has not been investigated. It is notably unknown whether the size of the nucleus and of the nucleolus are controlled by the same mechanism. We describe a morphological remodeling of the nucleus and its main subcompartment, the nucleolus, during adipogenesis of native human adipose stem cells (ASCs). We find that cell cycle arrest triggers a change in nucleoli structure which correlates with a decreased protein synthesis. Strikingly, triggering cytoskeletal rearrangements alone mimics the nucleolar remodeling observed in adipogenesis. Altogether, our results point to nucleolar remodeling as an active, mechano-regulated mechanism during adipogenic differentiation and demonstrate a key role of the actin cytoskeleton in defining nuclear and nucleolar architecture in differentiating human ASCs.

Chapter 4

Discussion

The work presented in this thesis aims to characterize the lncRNA *HOTAIR* in ASCs and dissect the cellular remodeling events affected by a downregulation of *HOTAIR* expression during adipogenesis. **Paper I** provides a transcriptomic characterization of *HOTAIR* and uncovers a tightly regulated pool of isoforms responsive to adipogenic induction. In **Paper II** we focus on the role of *HOTAIR* in adipogenesis by performing a stable knockdown (KD). In *HOTAIR* KD ASC lines, we describe cytoskeleton remodeling defects that lead to decreased lipid storage. Finally, in **Paper III** we further explore how the nucleus and nucleolus respond to cytoskeletal remodeling and describe how nucleolar phenotype changes during adipogenesis. The findings of **Paper II** and **Paper III** raise further questions about the connection between translation and the cytoskeleton in complex cellular processes such as stem cell differentiation.

4.1 The multiple isoforms of *HOTAIR*

The main finding of **Paper I** is that a previously unstudied group of *HOTAIR* isoforms is dominant in undifferentiated ASCs and is suppressed upon induction of adipogenesis, but not osteogenesis. LncRNAs can have many isoforms, yet little is known about their diversity (Deveson et al., 2018). To address this issue, the first step in **Paper I** was a general characterization and classification of *HOTAIR* isoforms from long-read sequencing data. In the process, we encountered issues when representing one isoform versus a group of isoforms with common characteristics. In the graphical representation of high-confidence isoforms selected in Fig. 2i (**Paper I**) ten isoforms are represented with the long E7 exon. However, these isoforms also exist with all four possible lengths of E7, making our representation a hidden graph. Concatenating E7 is allowed, since full-splice match transcripts are considered one isoform even if the last 3'-end exon length varies (Tardaguila et al., 2018). This is because alterations in the length of the last exon (E7) do not affect the combination of splice junctions used. Concatenating the last exon is a valid approach for protein-coding sequences that contain 3'-UTRs. In the case of *HOTAIR*, the distal 3'-end of E7 contains the LSD1-binding domain. While a simplification of the data is required due to the number of splicing options, such visual

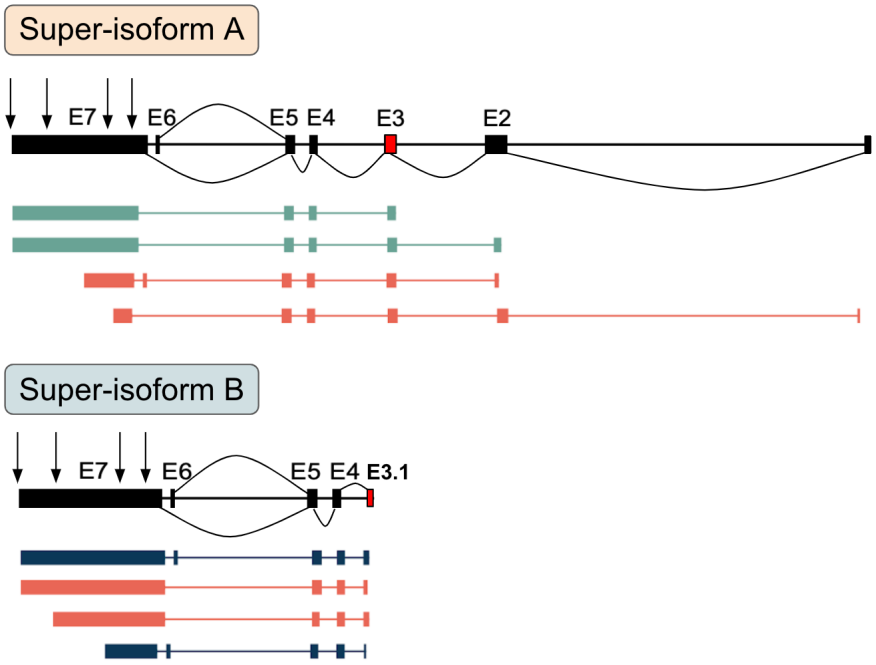

Figure 4.1: Supertranscript visualization approach to multiple isoforms. Superisoform A: isoforms containing E3 with examples of isoforms from **Paper I**; super-isoform B: isoforms starting with E3.1. with examples from **Paper I**. ↓ - pAs location; exons in red - defining superisoforms features.

representation of all isoforms can be misleading in relation to the length of E7.

Overall, due to the degree of variability and the number of splicing events, it could be helpful to use a graph-based approach to create a "consensus" superisoform representing several isoforms (Davidson et al., 2017). For lncRNAs, or *HOTAIR* in particular, we believe a representation with "isoform A" switching to "isoform B" is too simplistic. However, a graph concept of "superisoform A" versus "superisoform B" would be a better solution, including the underlying complexity of the splicing and making the classification more intelligible (Figure 4.1).

Detailed characterizations of the isoform pool are needed to interpret the data across different cellular models (cell types or differentiation systems) and might explain part of the inconsistencies between the results of *HOTAIR* studies (see Chapter 1.3.5). When working with *HOX* genes expressed in a gradient manner in organisms, anatomical location of the sample is essential to understand their mode of regulation. Thus, the

frequent absence of a correct anatomical source of human material used in most studies limits the use of public datasets for accurate comparative analyses.

Importantly, the findings of **Paper I** bring new considerations for functional studies of *HOTAIR*. Taking into account the complex isoform pool, careful consideration is needed when selecting the specific sequence to knockdown *HOTAIR*. Accordingly, commercially available siRNAs and custom-designed shRNAs target the area common to all isoforms (Figure 4.2). Arguably, if an siRNA was designed on E3, around 40-50% of the transcripts would not be targeted in ASCs.

Regarding overexpression, most studies use the only available vector LZRS-*HOTAIR* (Kalwa et al., 2016; Kuo, Huang, et al., 2022; Portoso et al., 2017; Zhai et al., 2016), which is truncated at both the 3' and 5' ends (Figure 4.2). Notably, the insert lacks part of E2 and the end E7, containing one of the PolyA signals. Assuming that the pool of isoforms is large and controlled, overexpression of an isoform that is a priori not normally expressed would likely disrupt the *HOTAIR* isoform balance. Ideally, functional overexpression studies should be conducted using the sequences of highly expressed isoforms. In addition, overexpression levels in functional studies are often 10-1000 fold (Kalwa et al., 2016; Kuo, Huang, et al., 2022; M. Lee et al., 2016; S. Wei et al., 2017), while fluctuations in physiological expression levels are less than 10 fold (**Paper II**) (Kuo, Neville, et al., 2022; B. Wei et al., 2017). Although the overexpression of various *HOTAIR* isoforms would inform on putative isoform-specific functions, designing a well-controlled experiment taking into account the isoform pool and its temporal dynamics would at present be technically challenging.

Interestingly, *HOTAIR* expression and TSS usage is regulated in adipogenesis but not osteogenesis (**Paper I** and **II**). The differential regulation of isoforms between lineages and the fact that ASCs express a pool of rare E3.1 isoforms highlight the importance of the cellular context in lncRNA studies. The adipogenic differentiation of gluteofemoral ASCs is a relevant dynamic system for characterizing the isoform composition of *HOTAIR* and unraveling the differential regulation of isoforms due to the relatively high expression level compared to multiple cell lines (**Paper I**). Similarly, functional studies of the lncRNA *Haunt*, which also belongs to a *Hox* cluster, could only be conducted in the context retinoic acid driven differentiation, where *Haunt* expression is highly induced (Yin et al., 2015). In that study, the authors highlight opposing roles for the gene locus versus the RNA transcript (Yin et al., 2015), a notion that is

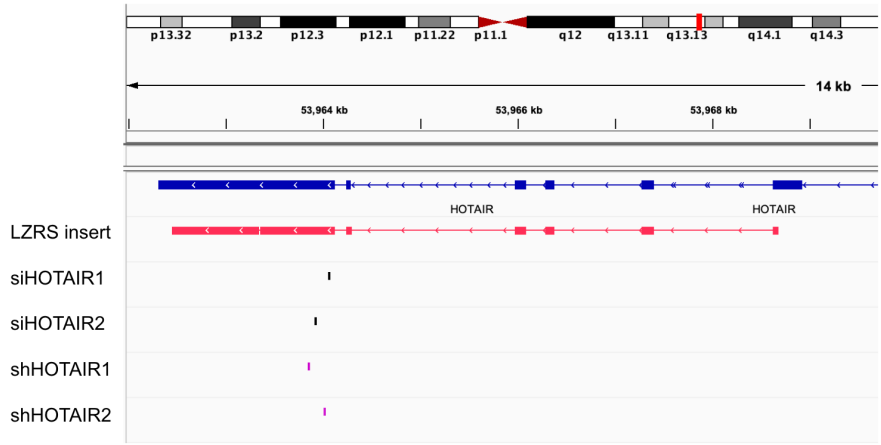

Figure 4.2: IGV screenshot with insert from the commonly used overexpression vector LZRS, location of siRNA sequences, and shRNA sequences.

reminiscent of early studies of *HOX* non-coding transcripts suggesting these loci are defining borders of epigenetic domains (Rinn et al., 2007). As we observe a switch in TSS usage, both the change in the state of regulatory elements and the downregulation of the E3.1 starting isoforms could be functionally significant. However, the fact that the histone modification landscape is not changing at the *HOTAIR* locus (**Paper I**) rather suggests the latter.

4.2 Can we predict the protein binding capacity of lncRNAs?

Several criteria contribute to defining the specificity of lncRNA-protein interactions and multiple approaches may be used to investigate whether *HOTAIR* isoforms differ in their ability to bind protein partners. Folding of the protein-binding domains in the RNA molecule depends on sequence composition. In **Paper I**, we find that the proportion of isoforms that include the PRC2 and LSD1/CoREST domains remains stable during adipogenic differentiation. Surprisingly, the main differences are in the composition of short 5'-end exons of *HOTAIR*, which could potentially affect the folding of the functional domains. The effect of short 5'-end exons on RNA folding is an attractive hypothesis since the short 52-bp novel E3.1 exon does not contain any specific RNA- or protein-binding motifs from known databases (data not shown). Therefore, functionality of the E3.1 exon may lie in the way it affects the folding of known

domains. *In silico* methods exist to predict the RNA secondary structure from sequence (Lorenz et al., 2011) and based on the folding of lncRNA, interactions with proteins can be predicted with tools such as lncPro (Q. Lu et al., 2013). We have attempted to use these tools to predict the folding of individual isoforms (E3 containing and E3.1 starting) and their binding affinity to published protein partners of *HOTAIR* (Busby et al., 2020). However, we found that reproducibility and accuracy of these approaches are low and thus have opted not use or present the data.

Another option would be to evaluate the folding of an artificially synthesized molecule *in vitro*. This approach could shed light on the folding of interaction domains in the presence of E3.1 instead of E3. The canonical sequence of *HOTAIR* folds into four separate domains (Somarowthu et al., 2015), where the first domain spans from E1 to the beginning of E7, and three others are located exclusively in E7. The first domain of the E3.1 starting isoforms should be folded differently, merely because it includes E3.1, but lacks all the upstream exons. However, it is currently challenging to speculate whether there would be any considerable impact on distant domains.

Even if we could predict differential folding in an accurate manner, the results may not give a direct link to differential functions of the isoforms. In general, the low conservation of exon sequence, the high conservation of splicing patterns, and the multiple identified roles of many lncRNAs (see Chapter 1.3) raise the conceptual question of specificity for lncRNAs. One of the roles of lncRNAs is to be a structural scaffold, and in that regard, the exact nucleotide sequence arguably plays a minor role compared to coding sequences.

Although looking at previously established protein-binding domains in lncRNAs and treating them similarly to functional domains in proteins seems an attractive avenue, careful consideration is needed when interpreting this type of data.

4.3 Is an interaction between *HOTAIR* and PRC2 relevant in a physiological context?

The interaction of *HOTAIR* with the PRC2 and LSD1/CoREST complexes and its function as an epigenetic scaffold is the most widely accepted *HOTAIR* function (Rinn et al., 2007; Tsai et al., 2010). This prompted us to to relate our findings to this scaffolding function in **Paper I** and **Paper II**.

In Paper I we did not detect a regulation of PRC2 or LSD1/CoREST

binding domains-containing isoforms during adipogenic differentiation, at least at the transcriptional level. Interestingly, only half of the expressed *HOTAIR* transcipts harbor the LSD1/CoREST binding domain; these are not regulated during adipogenesis, suggesting a constitutive function or a presumed functional irrelevance of these *HOTAIR* domains in adipogenesis. In **Paper II**, we do not see enrichment in PRC2 target genes in our transcriptomic data after *HOTAIR* knockdown. This contrasts with several functional studies (Gupta et al., 2010; K. Kim et al., 2013; Kogo et al., 2011), but agrees with studies in primary ASCs (Erdos et al., 2022; Kalwa et al., 2016).

These and other findings led us to critically discuss the concept of the PRC2-*HOTAIR* interaction, especially in primary cells.

1. PRC2 has been shown to bind hundreds of lncRNAs as identified by RNA immunoprecipitation sequencing (Khalil et al., 2009; Zhao et al., 2010), confirming the low specificity of PRC2 to RNA (Davidovich and Cech, 2015).

2. Polycomb recognition sequences identified in Drosophila (Ringrose and Paro, 2007) are apparently lacking in vertebrates where PRC2 targets represent a large and poorly defined group of genes (Margueron and Reinberg, 2011). The commonly accepted PRC2 target genes are characterized by H3K27me3 marking and comprise at least 10% of all genes, as identified in human embryonic stem cells (Margueron and Reinberg, 2011).

3. Recent proteomic studies fail to find PRC2 components in the protein interactome of *HOTAIR* (Delhaye et al., 2022; S. Li et al., 2021). Chromatin isolation by RNA purification coupled with mass spectrometry (ChIRP-ms) (Chu and Chang, 2018) does not detect these proteins associated with endogenous *HOTAIR* (Delhaye et al., 2022). Notably, BioID, a biotynilation-based tool for protein interactions, performed with an overexpression system returns components of the CoREST complex, but not of PRC2 (Delhaye et al., 2022).

An explanation that partly addresses these points is that additional cofactors define the specificity of the *HOTAIR* interaction with PRC2. This concept is widely assumed for epigenetic complexes such as PRC2 (van Mierlo et al., 2019). However, little is known so far about which cofactors would provide such specificity. *HOTAIR* is shown to bind to the heterogeneous nuclear ribonucleoprotein (hnRNP) A2/B1, an RNA

processing and matchmaking protein, which would provide specificity to PRC2-*HOTAIR* complex in some contexts (Balas et al., 2021; Meredith et al., 2016). Although the role of *HOTAIR* in ASCs was not extensively studied previously, recent publications report changes in gene expression either completely non-overlapping with PRC2 (**Paper II**) (Erdos et al., 2022; Kuo, Huang, et al., 2022) or with a slight enrichment in PRC2 target genes (Kuo, Neville, et al., 2022). Many assumed connections between *HOTAIR* and PRC2 in the literature, particularly cancer-related, stem from an indirect evaluation of gene expression upon removal of the RNA (Hajjari and Salavaty, 2015). Gene expression measures alone are not sufficient to distinguish genes directly regulated by the lncRNA binding or through various downstream effects. In **Paper II** we identify the genes affected by *HOTAIR* knockdown, however, we cannot argue whether *HOTAIR* directly regulates the expression of these genes or not. Methodologically, ChIRP coupled with sequencing can identify genes directly bound by RNA, allowing evaluation of direct gene expression regulation by lncRNAs (Chu et al., 2012). Using ChIRP-Seq, Erdos et al. find that *HOTAIR* is bound to highly expressed gene bodies in gluteofemoral ASCs (Erdos et al., 2022). The authors define two gene sets, directly and indirectly regulated by *HOTAIR*, where the directly regulated genes are found both in ChIRP-Seq and transcriptionally affected by the knockdown and overexpression of *HOTAIR* (Erdos et al., 2022). The affected genes are related to EMT and the cell cycle, with EMT-related genes mainly involved in the organization of the cytoskeleton (Erdos et al., 2022), supporting our findings of **Paper II**.

Overall, while highly cited literature established a role for *HOTAIR* as an epigenetic regulator acting via PRC2 or independently (Portoso et al., 2017; Rinn et al., 2007; Tsai et al., 2010), multiple other studies do not find a significant deregulation of PRC2-target genes when manipulating *HOTAIR* RNA levels (Ishibashi et al., 2013; Kalwa et al., 2016; Yoon et al., 2013; Zheng et al., 2015) (**Paper II**). Instead, these studies suggest other roles for *HOTAIR* (**Paper II**) (Yoon et al., 2013; Zheng et al., 2015). Although the concept of *HOTAIR* and the PRC2 duet should not be ignored, it is certainly not the only and likely not the central role of *HOTAIR* in the primary cell context. In ASCs, *HOTAIR* is both nuclear and cytoplasmic, and as such, is likely to act on gene expression both directly and indirectly (Tsai et al., 2010; Xu and Zhang, 2017; Yoon et al., 2013). Thus, gene deregulation upon *HOTAIR* KD in ASCs likely occurs downstream of multiple affected pathways.

4.4 Actin cytoskeleton remodeling is involved in adipogenesis

Remodeling of the cytoskeleton and the ECM is critical for commitment of ASCs to the adipocyte lineage (Mor-Yossef Moldovan et al., 2019; Rosen et al., 2000; W. Yang et al., 2014). In **Paper II**, cells depleted of *HOTAIR* which fail to dissasemble an actin cytoskeleton display decreased lipid storage and smaller lipid droplets. Accordingly, stabilizing the actin cytoskeleton has been suggested to be detrimental to adipogenesis (Chen et al., 2018; McColloch et al., 2019).

How is actin cytoskeleton disassembly favorable for adipogenesis? First, the negative impact of the cytoskeleton could be physical. In a cytoplasm with a rigid and well-defined F-actin cytoskeleton, accumulation and fusion of lipid droplets could be difficult due to spatial constraints. Second, it is logical to assume that lipid accumulation could generate a positive feedback to the nucleus via biomechanical cues (McColloch et al., 2019; Tharp et al., 2018; Torrino and Bertero, 2022). Indeed, adipocytes have a small, condensed nucleus, while lipid droplets occupy most of the cytoplasm (**Paper III**). Lipid droplets can not only press on the nucleus, but also enter the nucleus and regulate gene expression by recruiting transcriptional regulators to their surface (Barbosa and Siniossoglou, 2020; Sołtysik et al., 2019). Positive regulation of adipogenesis via growing lipid droplets also appears plausible in light of mechanosensitive transcription factors. For example, one of the key transcription factors for lipid accumulation, SREBP1c, is downregulated in differentiated *HOTAIR* KD cells (**Paper II**) and was shown to be mechanosensitive (Bertolio et al., 2019).

A recent study identified a transcription factor, Zc3h10, that regulates cytoskeleton organization in murine preadipocytes (MSCs of which ASCs are a subtype) (Audano et al., 2021). Interestingly, Zc3h10 KD in these cells mirrors the phenotype we demonstrate in **Paper II** after *HOTAIR* KD. Transcriptomic analysis of undifferentiated mouse MSCs reveals an increase in translation-related genes and a decrease in cytoskeletal genes (Audano et al., 2021). Furthermore, the studies describe opposite effects on LD size (Audano et al., 2021) (**Paper II**). Interestingly, in both **Paper II** and (Audano et al., 2021) differentiation efficiency is decreased, suggesting the importance of the temporal dynamics of the cytoskeleton for adipogenesis. Together, the two studies point to the co-regulation of lipid accumulation, cytoskeleton, and translation.

4.5 Relationship between protein synthesis and the cytoskeleton

In **Paper II** we find that genes co-expressed with *HOTAIR* during adipogenesis are related to the ECM and the cytoskeleton. The involvement of *HOTAIR* in the interplay between translation and the ECM or cytoskeleton can also be confirmed in multiple public datasets. Using the SEEK database (Zhu et al., 2015), we confirm that expression of *HOTAIR* is positively correlated with that of genes with GO terms related to ECM and development, while negatively correlated genes include some related to translation, ribosome biogenesis and respiration (Figure 4.3). These GO terms strikingly resemble those enriched in our RNA-seq data for *HOTAIR* KD cells.

Correlated genes

Term	p-value	q-value
extracellular matrix organization	1.1E-12	8.93E-12
skeletal system development	1.1E-12	1.7E-11
collagen fibril organization	7.9E-11	1.56E-8
collagen catabolic process	1.53E-9	7.79E-8
extracellular matrix disassembly	7.39E-9	2.85E-7

Anticorrelated genes

Term	p-value	q-value
mRNA metabolic process	2.19E-29	1.81E-28
cellular respiration	1.58E-24	5.21E-23
translation	1.18E-23	1.24E-22
ribonucleoprotein complex biogenesis	4.7E-22	9.39E-21
RNA processing	1.42E-20	1.08E-19
respiratory electron transport chain	2.1E-20	1.03E-18

Figure 4.3: GO terms for top 500 genes correlated and anticorrelated with HOTAIR expression patterns; SEEK database (Zhu et al., 2015) querying non-cancerous entries.

The relationship between the cytoskeleton and the translation machinery is intriguing. A physical connection was initially established when polysomes were discovered to be bound to the cytoskeleton (Hesketh and Pryme, 1991; Wolosewick and Porter, 1976). Later, multiple components of the translation machinery were found at migrating tips of cells and at focal adhesion points (Chicurel et al., 1998; Dermit et al., 2020; Hafner et al., 2019; Willett et al., 2011). However, it is unclear how and

why translation and cytoskeleton are co-regulated at the transcriptional level, as we note in **Paper II** (see also (Audano et al., 2021).

Interestingly, a recent report demonstrates a link between translation and the cytoskeleton outside a differentiation context, by describing a new role for the eukaryotic initiation factor eIF6 in endothelial cells, where it regulates mechanical responses (Keen et al., 2022). Keen et al. find no differences in *de novo* protein synthesis, rRNA expression levels, and polysome profiles after eIF6 KD. However, the ability to increase *de novo* protein synthesis upon insulin stimulation is impaired in eIF6 KD cells (Keen et al., 2022). Similarly, in **Paper II**, we report a lack of translation activation upon stimulation, as *HOTAIR* KD cell lines fail to respond to the fasting/refeeding challenge. In addition, eIF6 KD leads to a small decrease in the number of nucleoli per cell (Keen et al., 2022), a trend we also observe after both transient and stable KD of *HOTAIR* (**Paper II**). Notably, deletion of another eukaryotic initiation factor, eIF4E, in mice does not result in a phenotype under basal conditions, but in striking resistance to high-fat diet-induced obesity (Conn et al., 2021). This could be a common feature of translation regulators, as *de novo* protein synthesis is a crucial process for cell survival, and its regulation is likely redundant under basal conditions.

Importantly, cells lacking eIF6 display a disorganized cytoskeleton with fewer focal adhesions, lower coherence of actin fibers, and an inability to remodel their cytoskeleton under mechanical stress (Keen et al., 2022). In **Paper II**, *HOTAIR* KD cells also fail to remodel the cytoskeleton upon reaching confluence, when a change in the surrounding mechanical environment occurs, as the density and frequency of cell contacts increase (see Chapter 1, Figure 1.2). Hence, cells lacking eIF6 or *HOTAIR* display impaired responses to both translation-related and cytoskeleton-related challenges.

The consequence of a disorganized cytoskeleton in eIF6 depleted cells is decreased cell tension (Keen et al., 2022), which was not measured in our system, but likely plays a role in the phenotype we observe after *HOTAIR* KD. Decreased cell tension is characterized by a larger cell area and a lower coherence of actin fibers (Keen et al., 2022). In *HOTAIR* KD at D0, actin fibers are also characterized by lower coherence (**Paper II**). Cell tension is primarily defined by the cytoskeleton, and therefore failure to remodel the cytoskeleton probably affects cell tension. Interestingly, indirectly affecting cell stiffness upstream of the cytoskeleton through a lower matrix stiffness leads to a decrease in the number of nucleoli per cell and a decrease in *de novo* protein synthesis due to lower rRNA expression

(Pundel et al., 2022).

The biomechanical aspect of the relationship between cytoskeleton and translation in ASCs led us to examine, in **Paper III**, changes in nucleolar phenotypes during adipogenesis, a system where cytoskeleton remodeling is crucial (Mor-Yossef Moldovan et al., 2019; Rosen et al., 2000; W. Yang et al., 2014).

4.6 The nucleolus is a dynamic organelle during adipogenesis

The actin cytoskeleton is reorganized during adipogenic differentiation (Kanzaki and Pessin, 2001; Nobusue et al., 2014; W. Yang et al., 2014). However, whether this reorganization affects nucleoli during adipogenesis is unknown. In general, little is known about the role and dynamics of nucleoli in differentiation. Adipogenesis presents a relevant model to explore nucleolar remodeling from the biomechanical angle, as cells change shape, disassemble the actin cytoskeleton, and synthesize a layer of ECM during differentiation (see Chapter 1.2). **Paper III** focuses on how adipose differentiation affects nucleolar morphology and function.

Nucleolar structure is altered upon cell cycle arrest

Paper III describes changes in nucleolar structure occuring upon growth arrest. One may argue that differences between GC compartment staining patterns in different cellular models (He et al., 2018; Sen Gupta et al., 2018; K. Yang et al., 2016) might be explained by variations in immuno-detection protocols, such as permeabilization or antibodies used. In our case, all samples are permeabilized identically, yet the change in the Nucleolin staining pattern between Pro and D0 is striking. We further confirmed our findings by staining with an antibody against Nucleophosmin, another major GC components which differ from Nucleolin by its size and interaction properties (Scott and Oeffinger, 2016). Both Nucleolin and Nucleophosmin display similar immunostaining profiles, confirming a change in nucleolar structure. A recent proteomic study suggests the existence of a novel nucleolar subcompartment, the nucleolar rim (Stenström et al., 2020), supporting our findings of GC proteins relocalization (**Paper III**). The authors spatially dissect the nucleolar proteome and identify 157 proteins localized to the nucleolar periphery. Although the nucleolar rim is more pronounced in the fixed conditions, it is also detectable in living cells (Stenström et al., 2020).

The remodeling of the nucleolus we observe upon cell cycle arrest of ASCs and during differentiation suggests a high degree of variation in nucleolar structure can exist under non-pathological conditions.

Why does nucleolar volume increase in adipocytes?

We find that between D0 and D15 of adipogenesis, total nucleolar volume per cell increases; however, this does not correlate with a change in translation rates. Our transcriptomic analysis reveals a marked increase in the expression of ribosomal protein genes by D15, suggesting higher nucleolar activity. An increase in ribosomal protein gene expression levels does not directly imply a higher number of ribosomes. However, if the expressed RNA is translated, ribosome assembly will take place and might require a larger nucleolus to accommodate all maturing ribosomes. Potentially, adipocytes as terminally differentiated cells possess a lineage-specific translation machinery which can be tuned to express a narrower set of relevant proteins (Genuth and Barna, 2018).

Another possibility is that the increase in nucleolus size in adipocytes is related to the unfolded protein response (UPR) pathway. The UPR occurs in both the nucleus and the cytoplasm. The cytosolic unfolded protein response is activated upon endoplasmic reticulum stress (C. Y. Liu and Kaufman, 2003) and plays a role in adipogenesis (J.-M. Lee et al., 2021; Zha and Zhou, 2012). In the nucleus, the nucleolus sequesters misfolded proteins from the nucleoplasm, acting as a protein quality control compartment (Alberti and Carra, 2019; Frottin et al., 2019). Sequestration in the nucleolus prevents misfolded proteins from forming toxic aggregates in the nucleus (Frottin et al., 2019). It is not known whether nuclear UPR is induced during adipogenesis, but storage of unfolded proteins could be one of the reasons nucleoli grow larger in late differentiation.

Finally, nucleoli are a platform for nucleolus-associated heterochromatin domains (NADs), which largely overlap with LADs, suggesting that heterochromatin can be anchored both at the nuclear lamina and in the vicinity of the nucleolus (Bersaglieri and Santoro, 2019; Németh et al., 2010; Vertii et al., 2019). From the point of spatial organization of the nucleus, the formation of a single large nucleolus could reflect the need for a larger nucleolar surface area to anchor heterochromatin, when the nuclear volume, and thus the surface of the nuclear lamina, decreases.

Is the nucleolus mechanosensitive?

Our findings in **Paper III** suggest that changes in nucleolar morphology are mainly driven by cytoskeletal dissassembly during differentiation. Although the cytoskeleton regulates the shape of the nucleus, the potential relationship between the cytoskeleton and nucleoli is not well established.

In HeLa cells, inhibition of actin polymerization does not lead to nucleolar fusion (Caragine et al., 2019). In our experiments, treatment with cytochalasin D leads to a sharp decrease in the number of nucleoli per cell. Similarly, lower cell or matrix stiffness leads to nucleolar fusion(Keen et al., 2022; Pundel et al., 2022). The discrepancy between our results and those of (Caragine et al., 2019) probably stems from the difference in cytoskeletal organization between ASCs and HeLa cells. HeLa cells do not have a strongly defined actin cytoskeleton with stress fibers, unlike elongated ASCs, and their shape is relatively round (Figure 4.4). We propose that as the stretch force created by the cytoskeleton is released and cellular tension decreases, allowing the nucleus to shrink. The contact frequency of individual nucleoli should therefore increase as the nuclear volume decreases, likely leading to nucleolar fusion.

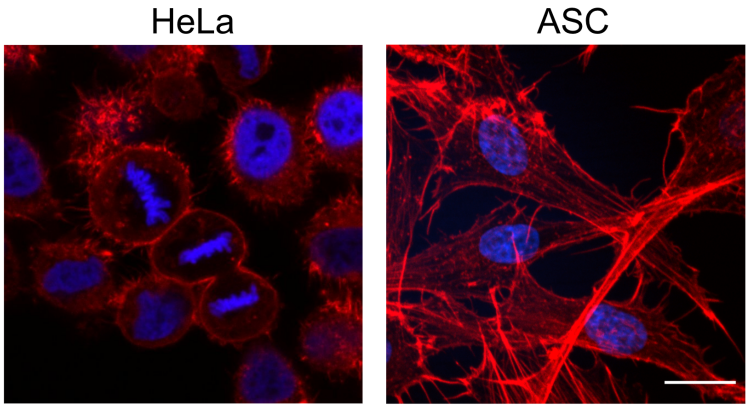

Figure 4.4: Phalloidin staining of the actin cytoskeleton in HeLa (left) and ASCs (right). HeLa - spirochrome gallery (https://spirochrome.com/gallery/), ASCs - own data. Scale bar - 20 µm.

The nucleolus is a drop-like condensate that is not physically connected to the cytoskeleton (Lafontaine et al., 2021). Therefore, the medium that exerts physical cues on the nucleolus is chromatin. In phase

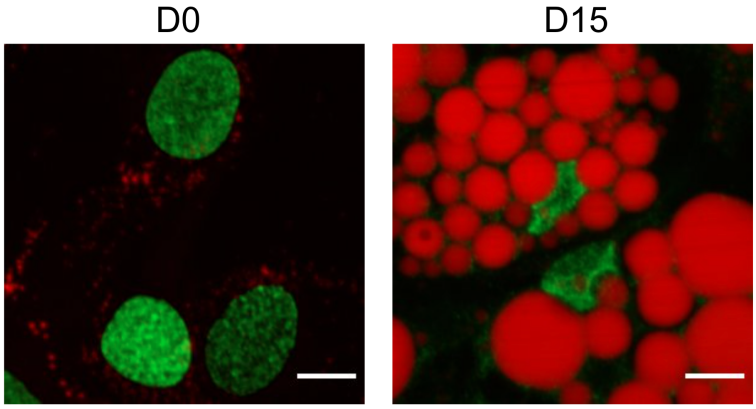

Figure 4.5: Immunofluorescence imaging of H3K9me3 (green), and bodipy staining of intracellular lipids (red), in D0 and D15 *in vitro* differentiated adipocytes; scale bar, 10 µm. Unpublished data.

separation processes within the nucleus, heterochromatin condensation supports the growth and fusion of droplets within softer regions of less dense chromatin (Shin et al., 2019). In agreement, cells with smaller nuclei and fewer nucleoli per nucleus have more H3K9me3-marked heterochromatin foci and overall lower chromatin mobility (Pundel et al., 2022). However, unpublished ChIP-seq data from our laboratory suggest that there is no increase in H3K9me3 levels in D15 adipocytes, and our immunofluorescence data does not show an apparent increase in H3K9me3 levels (Figure 4.5). Moreover, inducing H3K9me3 deposition in ASCs leads to a reduced nuclear volume, however, the number of nucleoli remains unchanged (**Paper III**), suggesting heterochromatin accumulation by itself does not induce nucleolar fusion. It remains unclear whether the nucleolus actively senses mechanical forces or is passively remodeled under the influence of the surrounding chromatin. The exact mechanism leading to nucleolar fusion and its functional role is yet to be determined.

Cell stiffness and heterochromatin in adipogenesis

In **Paper III**, we show a decrease in the ratio of lamin A/C to lamin B1 during differentiation, and an overall decrease in lamin protein levels. Although we do not have direct measures of nuclear lamina or cell stiffness, both actin cytoskeleton dissassembly and downregulation of lamins at the protein level suggest lower nuclear and cell stiffness (Swift et al., 2013).

Immunofluorescence and ChIP-ceq data (Figure 4.5, and unpublished data from the lab [not shown]) suggest preserved or lower levels of H3K9me3, a key heterochromatin histone modification. The finding seems contraintuitive, as one might expect a terminally differentiated cell to have a less permissive chromatin environment (Bártová, Krejcıé, Harnicarová, and Kozubek, 2008; Ugarte et al., 2015) . However, softening of the nucleus through loss of H3K9me3 heterochromatin could be a protective mechanism for the genome against mechanical stress (Nava et al., 2020), such as stress imposed by lipid droplets in our system. Additional studies on the mechanisms of chromatin homeostasis under mechanical stress would be informative to better appreciate structural and conformational chromatin changes taking place during adipogenesis (Paulsen et al., 2019; Siersbæk et al., 2017).

4.7 Perspectives

The work presented in this thesis provides new insights on the regulation of protein synthesis in various contexts: through the lncRNA *HOTAIR*, during adipogenesis, and at the physical level through the interdependence between the cytoskeleton, the nucleus and the nucleolus. Although primarily relevant in an adipose tissue context, the results presented in this thesis will be of interest to researchers working with other cellular models where cells transit from state to state and where the transition is accompanied by a change in the external or internal mechanical environment. For instance, cytoskeletal reorganization, extracellular matrix remodeling and stiffness changes occur in other differentiation lineages and in cancer progression, such as the epithelial-to-mesenchymal transition. Furthermore, a deeper understanding of translation regulation by various stimuli will be relevant in pathological contexts where the nucleolus plays a role, such as progeria, ribosomopathies, and aging.

Bibliography

Ackema, K. B., & Charité, J. (2008). Mesenchymal stem cells from different organs are characterized by distinct topographic Hox codes. *Stem Cells Dev.*, *17*(5), 979–991. https://doi.org/10.1089/scd.2007.0220

Ackerman, G. E., Smith, M. E., Mendelson, C. R., MacDonald, P. C., & Simpson, E. R. (1981). Aromatization of androstenedione by human adipose tissue stromal cells in monolayer culture. *J. Clin. Endocrinol. Metab.*, *53*(2), 412–417. https://doi.org/10.1210/jcem-53-2-412

Alberti, S., & Carra, S. (2019). Nucleolus: A Liquid Droplet Compartment for Misbehaving Proteins. *Curr. Biol.*, *29*(19), R930–R932. https://doi.org/10.1016/j.cub.2019.08.013

Amândio, A. R., Necsulea, A., Joye, E., Mascrez, B., & Duboule, D. (2016). Hotair Is Dispensible for Mouse Development. *PLoS Genet.*, *12*(12), e1006232. https://doi.org/10.1371/journal.pgen.1006232

Ambardar, S., Gupta, R., Trakroo, D., Lal, R., & Vakhlu, J. (2016). High Throughput Sequencing: An Overview of Sequencing Chemistry. *Indian J. Microbiol.*, *56*(4), 394–404. https://doi.org/10.1007/s12088-016-0606-4

Ameer, F., Scandiuzzi, L., Hasnain, S., Kalbacher, H., & Zaidi, N. (2014). De novo lipogenesis in health and disease. *Metabolism*, *63*(7), 895–902. https://doi.org/10.1016/j.metabol.2014.04.003

Anderson, R., Agarwal, A., Ghosh, A., Guan, B.-J., Casteel, J., Dvorina, N., Baldwin, W. M., 3rd, Mazumder, B., Nazarko, T. Y., Merrick, W. C., Buchner, D. A., Hatzoglou, M., Kondratov, R. V., & Komar, A. A. (2021). eIF2A-knockout mice reveal decreased life span and metabolic syndrome. *FASEB J.*, *35*(11), e21990. https://doi.org/10.1096/fj.202101105R

Audano, M., Pedretti, S., Ligorio, S., Gualdrini, F., Polletti, S., Russo, M., Ghisletti, S., Bean, C., Crestani, M., Caruso, D., De Fabiani, E., & Mitro, N. (2021). Zc3h10 regulates adipogenesis by controlling translation and F-actin/mitochondria interaction. *J. Cell Biol.*, *220*(3). https://doi.org/10.1083/jcb.202003173

Baker, N. E. (2013). Developmental regulation of nucleolus size during Drosophila eye differentiation. *PLoS One*, *8*(3), e58266. https://doi.org/10.1371/journal.pone.0058266

Balas, M. M., Hartwick, E. W., Barrington, C., Roberts, J. T., Wu, S. K., Bettcher, R., Griffin, A. M., Kieft, J. S., & Johnson, A. M. (2021). Establishing RNA-RNA interactions remodels lncRNA structure and promotes PRC2 activity. *Sci. Adv.*, *7*(16). https://doi.org/10.1126/sciadv.abc9191

Barak, Y., Nelson, M. C., Ong, E. S., Jones, Y. Z., Ruiz-Lozano, P., Chien, K. R., Koder, A., & Evans, R. M. (1999). PPARγ Is Required for Placental, Cardiac, and Adipose Tissue Development. *Mol. Cell*, *4*(4), 585–595. https://doi.org/10.1016/S1097-2765(00)80209-9

Barbosa, A. D., & Siniossoglou, S. (2020). New kid on the block: lipid droplets in the nucleus. *FEBS J.*, *287*(22), 4838–4843. https://doi.org/10.1111/febs.15307

Bártová, E., Krejcıé, J., Harnicarová, A., Galiová, G., & Kozubek, S. (2008). Histone modifications and nuclear architecture: a review. *J. Histochem. Cytochem.*, *56*(8), 711–721. https://doi.org/10.1369/jhc.2008.951251

Bártová, E., Krejcıé, J., Harnicarová, A., & Kozubek, S. (2008). Differentiation of human embryonic stem cells induces condensation of chromosome territories and formation of heterochromatin protein 1 foci. *Differentiation*, *76*(1), 24–32. https://doi.org/10.1111/j.1432-0436.2007.00192.x

Bersaglieri, C., Kresoja-Rakic, J., Gupta, S., Bär, D., Kuzyakiv, R., Panatta, M., & Santoro, R. (2022). Genome-wide maps of nucleolus interactions reveal distinct layers of repressive

chromatin domains. *Nat. Commun.*, *13*(1), 1–18. https://doi.org/10.1038/s41467-022-29146-2

Bersaglieri, C., & Santoro, R. (2019). Genome Organization in and around the Nucleolus. *Cells*, *8*(6). https://doi.org/10.3390/cells8060579

Bertolio, R., Napoletano, F., Mano, M., Maurer-Stroh, S., Fantuz, M., Zannini, A., Bicciato, S., Sorrentino, G., & Del Sal, G. (2019). Sterol regulatory element binding protein 1 couples mechanical cues and lipid metabolism. *Nat. Commun.*, *10*(1), 1–11. https://doi.org/10.1038/s41467-019-09152-7

Bhan, A., Hussain, I., Ansari, K. I., Kasiri, S., Bashyal, A., & Mandal, S. S. (2013). Antisense transcript long noncoding RNA (lncRNA) HOTAIR is transcriptionally induced by estradiol. *J. Mol. Biol.*, *425*(19), 3707–3722. https://doi.org/10.1016/j.jmb.2013.01.022

Bhan, A., & Mandal, S. S. (2015). LncRNA HOTAIR: A master regulator of chromatin dynamics and cancer. *Biochim. Biophys. Acta*, *1856*(1), 151–164. https://doi.org/10.1016/j.bbcan.2015.07.001

Birman, S., Morgan, B., Anzivino, M., & Hirsh, J. (1994). A novel and major isoform of tyrosine hydroxylase in Drosophila is generated by alternative RNA processing. *J. Biol. Chem.*, *269*(42), 26559–26567. https://doi.org/10.1016/S0021-9258(18)47231-6

Birsoy, K., Chen, Z., & Friedman, J. (2008). Transcriptional regulation of adipogenesis by KLF4. *Cell Metab.*, *7*(4), 339–347. https://doi.org/10.1016/j.cmet.2008.02.001

Björntorp, P., & Sjöström, L. (1978). Carbohydrate storage in man: speculations and some quantitative considerations. *Metabolism*, *27*(12 Suppl 2), 1853–1865. https://doi.org/10.1016/s0026-0495(78)80004-3

Boisvert, F.-M., van Koningsbruggen, S., Navascués, J., & Lamond, A. I. (2007). The multifunctional nucleolus. *Nat. Rev. Mol. Cell Biol.*, *8*(7), 574–585. https://doi.org/10.1038/nrm2184

Bonasio, R., & Shiekhattar, R. (2014). Regulation of transcription by long noncoding RNAs. *Annu. Rev. Genet.*, *48*, 433–455. https://doi.org/10.1146/annurev-genet-120213-092323

Boquest, A. C., Shahdadfar, A., Frønsdal, K., Sigurjonsson, O., Tunheim, S. H., Collas, P., & Brinchmann, J. E. (2005). Isolation and transcription profiling of purified uncultured human stromal stem cells: alteration of gene expression after in vitro cell culture. *Mol. Biol. Cell*, *16*(3), 1131–1141. https://doi.org/10.1091/mbc.e04-10-0949

Bouzid, T., Kim, E., Riehl, B. D., Esfahani, A. M., Rosenbohm, J., Yang, R., Duan, B., & Lim, J. Y. (2019). The LINC complex, mechanotransduction, and mesenchymal stem cell function and fate. *J. Biol. Eng.*, *13*, 68. https://doi.org/10.1186/s13036-019-0197-9

Branco, M. R., & Pombo, A. (2006). Intermingling of chromosome territories in interphase suggests role in translocations and transcription-dependent associations. *PLoS Biol.*, *4*(5), e138. https://doi.org/10.1371/journal.pbio.0040138

Brannan, C. I., Dees, E. C., Ingram, R. S., & Tilghman, S. M. (1990). The product of the H19 gene may function as an RNA. *Mol. Cell. Biol.*, *10*(1), 28–36. https://doi.org/10.1128/mcb.10.1.28-36.1990

Briand, N., & Collas, P. (2020). Lamina-associated domains: peripheral matters and internal affairs. *Genome Biol.*, *21*(1), 85. https://doi.org/10.1186/s13059-020-02003-5

Brockdorff, N., Ashworth, A., Kay, G. F., McCabe, V. M., Norris, D. P., Cooper, P. J., Swift, S., & Rastan, S. (1992). The product of the mouse Xist gene is a 15 kb inactive X-specific transcript containing no conserved ORF and located in the nucleus. *Cell*, *71*(3), 515–526. https://doi.org/10.1016/0092-8674(92)90519-i

Broers, J. L. V., Peeters, E. A. G., Kuijpers, H. J. H., Endert, J., Bouten, C. V. C., Oomens, C. W. J., Baaijens, F. P. T., & Ramaekers, F. C. S. (2004). Decreased mechanical stiffness in LMNA-/- cells is caused by defective nucleo-cytoskeletal integrity: implications for the development of laminopathies. *Hum. Mol. Genet.*, *13*(21), 2567–2580. https://doi.org/10.1093/hmg/ddh295

Brown, C. J., Hendrich, B. D., Rupert, J. L., Lafrenière, R. G., Xing, Y., Lawrence, J., & Willard, H. F. (1992). The human XIST gene: analysis of a 17 kb inactive X-specific RNA that contains conserved repeats and is highly localized within the nucleus. *Cell*, *71*(3), 527–542. https://doi.org/10.1016/0092-8674(92)90520-m

Brunmeir, R., Wu, J., Peng, X., Kim, S.-Y., Julien, S. G., Zhang, Q., Xie, W., & Xu, F. (2016). Comparative Transcriptomic and Epigenomic Analyses Reveal New Regulators of Murine Brown Adipogenesis. *PLoS Genet.*, *12*(12), e1006474. https://doi.org/10.1371/journal.pgen.1006474

Buchwalter, A., & Hetzer, M. W. (2017). Nucleolar expansion and elevated protein translation in premature aging. *Nat. Commun.*, *8*(1), 328. https://doi.org/10.1038/s41467-017-00322-z

Bunnell, B. A., Flaat, M., Gagliardi, C., Patel, B., & Ripoll, C. (2008). Adipose-derived stem cells: isolation, expansion and differentiation. *Methods*, *45*(2), 115–120. https://doi.org/10.1016/j.ymeth.2008.03.006

Burke, B., & Stewart, C. L. (2013). The nuclear lamins: flexibility in function. *Nat. Rev. Mol. Cell Biol.*, *14*(1), 13–24. https://doi.org/10.1038/nrm3488

Busby, K. N., Fulzele, A., Zhang, D., Bennett, E. J., & Devaraj, N. K. (2020). Enzymatic RNA Biotinylation for Affinity Purification and Identification of RNA-Protein Interactions. *ACS Chem. Biol.*, *15*(8), 2247–2258. https://doi.org/10.1021/acschembio.0c00445

Cabili, M. N., Trapnell, C., Goff, L., Koziol, M., Tazon-Vega, B., Regev, A., & Rinn, J. L. (2011). Integrative annotation of human large intergenic noncoding RNAs reveals global properties and specific subclasses. *Genes Dev.*, *25*(18), 1915–1927. https://doi.org/10.1101/gad.17446611

Caille, N., Thoumine, O., Tardy, Y., & Meister, J.-J. (2002). Contribution of the nucleus to the mechanical properties of endothelial cells. *J. Biomech.*, *35*(2), 177–187. https://doi.org/10.1016/s0021-9290(01)00201-9

Cantile, M., Di Bonito, M., Tracey De Bellis, M., & Botti, G. (2021). Functional Interaction among lncRNA HOTAIR and MicroRNAs in Cancer and Other Human Diseases. *Cancers*, *13*(3). https://doi.org/10.3390/cancers13030570

Cao, R., Wang, L., Wang, H., Xia, L., Erdjument-Bromage, H., Tempst, P., Jones, R. S., & Zhang, Y. (2002). Role of histone H3 lysine 27 methylation in Polycomb-group silencing. *Science*, *298*(5595), 1039–1043. https://doi.org/10.1126/science.1076997

Cao, Z., Umek, R. M., & McKnight, S. L. (1991). Regulated expression of three C/EBP isoforms during adipose conversion of 3T3-L1 cells. *Genes Dev.*, *5*(9), 1538–1552. https://doi.org/10.1101/gad.5.9.1538

Caragine, C. M., Haley, S. C., & Zidovska, A. (2019). Nucleolar dynamics and interactions with nucleoplasm in living cells. *Elife*, *8*. https://doi.org/10.7554/eLife.47533

Carnevalli, L. S., Masuda, K., Frigerio, F., Le Bacquer, O., Um, S. H., Gandin, V., Topisirovic, I., Sonenberg, N., Thomas, G., & Kozma, S. C. (2010). S6K1 plays a critical role in early adipocyte differentiation. *Dev. Cell*, *18*(5), 763–774. https://doi.org/10.1016/j.devcel.2010.02.018

Carninci, P., Kasukawa, T., Katayama, S., Gough, J., Frith, M. C., Maeda, N., Oyama, R., Ravasi, T., Lenhard, B., Wells, C., Kodzius, R., Shimokawa, K., Bajic, V. B., Brenner, S. E., Batalov, S., Forrest, A. R. R., Zavolan, M., Davis, M. J., Wilming, L. G., ... RIKEN Genome Exploration Research Group and Genome Science Group (Genome Network Project Core Group). (2005). The transcriptional landscape of the mammalian genome. *Science*, *309*(5740), 1559–1563. https://doi.org/10.1126/science.1112014

Carroll, S. B. (1995). Homeotic genes and the evolution of arthropods and chordates. *Nature*, *376*(6540), 479–485. https://doi.org/10.1038/376479a0

Carver, W., & Goldsmith, E. C. (2013). Regulation of tissue fibrosis by the biomechanical environment. *Biomed Res. Int.*, *2013*, 101979. https://doi.org/10.1155/2013/101979

Casado-Dıéaz, A., Anter, J., Müller, S., Winter, P., Quesada-Gómez, J. M., & Dorado, G. (2017). Transcriptomic Analyses of Adipocyte Differentiation From Human Mesenchymal Stromal-Cells (MSC). *J. Cell. Physiol.*, *232*(4), 771–784. https://doi.org/10.1002/jcp.25472

Chehab, F. F. (2008). Obesity and lipodystrophy–where do the circles intersect? *Endocrinology*, *149*(3), 925–934. https://doi.org/10.1210/en.2007-1355

Chen, L., Hu, H., Qiu, W., Shi, K., & Kassem, M. (2018). Actin depolymerization enhances adipogenic differentiation in human stromal stem cells. *Stem Cell Res.*, *29*, 76–83. https://doi.org/10.1016/j.scr.2018.03.010

Cheng, D., Deng, J., Zhang, B., He, X., Meng, Z., Li, G., Ye, H., Zheng, S., Wei, L., Deng, X., Chen, R., & Zhou, J. (2018). LncRNA HOTAIR epigenetically suppresses miR-122 expression in hepatocellular carcinoma via DNA methylation. *EBioMedicine*, *36*, 159–170. https://doi.org/10.1016/j.ebiom.2018.08.055

Cheng, K.-H., Kuo, T.-L., Kuo, K.-K., & Hsiao, C.-C. (2011). Human adipose-derived stem cells: Isolation, characterization and current application in regeneration medicine. *Genomic Medicine, Biomarkers, and Health Sciences*, *3*(2), 53–62. https://doi.org/10.1016/j.gmbhs.2011.08.003

Chew, G.-L., Pauli, A., Rinn, J. L., Regev, A., Schier, A. F., & Valen, E. (2013). Ribosome profiling reveals resemblance between long non-coding RNAs and 5' leaders of coding RNAs. *Development*, *140*(13), 2828–2834. https://doi.org/10.1242/dev.098343

Chicurel, M. E., Singer, R. H., Meyer, C. J., & Ingber, D. E. (1998). Integrin binding and mechanical tension induce movement of mRNA and ribosomes to focal adhesions. *Nature*, *392*(6677), 730–733. https://doi.org/10.1038/33719

Chu, C., & Chang, H. Y. (2018). ChIRP-MS: RNA-Directed Proteomic Discovery. *Methods Mol. Biol.*, *1861*, 37–45. https://doi.org/10.1007/978-1-4939-8766-5_3

Chu, C., Quinn, J., & Chang, H. Y. (2012). Chromatin isolation by RNA purification (ChIRP). *J. Vis. Exp.*, (61). https://doi.org/10.3791/3912

Clark, M. B., Mercer, T. R., Bussotti, G., Leonardi, T., Haynes, K. R., Crawford, J., Brunck, M. E., Cao, K.-A. L., Thomas, G. P., Chen, W. Y., Taft, R. J., Nielsen, L. K., Enright, A. J., Mattick, J. S., & Dinger, M. E. (2015). Quantitative gene profiling of long noncoding RNAs with targeted RNA sequencing. *Nat. Methods*, *12*(4), 339–342. https://doi.org/10.1038/nmeth.3321

Clark, M. B., Wrzesinski, T., Garcia, A. B., Hall, N. A. L., Kleinman, J. E., Hyde, T., Weinberger, D. R., Harrison, P. J., Haerty, W., & Tunbridge, E. M. (2019). Long-read sequencing reveals the complex splicing profile of the psychiatric risk gene CACNA1C in human brain. *Mol. Psychiatry*, *25*(1), 37–47. https://doi.org/10.1038/s41380-019-0583-1

Coelho, M., Oliveira, T., & Fernandes, R. (2013). Biochemistry of adipose tissue: an endocrine organ. *Arch. Med. Sci.*, *9*(2), 191–200. https://doi.org/10.5114/aoms.2013.33181

Collins, J. M., Neville, M. J., Pinnick, K. E., Hodson, L., Ruyter, B., van Dijk, T. H., Reijngoud, D.-J., Fielding, M. D., & Frayn, K. N. (2011). De novo lipogenesis in the differentiating human adipocyte can provide all fatty acids necessary for maturation. *J. Lipid Res.*, *52*(9), 1683–1692. https://doi.org/10.1194/jlr.M012195

Conn, C. S., Yang, H., Tom, H. J., Ikeda, K., Oses-Prieto, J. A., Vu, H., Oguri, Y., Nair, S., Gill, R. M., Kajimura, S., DeBerardinis, R. J., Burlingame, A. L., & Ruggero, D. (2021). The major cap-binding protein eIF4E regulates lipid homeostasis and diet-induced obesity. *Nat Metab*, *3*(2), 244–257. https://doi.org/10.1038/s42255-021-00349-z

Cremer, T., & Cremer, M. (2010). Chromosome territories. *Cold Spring Harb. Perspect. Biol.*, *2*(3), a003889. https://doi.org/10.1101/cshperspect.a003889

Crewe, C., Zhu, Y., Paschoal, V. A., Joffin, N., Ghaben, A. L., Gordillo, R., Oh, D. Y., Liang, G., Horton, J. D., & Scherer, P. E. (2019). SREBP-regulated adipocyte lipogenesis is dependent on substrate availability and redox modulation of mTORC1. *JCI Insight*, *5*. https://doi.org/10.1172/jci.insight.129397

Daftary, G. S., & Taylor, H. S. (2006). Endocrine regulation of HOX genes. *Endocr. Rev.*, *27*(4), 331–355. https://doi.org/10.1210/er.2005-0018

Davidovich, C., & Cech, T. R. (2015). The recruitment of chromatin modifiers by long noncoding RNAs: lessons from PRC2. *RNA*, *21*(12), 2007–2022. https://doi.org/10.1261/rna.053918.115

Davidson, N. M., Hawkins, A. D. K., & Oshlack, A. (2017). SuperTranscripts: a data driven reference for analysis and visualisation of transcriptomes. *Genome Biol.*, *18*(1), 148. https://doi.org/10.1186/s13059-017-1284-1

De Francesco, F., Ricci, G., D'Andrea, F., Nicoletti, G. F., & Ferraro, G. A. (2015). Human Adipose Stem Cells: From Bench to Bedside. *Tissue Eng. Part B Rev.*, *21*(6), 572–584. https://doi.org/10.1089/ten.TEB.2014.0608

De Kumar, B., & Krumlauf, R. (2016). *Hox*s and lincrnas: two sides of the same coin. *Sci Adv*, *2*(1), e1501402. https://doi.org/10.1126/sciadv.1501402

De Paoli-Iseppi, R., Gleeson, J., & Clark, M. B. (2021). Isoform Age - Splice Isoform Profiling Using Long-Read Technologies. *Front Mol Biosci*, *8*, 711733. https://doi.org/10.3389/fmolb.2021.711733

Dechat, T., Adam, S. A., Taimen, P., Shimi, T., & Goldman, R. D. (2010). Nuclear lamins. *Cold Spring Harb. Perspect. Biol.*, *2*(11), a000547. https://doi.org/10.1101/cshperspect.a000547

de Klerk, E., Fokkema, I. F. A. C., Thiadens, K. A. M. H., Goeman, J. J., Palmblad, M., den Dunnen, J. T., von Lindern, M., & 't Hoen, P. A. C. (2015). Assessing the translational landscape of myogenic differentiation by ribosome profiling. *Nucleic Acids Res.*, *43*(9), 4408–4428. https://doi.org/10.1093/nar/gkv281

DeLany, J. P., Floyd, Z. E., Zvonic, S., Smith, A., Gravois, A., Reiners, E., Wu, X., Kilroy, G., Lefevre, M., & Gimble, J. M. (2005). Proteomic Analysis of Primary Cultures of Human Adipose-derived Stem Cells: Modulation by Adipogenesis*S. *Mol. Cell. Proteomics*, *4*(6), 731–740. https://doi.org/10.1074/mcp.M400198-MCP200

Delhaye, L., De Bruycker, E., Volders, P.-J., Fijalkowska, D., De Sutter, D., Degroeve, S., Martens, L., Mestdagh, P., & Eyckerman, S. (2022). Orthogonal proteomics methods to unravel the HOTAIR interactome. *Sci. Rep.*, *12*(1), 1513. https://doi.org/10.1038/s41598-022-05405-6

Dermit, M., Dodel, M., Lee, F. C. Y., Azman, M. S., Schwenzer, H., Jones, J. L., Blagden, S. P., Ule, J., & Mardakheh, F. K. (2020). Subcellular mRNA Localization Regulates Ribosome Biogenesis in Migrating Cells. *Dev. Cell*, *55*(3), 298–313.e10. https://doi.org/10.1016/j.devcel.2020.10.006

Derrien, T., Johnson, R., Bussotti, G., Tanzer, A., Djebali, S., Tilgner, H., Guernec, G., Martin, D., Merkel, A., Knowles, D. G., Lagarde, J., Veeravalli, L., Ruan, X., Ruan, Y., Lassmann, T., Carninci, P., Brown, J. B., Lipovich, L., Gonzalez, J. M., ... Guigó, R. (2012). The GENCODE v7 catalog of human long noncoding RNAs: analysis of their gene structure, evolution, and expression. *Genome Res.*, *22*(9), 1775–1789. https://doi.org/10.1101/gr.132159.111

Deveson, I. W., Brunck, M. E., Blackburn, J., Tseng, E., Hon, T., Clark, T. A., Clark, M. B., Crawford, J., Dinger, M. E., Nielsen, L. K., Mattick, J. S., & Mercer, T. R. (2018). Universal Alternative Splicing of Noncoding Exons. *Cell Syst*, *6*(2), 245–255.e5. https://doi.org/10.1016/j.cels.2017.12.005

Di Caprio, N., & Bellas, E. (2020). Collagen Stiffness and Architecture Regulate Fibrotic Gene Expression in Engineered Adipose Tissue. *Adv Biosyst*, *4*(6), e1900286. https://doi.org/10.1002/adbi.201900286

Dillinger, S., Straub, T., & Németh, A. (2017). Nucleolus association of chromosomal domains is largely maintained in cellular senescence despite massive nuclear reorganisation. *PLoS One*, *12*(6), e0178821. https://doi.org/10.1371/journal.pone.0178821

Dittmer, T. A., & Misteli, T. (2011). The lamin protein family. *Genome Biol.*, *12*(5), 1–14. https://doi.org/10.1186/gb-2011-12-5-222

Divoux, A., Karastergiou, K., Xie, H., Guo, W., Perera, R. J., Fried, S. K., & Smith, S. R. (2014). Identification of a novel lncRNA in gluteal adipose tissue and evidence for its positive effect on preadipocyte differentiation. *Obesity*, *22*(8), 1781–1785. https://doi.org/10.1002/oby.20793

Dupont, S., Morsut, L., Aragona, M., Enzo, E., Giulitti, S., Cordenonsi, M., Zanconato, F., Le Digabel, J., Forcato, M., Bicciato, S., Elvassore, N., & Piccolo, S. (2011). Role of YAP/TAZ in mechanotransduction. *Nature*, *474*(7350), 179–183. https://doi.org/10.1038/nature10137

Eberlé, D., Hegarty, B., Bossard, P., Ferré, P., & Foufelle, F. (2004). SREBP transcription factors: master regulators of lipid homeostasis. *Biochimie*, *86*(11), 839–848. https://doi.org/10.1016/j.biochi.2004.09.018

Egecioglu, D., & Brickner, J. H. (2011). Gene positioning and expression. *Curr. Opin. Cell Biol.*, *23*(3), 338–345. https://doi.org/10.1016/j.ceb.2011.01.001

Erdos, E., Divoux, A., Sandor, K., Halasz, L., Smith, S. R., & Osborne, T. F. (2022). Unique role for lncRNA HOTAIR in defining depot-specific gene expression patterns in human adipose-derived stem cells. *Genes Dev.*, *36*(9-10), 566–581. https://doi.org/10.1101/gad.349393.122

Estève, D., Boulet, N., Belles, C., Zakaroff-Girard, A., Decaunes, P., Briot, A., Veeranagouda, Y., Didier, M., Remaury, A., Guillemot, J. C., Ledoux, S., Dani, C., Bouloumié, A., & Galitzky, J. (2019). Lobular architecture of human adipose tissue defines the niche and fate of progenitor cells. *Nat. Commun.*, *10*(1), 2549. https://doi.org/10.1038/s41467-019-09992-3

Feng, T., Szabo, E., Dziak, E., & Opas, M. (2010). Cytoskeletal disassembly and cell rounding promotes adipogenesis from ES cells. *Stem Cell Rev Rep*, *6*(1), 74–85. https://doi.org/10.1007/s12015-010-9115-8

Ferré, P., & Foufelle, F. (2007). SREBP-1c transcription factor and lipid homeostasis: clinical perspective. *Horm. Res.*, *68*(2), 72–82. https://doi.org/10.1159/000100426

Festa, A., D'Agostino, R., Jr, Williams, K., Karter, A. J., Mayer-Davis, E. J., Tracy, R. P., & Haffner, S. M. (2001). The relation of body fat mass and distribution to markers of chronic inflammation. *Int. J. Obes. Relat. Metab. Disord.*, *25*(10), 1407–1415. https://doi.org/10.1038/sj.ijo.0801792

Fletcher, D. A., & Mullins, R. D. (2010). Cell mechanics and the cytoskeleton. *Nature*, *463*(7280), 485–492. https://doi.org/10.1038/nature08908

Frankish, A., Diekhans, M., Ferreira, A.-M., Johnson, R., Jungreis, I., Loveland, J., Mudge, J. M., Sisu, C., Wright, J., Armstrong, J., Barnes, I., Berry, A., Bignell, A., Carbonell Sala, S., Chrast, J., Cunningham, F., Di Domenico, T., Donaldson, S., Fiddes, I. T., … Flicek, P. (2019). GENCODE reference annotation for the human and mouse genomes. *Nucleic Acids Res.*, *47*(D1), D766–D773. https://doi.org/10.1093/nar/gky955

Frottin, F., Schueder, F., Tiwary, S., Gupta, R., Körner, R., Schlichthaerle, T., Cox, J., Jungmann, R., Hartl, F. U., & Hipp, M. S. (2019). The nucleolus functions as a phase-separated protein quality control compartment. *Science*, *365*(6451), 342–347. https://doi.org/10.1126/science.aaw9157

Garg, A. (2006). Adipose tissue dysfunction in obesity and lipodystrophy. *Clin. Cornerstone*, *8 Suppl 4*, S7–S13. https://doi.org/10.1016/s1098-3597(06)80039-6

Gdula, M. R., Poterlowicz, K., Mardaryev, A. N., Sharov, A. A., Peng, Y., Fessing, M. Y., & Botchkarev, V. A. (2013). Remodeling of three-dimensional organization of the nucleus during terminal keratinocyte differentiation in the epidermis. *J. Invest. Dermatol.*, *133*(9), 2191–2201. https://doi.org/10.1038/jid.2013.66

Geiger, B., Spatz, J. P., & Bershadsky, A. D. (2009). Environmental sensing through focal adhesions. *Nat. Rev. Mol. Cell Biol.*, *10*(1), 21–33. https://doi.org/10.1038/nrm2593

Genuth, N. R., & Barna, M. (2018). The Discovery of Ribosome Heterogeneity and Its Implications for Gene Regulation and Organismal Life. *Mol. Cell*, *71*(3), 364–374. https://doi.org/10.1016/j.molcel.2018.07.018

Giralt, M., & Villarroya, F. (2013). White, brown, beige/brite: different adipose cells for different functions? *Endocrinology*, *154*(9), 2992–3000. https://doi.org/10.1210/en.2013-1403

Gomes, C. P. d. C., Ágg, B., Andova, A., Arslan, S., Baker, A., Barteková, M., Beis, D., Betsou, F., Wettinger, S. B., Bugarski, B., Condorelli, G., Silva, G. J. J. d., Danilin, S., de Gonzalo-Calvo, D., Buil, A., Carmo-Fonseca, M., Enguita, F. J., Felekkis, K., Ferdinandy, P., … on behalf of the EU-CardioRNA COST Action (CA17129). (2019). Catalyzing Transcriptomics Research in Cardiovascular Disease: The CardioRNA COST Action CA17129. *Noncoding RNA*, *5*(2). https://doi.org/10.3390/ncrna5020031

Green, H., & Meuth, M. (1974a). An established pre-adipose cell line and its differentiation in culture. *Cell*, *3*(2), 127–133. https://doi.org/10.1016/0092-8674(74)90116-0

Green, H., & Meuth, M. (1974b). An established pre-adipose cell line and its differentiation in culture. *Cell*, *3*(2), 127–133. https://doi.org/10.1016/0092-8674(74)90116-0

Gruber, H. E., Somayaji, S., Riley, F., Hoelscher, G. L., Norton, H. J., Ingram, J., & Hanley, E. N., Jr. (2012). Human adipose-derived mesenchymal stem cells: serial passaging, doubling time and cell senescence. *Biotech. Histochem.*, *87*(4), 303–311. https://doi.org/10.3109/10520295.2011.649785

Gruenbaum, Y., Margalit, A., Goldman, R. D., Shumaker, D. K., & Wilson, K. L. (2005). The nuclear lamina comes of age. *Nat. Rev. Mol. Cell Biol.*, *6*(1), 21–31. https://doi.org/10.1038/nrm1550

Guo, L., Li, X., & Tang, Q.-Q. (2015). Transcriptional regulation of adipocyte differentiation: a central role for CCAAT/enhancer-binding protein (C/EBP) *β*. *J. Biol. Chem.*, *290*(2), 755–761. https://doi.org/10.1074/jbc.R114.619957

Gupta, R. A., Shah, N., Wang, K. C., Kim, J., Horlings, H. M., Wong, D. J., Tsai, M.-C., Hung, T., Argani, P., Rinn, J. L., Wang, Y., Brzoska, P., Kong, B., Li, R., West, R. B., van de Vijver, M. J., Sukumar, S., & Chang, H. Y. (2010). Long non-coding RNA HOTAIR reprograms chromatin state to promote cancer metastasis. *Nature*, *464*(7291), 1071–1076. https://doi.org/10.1038/nature08975

Guttman, M., Amit, I., Garber, M., French, C., Lin, M. F., Feldser, D., Huarte, M., Zuk, O., Carey, B. W., Cassady, J. P., Cabili, M. N., Jaenisch, R., Mikkelsen, T. S., Jacks, T., Hacohen, N., Bernstein, B. E., Kellis, M., Regev, A., Rinn, J. L., & Lander, E. S. (2009). Chromatin signature reveals over a thousand highly conserved large non-coding RNAs in mammals. *Nature*, *458*(7235), 223–227. https://doi.org/10.1038/nature07672

Haerty, W., & Ponting, C. P. (2013). Mutations within lncRNAs are effectively selected against in fruitfly but not in human. *Genome Biol.*, *14*(5), R49. https://doi.org/10.1186/gb-2013-14-5-r49

Haerty, W., & Ponting, C. P. (2015). Unexpected selection to retain high GC content and splicing enhancers within exons of multiexonic lncRNA loci. *RNA*, *21*(3), 333–346. https://doi.org/10.1261/rna.047324.114

Hafner, A.-S., Donlin-Asp, P. G., Leitch, B., Herzog, E., & Schuman, E. M. (2019). Local protein synthesis is a ubiquitous feature of neuronal pre- and postsynaptic compartments. *Science*, *364*(6441). https://doi.org/10.1126/science.aau3644

Hajjari, M., & Rahnama, S. (2017). HOTAIR Long Non-coding RNA: Characterizing the Locus Features by the In Silico Approaches. *Genomics Inform.*, *15*(4), 170–177. https://doi.org/10.5808/GI.2017.15.4.170

Hajjari, M., & Salavaty, A. (2015). HOTAIR: an oncogenic long non-coding RNA in different cancers. *Cancer Biol Med*, *12*(1), 1–9. https://doi.org/10.7497/j.issn.2095-3941.2015.0006

Hangauer, M. J., Vaughn, I. W., & McManus, M. T. (2013). Pervasive transcription of the human genome produces thousands of previously unidentified long intergenic noncoding RNAs. *PLoS Genet.*, *9*(6), e1003569. https://doi.org/10.1371/journal.pgen.1003569

Hansson, B., Morén, B., Fryklund, C., Vliex, L., Wasserstrom, S., Albinsson, S., Berger, K., & Stenkula, K. G. (2019). Adipose cell size changes are associated with a drastic actin remodeling. *Sci. Rep.*, *9*(1), 12941. https://doi.org/10.1038/s41598-019-49418-0

He, J.-S., Soo, P., Evers, M., Parsons, K. M., Hein, N., Hannan, K. M., Hannan, R. D., & George, A. J. (2018). High-Content Imaging Approaches to Quantitate Stress-Induced Changes in Nucleolar Morphology. *Assay Drug Dev. Technol.*, *16*(6), 320–332. https://doi.org/10.1089/adt.2018.861

Hegele, R. A., Joy, T. R., Al-Attar, S. A., & Rutt, B. K. (2007). Thematic review series: Adipocyte Biology. Lipodystrophies: windows on adipose biology and metabolism. *J. Lipid Res.*, *48*(7), 1433–1444. https://doi.org/10.1194/jlr.R700004-JLR200

Hepler, C., & Gupta, R. K. (2017). The expanding problem of adipose depot remodeling and postnatal adipocyte progenitor recruitment. *Mol. Cell. Endocrinol.*, *445*, 95–108. https://doi.org/10.1016/j.mce.2016.10.011

Herman, M. A., Peroni, O. D., Villoria, J., Schön, M. R., Abumrad, N. A., Blüher, M., Klein, S., & Kahn, B. B. (2012). A novel ChREBP isoform in adipose tissue regulates systemic glucose metabolism. *Nature*, *484*(7394), 333–338. https://doi.org/10.1038/nature10986

Hesketh, J. E., & Pryme, I. F. (1991). Interaction between mRNA, ribosomes and the cytoskeleton. *Biochem. J*, *277 (Pt 1)*, 1–10. https://doi.org/10.1042/bj2770001

Hoefner, C., Muhr, C., Horder, H., Wiesner, M., Wittmann, K., Lukaszyk, D., Radeloff, K., Winnefeld, M., Becker, M., Blunk, T., & Bauer-Kreisel, P. (2020). Human Adipose-Derived Mesenchymal Stromal/Stem Cell Spheroids Possess High Adipogenic Capacity and Acquire an Adipose Tissue-like Extracellular Matrix Pattern. *Tissue Eng. Part A*, *26*(15-16), 915–926. https://doi.org/10.1089/ten.TEA.2019.0206

Hon, T., Mars, K., Young, G., Tsai, Y.-C., Karalius, J. W., Landolin, J. M., Maurer, N., Kudrna, D., Hardigan, M. A., Steiner, C. C., Knapp, S. J., Ware, D., Shapiro, B., Peluso, P., & Rank, D. R. (2020). Highly accurate long-read HiFi sequencing data for five complex genomes. *Sci Data*, *7*(1), 399. https://doi.org/10.1038/s41597-020-00743-4

Hoque, M., Ji, Z., Zheng, D., Luo, W., Li, W., You, B., Park, J. Y., Yehia, G., & Tian, B. (2013). Analysis of alternative cleavage and polyadenylation by 3' region extraction and deep sequencing. *Nat. Methods*, *10*(2), 133–139. https://doi.org/10.1038/nmeth.2288

Hwang, C. S., Loftus, T. M., Mandrup, S., & Lane, M. D. (1997). Adipocyte differentiation and leptin expression. *Annu. Rev. Cell Dev. Biol.*, *13*, 231–259. https://doi.org/10.1146/annurev.cellbio.13.1.231

Hyman, A. A., Weber, C. A., & Jülicher, F. (2014). Liquid-liquid phase separation in biology. *Annu. Rev. Cell Dev. Biol.*, *30*, 39–58. https://doi.org/10.1146/annurev-cellbio-100913-013325

Iimura, T., & Pourquié, O. (2007). Hox genes in time and space during vertebrate body formation. *Dev. Growth Differ.*, *49*(4), 265–275. https://doi.org/10.1111/j.1440-169X.2007.00928.x

Iizuka, K., Bruick, R. K., Liang, G., Horton, J. D., & Uyeda, K. (2004). Deficiency of carbohydrate response element-binding protein (ChREBP) reduces lipogenesis as well as glycolysis. *Proc. Natl. Acad. Sci. U. S. A.*, *101*(19), 7281–7286. https://doi.org/10.1073/pnas.0401516101

Ingolia, N. T., Brar, G. A., Stern-Ginossar, N., Harris, M. S., Talhouarne, G. J. S., Jackson, S. E., Wills, M. R., & Weissman, J. S. (2014). Ribosome profiling reveals pervasive translation outside of annotated protein-coding genes. *Cell Rep.*, *8*(5), 1365–1379. https://doi.org/10.1016/j.celrep.2014.07.045

Ishibashi, M., Kogo, R., Shibata, K., Sawada, G., Takahashi, Y., Kurashige, J., Akiyoshi, S., Sasaki, S., Iwaya, T., Sudo, T., Sugimachi, K., Mimori, K., Wakabayashi, G., & Mori, M. (2013). Clinical significance of the expression of long non-coding RNA HOTAIR in primary hepatocellular carcinoma. *Oncol. Rep.*, *29*(3), 946–950. https://doi.org/10.3892/or.2012.2219

Iyer, K. V., Pulford, S., Mogilner, A., & Shivashankar, G. V. (2012). Mechanical activation of cells induces chromatin remodeling preceding MKL nuclear transport. *Biophys. J.*, *103*(7), 1416–1428. https://doi.org/10.1016/j.bpj.2012.08.041

Jääger, K., Islam, S., Zajac, P., Linnarsson, S., & Neuman, T. (2012). RNA-seq analysis reveals different dynamics of differentiation of human dermis- and adipose-derived stromal stem cells. *PLoS One*, *7*(6), e38833. https://doi.org/10.1371/journal.pone.0038833

Jackson, R. J., Hellen, C. U. T., & Pestova, T. V. (2010). The mechanism of eukaryotic translation initiation and principles of its regulation. *Nat. Rev. Mol. Cell Biol.*, *11*(2), 113–127. https://doi.org/10.1038/nrm2838

Jacobs, S. A., Taverna, S. D., Zhang, Y., Briggs, S. D., Li, J., Eissenberg, J. C., Allis, C. D., & Khorasanizadeh, S. (2001). Specificity of the HP1 chromo domain for the methylated N-terminus of histone H3. *EMBO J.*, *20*(18), 5232–5241. https://doi.org/10.1093/emboj/20.18.5232

Jeffery, E., Church, C. D., Holtrup, B., Colman, L., & Rodeheffer, M. S. (2015). Rapid depot-specific activation of adipocyte precursor cells at the onset of obesity. *Nat. Cell Biol.*, *17*(4), 376–385. https://doi.org/10.1038/ncb3122

Jones, J. E. C., Rabhi, N., Orofino, J., Gamini, R., Perissi, V., Vernochet, C., & Farmer, S. R. (2020). The Adipocyte Acquires a Fibroblast-Like Transcriptional Signature in Response to a High Fat Diet. *Sci. Rep.*, *10*(1), 2380. https://doi.org/10.1038/s41598-020-59284-w

Kalwa, M., Hänzelmann, S., Otto, S., Kuo, C.-C., Franzen, J., Joussen, S., Fernandez-Rebollo, E., Rath, B., Koch, C., Hofmann, A., Lee, S.-H., Teschendorff, A. E., Denecke, B., Lin, Q., Widschwendter, M., Weinhold, E., Costa, I. G., & Wagner, W. (2016). The lncRNA HOTAIR impacts on mesenchymal stem cells via triple helix formation. *Nucleic Acids Res.*, *44*(22), 10631–10643. https://doi.org/10.1093/nar/gkw802

Kanzaki, M., & Pessin, J. E. (2001). Insulin-stimulated GLUT4 Translocation in Adipocytes Is Dependent upon Cortical Actin Remodeling*210. *J. Biol. Chem.*, *276*(45), 42436–42444. https://doi.org/10.1074/jbc.M108297200

Kanzaki, M., & Pessin, J. E. (2002). Caveolin-associated filamentous actin (Cav-actin) defines a novel F-actin structure in adipocytes. *J. Biol. Chem.*, *277*(29), 25867–25869. https://doi.org/10.1074/jbc.C200292200

Kappen, C., Schughart, K., & Ruddle, F. H. (1993). Early evolutionary origin of major homeodomain sequence classes. *Genomics*, *18*(1), 54–70. https://doi.org/10.1006/geno.1993.1426

Karastergiou, K., Fried, S. K., Xie, H., Lee, M.-J., Divoux, A., Rosencrantz, M. A., Chang, R. J., & Smith, S. R. (2013). Distinct developmental signatures of human abdominal and gluteal subcutaneous adipose tissue depots. *J. Clin. Endocrinol. Metab.*, *98*(1), 362–371. https://doi.org/10.1210/jc.2012-2953

Karastergiou, K., Smith, S. R., Greenberg, A. S., & Fried, S. K. (2012). Sex differences in human adipose tissues - the biology of pear shape. *Biol. Sex Differ.*, *3*(1), 13. https://doi.org/10.1186/2042-6410-3-13

Karpe, F., & Pinnick, K. E. (2015). Biology of upper-body and lower-body adipose tissue–link to whole-body phenotypes. *Nat. Rev. Endocrinol.*, *11*(2), 90–100. https://doi.org/10.1038/nrendo.2014.185

Keen, A. N., Payne, L. A., Mehta, V., Rice, A., Simpson, L. J., Pang, K. L., del Rio Hernandez, A., Reader, J. S., & Tzima, E. (2022). Eukaryotic initiation factor 6 regulates mechanical responses in endothelial cells. *J. Cell Biol.*, *221*(2). https://doi.org/10.1083/jcb.202005213

Kershaw, E. E., & Flier, J. S. (2004). Adipose tissue as an endocrine organ. *J. Clin. Endocrinol. Metab.*, *89*(6), 2548–2556. https://doi.org/10.1210/jc.2004-0395

Khalil, A. M., Guttman, M., Huarte, M., Garber, M., Raj, A., Rivea Morales, D., Thomas, K., Presser, A., Bernstein, B. E., van Oudenaarden, A., Regev, A., Lander, E. S., & Rinn, J. L. (2009). Many human large intergenic noncoding RNAs associate with chromatin-modifying complexes and affect gene expression. *Proc. Natl. Acad. Sci. U. S. A.*, *106*(28), 11667–11672. https://doi.org/10.1073/pnas.0904715106

Khilan, A. A., Al-Maslamani, N. A., & Horn, H. F. (2021). Cell stretchers and the LINC complex in mechanotransduction. *Arch. Biochem. Biophys.*, *702*, 108829. https://doi.org/10.1016/j.abb.2021.108829

Killinger, D. W., Perel, E., Daniilescu, D., Kharlip, L., & Blackstein, M. E. (1987). Aromatase activity in the breast and other peripheral tissues and its therapeutic regulation. *Steroids*, *50*(4-6), 523–536. https://doi.org/10.1016/0039-128x(87)90036-5

Kim, J. B., & Spiegelman, B. M. (1996). ADD1/SREBP1 promotes adipocyte differentiation and gene expression linked to fatty acid metabolism. *Genes Dev.*, *10*(9), 1096–1107. https://doi.org/10.1101/gad.10.9.1096

Kim, K., Jutooru, I., Chadalapaka, G., Johnson, G., Frank, J., Burghardt, R., Kim, S., & Safe, S. (2013). HOTAIR is a negative prognostic factor and exhibits pro-oncogenic activity in pancreatic cancer. *Oncogene*, *32*(13), 1616–1625. https://doi.org/10.1038/onc.2012.193

Kimura, H. (2013). Histone modifications for human epigenome analysis. *J. Hum. Genet.*, *58*(7), 439–445. https://doi.org/10.1038/jhg.2013.66

Kissebah, A. H., Vydelingum, N., Murray, R., Evans, D. J., Hartz, A. J., Kalkhoff, R. K., & Adams, P. W. (1982). Relation of body fat distribution to metabolic complications of obesity. *J. Clin. Endocrinol. Metab.*, *54*(2), 254–260. https://doi.org/10.1210/jcem-54-2-254

Kogo, R., Shimamura, T., Mimori, K., Kawahara, K., Imoto, S., Sudo, T., Tanaka, F., Shibata, K., Suzuki, A., Komune, S., Miyano, S., & Mori, M. (2011). Long noncoding RNA HOTAIR regulates polycomb-dependent chromatin modification and is associated with poor prognosis in colorectal cancers. *Cancer Res.*, *71*(20), 6320–6326. https://doi.org/10.1158/0008-5472.CAN-11-1021

Krumlauf, R. (1994). Hox genes in vertebrate development. *Cell*, *78*(2), 191–201. https://doi.org/10.1016/0092-8674(94)90290-9

Kuo, F.-C., Huang, Y.-C., Yen, M.-R., Lee, C.-H., Hsu, K.-F., Yang, H.-Y., Wu, L.-W., Lu, C.-H., Hsu, Y.-J., & Chen, P.-Y. (2022). Aberrant overexpression of HOTAIR inhibits abdominal adipogenesis through remodelling of genome-wide DNA methylation and transcription. *Mol Metab*, *60*, 101473. https://doi.org/10.1016/j.molmet.2022.101473

Kuo, F.-C., Neville, M. J., Sabaratnam, R., Wesolowska-Andersen, A., Phillips, D., Wittemans, L. B. L., van Dam, A. D., Loh, N. Y., Todorčević, M., Denton, N., Kentistou, K. A., Joshi, P. K., Christodoulides, C., Langenberg, C., Collas, P., Karpe, F., & Pinnick, K. E. (2022). HOTAIR interacts with PRC2 complex regulating the regional preadipocyte transcriptome and human fat distribution. *Cell Rep.*, *40*(4), 111136. https://doi.org/10.1016/j.celrep.2022.111136

Kuroda, M., Tanabe, H., Yoshida, K., Oikawa, K., Saito, A., Kiyuna, T., Mizusawa, H., & Mukai, K. (2004). Alteration of chromosome positioning during adipocyte differentiation. *J. Cell Sci.*, *117*(Pt 24), 5897–5903. https://doi.org/10.1242/jcs.01508

Lafontaine, D. L. J., Riback, J. A., Bascetin, R., & Brangwynne, C. P. (2021). The nucleolus as a multiphase liquid condensate. *Nat. Rev. Mol. Cell Biol.*, *22*(3), 165–182. https://doi.org/10.1038/s41580-020-0272-6

Lammerding, J., Fong, L. G., Ji, J. Y., Reue, K., Stewart, C. L., Young, S. G., & Lee, R. T. (2006). Lamins A and C but not lamin B1 regulate nuclear mechanics. *J. Biol. Chem.*, *281*(35), 25768–25780.

Lamming, D. W., Ye, L., Sabatini, D. M., & Baur, J. A. (2013). Rapalogs and mTOR inhibitors as anti-aging therapeutics. *J. Clin. Invest.*, *123*(3), 980–989. https://doi.org/10.1172/JCI64099

Lappin, T. R. J., Grier, D. G., Thompson, A., & Halliday, H. L. (2006). HOX genes: seductive science, mysterious mechanisms. *Ulster Med. J.*, *75*(1), 23–31.

Lee, J.-E., Schmidt, H., Lai, B., & Ge, K. (2019). Transcriptional and Epigenomic Regulation of Adipogenesis. *Mol. Cell. Biol.*, *39*(11). https://doi.org/10.1128/MCB.00601-18

Lee, J.-M., Park, S., Lee, D., Ginting, R. P., Lee, M. R., Lee, M.-W., & Han, J. (2021). Reduction in endoplasmic reticulum stress activates beige adipocytes differentiation and alleviates high fat diet-induced metabolic phenotypes. *Biochim. Biophys. Acta Mol. Basis Dis.*, *1867*(5), 166099. https://doi.org/10.1016/j.bbadis.2021.166099

Lee, M., Kim, H. J., Kim, S. W., Park, S.-A., Chun, K.-H., Cho, N. H., Song, Y. S., & Kim, Y. T. (2016). The long non-coding RNA HOTAIR increases tumour growth and invasion in cervical cancer by targeting the Notch pathway. *Oncotarget*, *7*(28), 44558–44571. https://doi.org/10.18632/oncotarget.10065

Lee, P. L., Jung, S. M., & Guertin, D. A. (2017). The Complex Roles of Mechanistic Target of Rapamycin in Adipocytes and Beyond. *Trends Endocrinol. Metab.*, *28*(5), 319–339. https://doi.org/10.1016/j.tem.2017.01.004

Lee, R. C., Feinbaum, R. L., & Ambros, V. (1993). The C. elegans heterochronic gene lin-4 encodes small RNAs with antisense complementarity to lin-14. *Cell*, *75*(5), 843–854. https://doi.org/10.1016/0092-8674(93)90529-y

Lefterova, M. I., Haakonsson, A. K., Lazar, M. A., & Mandrup, S. (2014). PPARγ and the global map of adipogenesis and beyond. *Trends Endocrinol. Metab.*, *25*(6), 293–302. https://doi.org/10.1016/j.tem.2014.04.001

Lemieux, I. (2004). Energy partitioning in gluteal-femoral fat: does the metabolic fate of triglycerides affect coronary heart disease risk? *Arterioscler. Thromb. Vasc. Biol.*, *24*(5), 795–797. https://doi.org/10.1161/01.ATV.0000126485.80373.33

Letexier, D., Pinteur, C., Large, V., Fréring, V., & Beylot, M. (2003). Comparison of the expression and activity of the lipogenic pathway in human and rat adipose tissue. *J. Lipid Res.*, *44*(11), 2127–2134. https://doi.org/10.1194/jlr.M300235-JLR200

Lewis, E. B. (1992). Clusters of Master Control Genes Regulate the Development of Higher Organisms. *JAMA*, *267*(11), 1524–1531. https://doi.org/10.1001/jama.1992.03480110100042

Li, L., Liu, B., Wapinski, O. L., Tsai, M.-C., Qu, K., Zhang, J., Carlson, J. C., Lin, M., Fang, F., Gupta, R. A., Helms, J. A., & Chang, H. Y. (2013). Targeted disruption of Hotair leads to homeotic transformation and gene derepression. *Cell Rep.*, *5*(1), 3–12. https://doi.org/10.1016/j.celrep.2013.09.003

Li, S., Xiong, Q., Chen, M., Wang, B., Yang, X., Yang, M., Wang, Q., Cui, Z., & Ge, F. (2021). Long noncoding RNA HOTAIR interacts with Y-Box Protein-1 (YBX1) to regulate cell proliferation. *Life Sci Alliance*, *4*(9). https://doi.org/10.26508/lsa.202101139

Linhart, H. G., Ishimura-Oka, K. et al. (2001). C/EBPα is required for differentiation of white, but not brown, adipose tissue [Accessed: 2022-5-19].

Liu, C. Y., & Kaufman, R. J. (2003). The unfolded protein response. *J. Cell Sci.*, *116*(Pt 10), 1861–1862. https://doi.org/10.1242/jcs.00408

Liu, Y.-W., Sun, M., Xia, R., Zhang, E.-B., Liu, X.-H., Zhang, Z.-H., Xu, T.-P., De, W., Liu, B.-R., & Wang, Z.-X. (2015). LincHOTAIR epigenetically silences miR34a by binding to PRC2 to promote the epithelial-to-mesenchymal transition in human gastric cancer. *Cell Death Dis.*, *6*, e1802. https://doi.org/10.1038/cddis.2015.150

López-Urrutia, E., Bustamante Montes, L. P., Ladrón de Guevara Cervantes, D., Pérez-Plasencia, C., & Campos-Parra, A. D. (2019). Crosstalk Between Long Non-coding RNAs, Micro-RNAs and mRNAs: Deciphering Molecular Mechanisms of Master Regulators in Cancer. *Front. Oncol.*, *9*, 669. https://doi.org/10.3389/fonc.2019.00669

Lorenz, R., Bernhart, S. H., Höner Zu Siederdissen, C., Tafer, H., Flamm, C., Stadler, P. F., & Hofacker, I. L. (2011). ViennaRNA Package 2.0. *Algorithms Mol. Biol.*, *6*, 26. https://doi.org/10.1186/1748-7188-6-26

Lowell, B. B. (1999). PPARgamma: an essential regulator of adipogenesis and modulator of fat cell function. *Cell*, *99*(3), 239–242. https://doi.org/10.1016/s0092-8674(00)81654-2

Lu, L., Zhu, G., Zhang, C., Deng, Q., Katsaros, D., Mayne, S. T., Risch, H. A., Mu, L., Canuto, E. M., Gregori, G., Benedetto, C., & Yu, H. (2012). Association of large noncoding RNA HOTAIR expression and its downstream intergenic CpG island methylation with survival in breast cancer. *Breast Cancer Res. Treat.*, *136*(3), 875–883. https://doi.org/10.1007/s10549-012-2314-z

Lu, Q., Ren, S., Lu, M., Zhang, Y., Zhu, D., Zhang, X., & Li, T. (2013). Computational prediction of associations between long non-coding RNAs and proteins. *BMC Genomics*, *14*, 651. https://doi.org/10.1186/1471-2164-14-651

Lundgren, M., Svensson, M., Lindmark, S., Renström, F., Ruge, T., & Eriksson, J. W. (2007). Fat cell enlargement is an independent marker of insulin resistance and 'hyperleptinaemia'. *Diabetologia*, *50*(3), 625–633. https://doi.org/10.1007/s00125-006-0572-1

Lusic, M., & Mhlanga, M. M. (2022). Walking the LINEs hidden in the dark matter of the genome. *Nat. Genet.*, *54*(2), 98–99. https://doi.org/10.1038/s41588-021-01003-w

Ma, M.-Z., Li, C.-X., Zhang, Y., Weng, M.-Z., Zhang, M.-D., Qin, Y.-Y., Gong, W., & Quan, Z.-W. (2014). Long non-coding RNA HOTAIR, a c-Myc activated driver of malignancy, negatively regulates miRNA-130a in gallbladder cancer. *Mol. Cancer*, *13*, 156. https://doi.org/10.1186/1476-4598-13-156

Ma, Q., & Chang, H. Y. (2016). Single-cell profiling of lncRNAs in the developing human brain. *Genome Biol.*, *17*, 68. https://doi.org/10.1186/s13059-016-0933-0

Madsen-Østerbye, J., Abdelhalim, M., Baudement, M.-O., & Collas, P. (2022). Local euchromatin enrichment in lamina-associated domains anticipates their repositioning in the adipogenic lineage. *Genome Biol.*, *23*(1), 91. https://doi.org/10.1186/s13059-022-02662-6

Mainguy, G., Koster, J., Woltering, J., Jansen, H., & Durston, A. (2007). Extensive polycistronism and antisense transcription in the mammalian Hox clusters. *PLoS One*, *2*(4), e356. https://doi.org/10.1371/journal.pone.0000356

Malhas, A., Lee, C. F., Sanders, R., Saunders, N. J., & Vaux, D. J. (2007). Defects in lamin B1 expression or processing affect interphase chromosome position and gene expression. *J. Cell Biol.*, *176*(5), 593–603. https://doi.org/10.1083/jcb.200607054

Mann, J. P., & Savage, D. B. (2019). What lipodystrophies teach us about the metabolic syndrome. *J. Clin. Invest.*, *129*(10), 4009–4021. https://doi.org/10.1172/JCI129190

Marcon, B. H., Holetz, F. B., Eastman, G., Origa-Alves, A. C., Amorós, M. A., de Aguiar, A. M., Rebelatto, C. K., Brofman, P. R. S., Sotelo-Silveira, J., & Dallagiovanna, B. (2017). Downregulation of the protein synthesis machinery is a major regulatory event during early adipogenic differentiation of human adipose-derived stromal cells. *Stem Cell Res.*, *25*, 191–201. https://doi.org/10.1016/j.scr.2017.10.027

Margueron, R., & Reinberg, D. (2011). The Polycomb complex PRC2 and its mark in life. *Nature*, *469*(7330), 343–349. https://doi.org/10.1038/nature09784

Mariman, E. C. M., & Wang, P. (2010). Adipocyte extracellular matrix composition, dynamics and role in obesity. *Cell. Mol. Life Sci.*, *67*(8), 1277–1292. https://doi.org/10.1007/s00018-010-0263-4

Martin, L., & Chang, H. Y. (2012). Uncovering the role of genomic "dark matter" in human disease. *J. Clin. Invest.*, *122*(5), 1589–1595. https://doi.org/10.1172/JCI60020

Martino, F., Perestrelo, A. R., Vinarský, V., Pagliari, S., & Forte, G. (2018). Cellular Mechanotransduction: From Tension to Function. *Front. Physiol.*, *9*, 824. https://doi.org/10.3389/fphys.2018.00824

McColloch, A., Rabiei, M., Rabbani, P., Bowling, A., & Cho, M. (2019). Correlation between Nuclear Morphology and Adipogenic Differentiation: Application of a Combined Experimental and Computational Modeling Approach. *Sci. Rep.*, *9*(1), 16381. https://doi.org/10.1038/s41598-019-52926-8

McGinnis, W., & Krumlauf, R. (1992). Homeobox genes and axial patterning. *Cell*, *68*(2), 283–302. https://doi.org/10.1016/0092-8674(92)90471-n

McStay, B., & Grummt, I. (2008). The epigenetics of rRNA genes: from molecular to chromosome biology. *Annu. Rev. Cell Dev. Biol.*, *24*, 131–157. https://doi.org/10.1146/annurev.cellbio.24.110707.175259

Mefford, H. C. (2014). Shedding Light on the Genome's Dark Matter. *Sci. Transl. Med.*, *6*(257), 257ec173–257ec173. https://doi.org/10.1126/scitranslmed.3010422

Menssen, A., Häupl, T., Sittinger, M., Delorme, B., Charbord, P., & Ringe, J. (2011). Differential gene expression profiling of human bone marrow-derived mesenchymal stem cells during adipogenic development. *BMC Genomics*, *12*, 461. https://doi.org/10.1186/1471-2164-12-461

Mercer, T. R., Clark, M. B., Crawford, J., Brunck, M. E., Gerhardt, D. J., Taft, R. J., Nielsen, L. K., Dinger, M. E., & Mattick, J. S. (2014). Targeted sequencing for gene discovery and quantification using RNA CaptureSeq. *Nat. Protoc.*, *9*(5), 989–1009. https://doi.org/10.1038/nprot.2014.058

Meredith, E. K., Balas, M. M., Sindy, K., Haislop, K., & Johnson, A. M. (2016). An RNA matchmaker protein regulates the activity of the long noncoding RNA HOTAIR. *RNA*, *22*(7), 995–1010. https://doi.org/10.1261/rna.055830.115

Meshorer, E., & Misteli, T. (2006). Chromatin in pluripotent embryonic stem cells and differentiation. *Nat. Rev. Mol. Cell Biol.*, *7*(7), 540–546. https://doi.org/10.1038/nrm1938

Mewborn, S. K., Puckelwartz, M. J., Abuisneineh, F., Fahrenbach, J. P., Zhang, Y., MacLeod, H., Dellefave, L., Pytel, P., Selig, S., Labno, C. M., Reddy, K., Singh, H., & McNally, E. (2010). Altered chromosomal positioning, compaction, and gene expression with a lamin A/C gene mutation. *PLoS One*, *5*(12), e14342. https://doi.org/10.1371/journal.pone.0014342

Mikkelsen, T. S., Ku, M., Jaffe, D. B., Issac, B., Lieberman, E., Giannoukos, G., Alvarez, P., Brockman, W., Kim, T.-K., Koche, R. P., Lee, W., Mendenhall, E., O'Donovan, A., Presser, A., Russ, C., Xie, X., Meissner, A., Wernig, M., Jaenisch, R., … Bernstein, B. E. (2007). Genome-wide maps of chromatin state in pluripotent and lineage-committed cells. *Nature*, *448*(7153), 553–560. https://doi.org/10.1038/nature06008

Mori, S., Kiuchi, S., Ouchi, A., Hase, T., & Murase, T. (2014). Characteristic expression of extracellular matrix in subcutaneous adipose tissue development and adipogenesis; comparison with visceral adipose tissue. *Int. J. Biol. Sci.*, *10*(8), 825–833. https://doi.org/10.7150/ijbs.8672

Mor-Yossef Moldovan, L., Lustig, M., Naftaly, A., Mardamshina, M., Geiger, T., Gefen, A., & Benayahu, D. (2019). Cell shape alteration during adipogenesis is associated with coordinated matrix cues. *J. Cell. Physiol.*, *234*(4), 3850–3863. https://doi.org/10.1002/jcp.27157

Mozdarani, H., Ezzatizadeh, V., & Rahbar Parvaneh, R. (2020). The emerging role of the long non-coding RNA HOTAIR in breast cancer development and treatment. *J. Transl. Med.*, *18*(1), 152. https://doi.org/10.1186/s12967-020-02320-0

Nava, M. M., Miroshnikova, Y. A., Biggs, L. C., Whitefield, D. B., Metge, F., Boucas, J., Vihinen, H., Jokitalo, E., Li, X., Garcıéa Arcos, J. M., Hoffmann, B., Merkel, R., Niessen, C. M., Dahl, K. N., & Wickström, S. A. (2020). Heterochromatin-Driven Nuclear Softening Protects the Genome against Mechanical Stress-Induced Damage. *Cell*, *181*(4), 800–817.e22. https://doi.org/10.1016/j.cell.2020.03.052

Németh, A., Conesa, A., Santoyo-Lopez, J., Medina, I., Montaner, D., Péterfia, B., Solovei, I., Cremer, T., Dopazo, J., & Längst, G. (2010). Initial genomics of the human nucleolus. *PLoS Genet.*, *6*(3), e1000889. https://doi.org/10.1371/journal.pgen.1000889

Nobusue, H., Onishi, N., Shimizu, T., Sugihara, E., Oki, Y., Sumikawa, Y., Chiyoda, T., Akashi, K., Saya, H., & Kano, K. (2014). Regulation of MKL1 via actin cytoskeleton dynamics drives adipocyte differentiation. *Nat. Commun.*, *5*(1), 1–12. https://doi.org/10.1038/ncomms4368

Ofek, G., Natoli, R. M., & Athanasiou, K. A. (2009). In situ mechanical properties of the chondrocyte cytoplasm and nucleus. *J. Biomech.*, *42*(7), 873–877. https://doi.org/10.1016/j.jbiomech.2009.01.024

Oishi, Y., Manabe, I., Tobe, K., Tsushima, K., Shindo, T., Fujiu, K., Nishimura, G., Maemura, K., Yamauchi, T., Kubota, N., Suzuki, R., Kitamura, T., Akira, S., Kadowaki, T., & Nagai, R. (2005). Krüppel-like transcription factor KLF5 is a key regulator of adipocyte differentiation. *Cell Metab.*, *1*(1), 27–39. https://doi.org/10.1016/j.cmet.2004.11.005

Ottaviani, E., Malagoli, D., & Franceschi, C. (2011). The evolution of the adipose tissue: a neglected enigma. *Gen. Comp. Endocrinol.*, *174*(1), 1–4. https://doi.org/10.1016/j.ygcen.2011.06.018

Ouchi, N., Parker, J. L., Lugus, J. J., & Walsh, K. (2011). Adipokines in inflammation and metabolic disease. *Nat. Rev. Immunol.*, *11*(2), 85–97. https://doi.org/10.1038/nri2921

Oyadomari, S., Harding, H. P., Zhang, Y., Oyadomari, M., & Ron, D. (2008). Dephosphorylation of translation initiation factor 2alpha enhances glucose tolerance and attenuates hepatosteatosis in mice. *Cell Metab.*, *7*(6), 520–532. https://doi.org/10.1016/j.cmet.2008.04.011

Ozawa, T., Kondo, M., & Isobe, M. (2004). 3' rapid amplification of cDNA ends (RACE) walking for rapid structural analysis of large transcripts. *J. Hum. Genet.*, *49*(2), 102–105. https://doi.org/10.1007/s10038-003-0109-0

Pajerowski, J. D., Dahl, K. N., Zhong, F. L., Sammak, P. J., & Discher, D. E. (2007). Physical plasticity of the nucleus in stem cell differentiation. *Proc. Natl. Acad. Sci. U. S. A.*, *104*(40), 15619–15624. https://doi.org/10.1073/pnas.0702576104

Pang, K. C., Frith, M. C., & Mattick, J. S. (2006). Rapid evolution of noncoding RNAs: lack of conservation does not mean lack of function. *Trends Genet.*, *22*(1), 1–5. https://doi.org/10.1016/j.tig.2005.10.003

Paulsen, J., Liyakat Ali, T. M., Nekrasov, M., Delbarre, E., Baudement, M.-O., Kurscheid, S., Tremethick, D., & Collas, P. (2019). Long-range interactions between topologically associating domains shape the four-dimensional genome during differentiation. *Nat. Genet.*, *51*(5), 835–843. https://doi.org/10.1038/s41588-019-0392-0

Payne, V. A., Au, W.-S., Lowe, C. E., Rahman, S. M., Friedman, J. E., O'Rahilly, S., & Rochford, J. J. (2009). C/EBP transcription factors regulate SREBP1c gene expression during adipogenesis. *Biochem. J*, *425*(1), 215–223. https://doi.org/10.1042/BJ20091112

Pelletier, J., Thomas, G., & Volarević, S. (2018). Ribosome biogenesis in cancer: new players and therapeutic avenues. *Nat. Rev. Cancer*, *18*(1), 51–63. https://doi.org/10.1038/nrc.2017.104

Pereira, S. S., & Alvarez-Leite, J. I. (2014). Adipokines: biological functions and metabolically healthy obese profile. *JRLCR*, *7*, 15–25. https://doi.org/10.2147/JRLCR.S36060

Pérez, L. M., Bernal, A., de Lucas, B., San Martin, N., Mastrangelo, A., Garcıéa, A., Barbas, C., & Gálvez, B. G. (2015). Altered metabolic and stemness capacity of adipose tissue-derived stem cells from obese mouse and human. *PLoS One*, *10*(4), e0123397. https://doi.org/10.1371/journal.pone.0123397

Picchi, J., Trombi, L., Spugnesi, L., Barachini, S., Maroni, G., Brodano, G. B., Boriani, S., Valtieri, M., Petrini, M., & Magli, M. C. (2013). HOX and TALE signatures specify human stromal stem cell populations from different sources. *J. Cell. Physiol.*, *228*(4), 879–889. https://doi.org/10.1002/jcp.24239

Pinnick, K. E., Neville, M. J., Fielding, B. A., Frayn, K. N., Karpe, F., & Hodson, L. (2012). Gluteofemoral adipose tissue plays a major role in production of the lipokine

palmitoleate in humans. *Diabetes*, *61*(6), 1399–1403. https://doi.org/10.2337/db11-1810

Pinnick, K. E., Nicholson, G., Manolopoulos, K. N., McQuaid, S. E., Valet, P., Frayn, K. N., Denton, N., Min, J. L., Zondervan, K. T., Fleckner, J., MolPAGE Consortium, McCarthy, M. I., Holmes, C. C., & Karpe, F. (2014). Distinct developmental profile of lower-body adipose tissue defines resistance against obesity-associated metabolic complications. *Diabetes*, *63*(11), 3785–3797. https://doi.org/10.2337/db14-0385

Pischedda, C., Cocco, S., Melis, A., Marini, M. G., Kan, Y. W., Cao, A., & Moi, P. (1995). Isolation of a differentially regulated splicing isoform of human NF-E2. *Proc. Natl. Acad. Sci. U. S. A.*, *92*(8), 3511–3515. https://doi.org/10.1073/pnas.92.8.3511

Poissonnet, C. M., Burdi, A. R., & Garn, S. M. (1984). The chronology of adipose tissue appearance and distribution in the human fetus. *Early Hum. Dev.*, *10*(1-2), 1–11. https://doi.org/10.1016/0378-3782(84)90106-3

Ponjavic, J., Ponting, C. P., & Lunter, G. (2007). Functionality or transcriptional noise? Evidence for selection within long noncoding RNAs. *Genome Res.*, *17*(5), 556–565. https://doi.org/10.1101/gr.6036807

Portoso, M., Ragazzini, R., Brenčič, Ž., Moiani, A., Michaud, A., Vassilev, I., Wassef, M., Servant, N., Sargueil, B., & Margueron, R. (2017). PRC2 is dispensable for HOTAIR-mediated transcriptional repression. *EMBO J.*, *36*(8), 981–994. https://doi.org/10.15252/embj.201695335

Poulos, S. P., Dodson, M. V., & Hausman, G. J. (2010). Cell line models for differentiation: preadipocytes and adipocytes. *Exp. Biol. Med.*, *235*(10), 1185–1193. https://doi.org/10.1258/ebm.2010.010063

Prieto González, E. A. (2019). Heterogeneity in Adipose Stem Cells. In A. Birbrair (Ed.), *Stem Cells Heterogeneity - Novel Concepts* (pp. 119–150). Springer International Publishing. https://doi.org/10.1007/978-3-030-11096-3_8

Pundel, O. J., Blowes, L. M., & Connelly, J. T. (2022). Extracellular Adhesive Cues Physically Define Nucleolar Structure and Function. *Adv. Sci.*, *9*(10), e2105545. https://doi.org/10.1002/advs.202105545

Quinonez, S. C., & Innis, J. W. (2014). Human HOX gene disorders. *Mol. Genet. Metab.*, *111*(1), 4–15. https://doi.org/10.1016/j.ymgme.2013.10.012

Qureshi, I. A., & Mehler, M. F. (2012). Emerging roles of non-coding RNAs in brain evolution, development, plasticity and disease. *Nat. Rev. Neurosci.*, *13*(8), 528–541. https://doi.org/10.1038/nrn3234

Rauch, A., Haakonsson, A. K., Madsen, J. G. S., Larsen, M., Forss, I., Madsen, M. R., Van Hauwaert, E. L., Wiwie, C., Jespersen, N. Z., Tencerova, M., Nielsen, R., Larsen, B. D., Röttger, R., Baumbach, J., Scheele, C., Kassem, M., & Mandrup, S. (2019). Osteogenesis depends on commissioning of a network of stem cell transcription factors that act as repressors of adipogenesis. *Nat. Genet.*, *51*(4), 716–727. https://doi.org/10.1038/s41588-019-0359-1

Rey, F., Urrata, V., Gilardini, L., Bertoli, S., Calcaterra, V., Zuccotti, G. V., Cancello, R., & Carelli, S. (2021). Role of long non-coding RNAs in adipogenesis: State of the art and implications in obesity and obesity-associated diseases. *Obes. Rev.*, *22*(7), e13203. https://doi.org/10.1111/obr.13203

Ringrose, L., & Paro, R. (2007). Polycomb/Trithorax response elements and epigenetic memory of cell identity. *Development*, *134*(2), 223–232. https://doi.org/10.1242/dev.02723

Rinn, J. L., & Chang, H. Y. (2012). Genome regulation by long noncoding RNAs. *Annu. Rev. Biochem.*, *81*, 145–166. https://doi.org/10.1146/annurev-biochem-051410-092902

Rinn, J. L., Kertesz, M., Wang, J. K., Squazzo, S. L., Xu, X., Brugmann, S. A., Goodnough, L. H., Helms, J. A., Farnham, P. J., Segal, E., & Chang, H. Y. (2007). Functional demarcation of active and silent chromatin domains in human HOX loci by noncoding RNAs. *Cell*, *129*(7), 1311–1323. https://doi.org/10.1016/j.cell.2007.05.022

Roberts, R., Hodson, L., Dennis, A. L., Neville, M. J., Humphreys, S. M., Harnden, K. E., Micklem, K. J., & Frayn, K. N. (2009). Markers of de novo lipogenesis in adipose tissue: associations with small adipocytes and insulin sensitivity in humans. *Diabetologia*, *52*(5), 882–890. https://doi.org/10.1007/s00125-009-1300-4

Rønningen, T., Shah, A., Oldenburg, A. R., Vekterud, K., Delbarre, E., Moskaug, J. Ø., & Collas, P. (2015). Prepatterning of differentiation-driven nuclear lamin A/C-associated chromatin domains by GlcNAcylated histone H2B. *Genome Res.*, *25*(12), 1825–1835. https://doi.org/10.1101/gr.193748.115

Rosen, E. D., Hsu, C.-H., Wang, X., Sakai, S., Freeman, M. W., Gonzalez, F. J., & Spiegelman, B. M. (2002). C/EBPalpha induces adipogenesis through PPARgamma: a unified pathway. *Genes Dev.*, *16*(1), 22–26. https://doi.org/10.1101/gad.948702

Rosen, E. D., & MacDougald, O. A. (2006). Adipocyte differentiation from the inside out. *Nat. Rev. Mol. Cell Biol.*, *7*(12), 885–896. https://doi.org/10.1038/nrm2066

Rosen, E. D., Walkey, C. J., Puigserver, P., & Spiegelman, B. M. (2000). Transcriptional regulation of adipogenesis. *Genes Dev.*, *14*(11), 1293–1307. https://doi.org/10.1101/gad.14.11.1293

Salans, L. B., Knittle, J. L., & Hirsch, J. (1968). The role of adipose cell size and adipose tissue insulin sensitivity in the carbohydrate intolerance of human obesity. *J. Clin. Invest.*, *47*(1), 153–165. https://doi.org/10.1172/JCI105705

Sarusi Portuguez, A., Schwartz, M., Siersbaek, R., Nielsen, R., Sung, M.-H., Mandrup, S., Kaplan, T., & Hakim, O. (2017). Hierarchical role for transcription factors and chromatin structure in genome organization along adipogenesis. *FEBS J.*, *284*(19), 3230–3244. https://doi.org/10.1111/febs.14183

Savić, N., Bär, D., Leone, S., Frommel, S. C., Weber, F. A., Vollenweider, E., Ferrari, E., Ziegler, U., Kaech, A., Shakhova, O., Cinelli, P., & Santoro, R. (2014). lncRNA maturation to initiate heterochromatin formation in the nucleolus is required for exit from pluripotency in ESCs. *Cell Stem Cell*, *15*(6), 720–734. https://doi.org/10.1016/j.stem.2014.10.005

Schorderet, P., & Duboule, D. (2011). Structural and functional differences in the long non-coding RNA hotair in mouse and human. *PLoS Genet.*, *7*(5), e1002071. https://doi.org/10.1371/journal.pgen.1002071

Schwarzacher, H. G., & Wachtler, F. (1993). The nucleolus. *Anat. Embryol.*, *188*(6), 515–536. https://doi.org/10.1007/BF00187008

Scott, D. D., & Oeffinger, M. (2016). Nucleolin and nucleophosmin: nucleolar proteins with multiple functions in DNA repair. *Biochem. Cell Biol.*, *94*(5), 419–432. https://doi.org/10.1139/bcb-2016-0068

Sekelsky, J. J., Brodsky, M. H., Rubin, G. M., & Hawley, R. S. (1999). Drosophila and human RecQ5 exist in different isoforms generated by alternative splicing. *Nucleic Acids Res.*, *27*(18), 3762–3769. https://doi.org/10.1093/nar/27.18.3762

Sen Gupta, A., Joshi, G., Pawar, S., & Sengupta, K. (2018). Nucleolin modulates compartmentalization and dynamics of histone 2B-ECFP in the nucleolus. *Nucleus*, *9*(1), 350–367. https://doi.org/10.1080/19491034.2018.1471936

Shen, W., Wang, Z., Punyanita, M., Lei, J., Sinav, A., Kral, J. G., Imielinska, C., Ross, R., & Heymsfield, S. B. (2003). Adipose tissue quantification by imaging methods: a proposed classification. *Obes. Res.*, *11*(1), 5–16. https://doi.org/10.1038/oby.2003.3

Shepherd, P. R., & Kahn, B. B. (1999). Glucose transporters and insulin action–implications for insulin resistance and diabetes mellitus. *N. Engl. J. Med.*, *341*(4), 248–257. https://doi.org/10.1056/NEJM199907223410406

Shin, Y., Chang, Y.-C., Lee, D. S. W., Berry, J., Sanders, D. W., Ronceray, P., Wingreen, N. S., Haataja, M., & Brangwynne, C. P. (2019). Liquid Nuclear Condensates Mechanically Sense and Restructure the Genome. *Cell*, *176*(6), 1518. https://doi.org/10.1016/j.cell.2019.02.025

Siddiqui, N., & Sonenberg, N. (2015). Signalling to eIF4E in cancer. *Biochem. Soc. Trans.*, *43*(5), 763–772. https://doi.org/10.1042/BST20150126

Siersbæk, R., Madsen, J. G. S., Javierre, B. M., Nielsen, R., Bagge, E. K., Cairns, J., Wingett, S. W., Traynor, S., Spivakov, M., Fraser, P., & Mandrup, S. (2017). Dynamic Rewiring of Promoter-Anchored Chromatin Loops during Adipocyte Differentiation. *Mol. Cell*, *66*(3), 420–435.e5. https://doi.org/10.1016/j.molcel.2017.04.010

Silva, K. R., Liechocki, S., Carneiro, J. R., Claudio-da-Silva, C., Maya-Monteiro, C. M., Borojevic, R., & Baptista, L. S. (2015). Stromal-vascular fraction content and adipose

stem cell behavior are altered in morbid obese and post bariatric surgery ex-obese women. *Stem Cell Res. Ther.*, *6*, 72. https://doi.org/10.1186/s13287-015-0029-x

Snijder, M. B., Dekker, J. M., Visser, M., Yudkin, J. S., Stehouwer, C. D. A., Bouter, L. M., Heine, R. J., Nijpels, G., & Seidell, J. C. (2003). Larger thigh and hip circumferences are associated with better glucose tolerance: the Hoorn study. *Obes. Res.*, *11*(1), 104–111. https://doi.org/10.1038/oby.2003.18

Sołtysik, K., Ohsaki, Y., Tatematsu, T., Cheng, J., & Fujimoto, T. (2019). Nuclear lipid droplets derive from a lipoprotein precursor and regulate phosphatidylcholine synthesis. *Nat. Commun.*, *10*(1), 473. https://doi.org/10.1038/s41467-019-08411-x

Somarowthu, S., Legiewicz, M., Chillón, I., Marcia, M., Liu, F., & Pyle, A. M. (2015). HOTAIR forms an intricate and modular secondary structure. *Mol. Cell*, *58*(2), 353–361. https://doi.org/10.1016/j.molcel.2015.03.006

Soneson, C., Matthes, K. L., Nowicka, M., Law, C. W., & Robinson, M. D. (2016). Isoform prefiltering improves performance of count-based methods for analysis of differential transcript usage. *Genome Biol.*, *17*, 12. https://doi.org/10.1186/s13059-015-0862-3

Song, Z., Xiaoli, A. M., & Yang, F. (2018). Regulation and Metabolic Significance of De Novo Lipogenesis in Adipose Tissues. *Nutrients*, *10*(10). https://doi.org/10.3390/nu10101383

Sørensen, K. P., Thomassen, M., Tan, Q., Bak, M., Cold, S., Burton, M., Larsen, M. J., & Kruse, T. A. (2013). Long non-coding RNA HOTAIR is an independent prognostic marker of metastasis in estrogen receptor-positive primary breast cancer. *Breast Cancer Res. Treat.*, *142*(3), 529–536. https://doi.org/10.1007/s10549-013-2776-7

Spalding, K. L., Arner, E., Westermark, P. O., Bernard, S., Buchholz, B. A., Bergmann, O., Blomqvist, L., Hoffstedt, J., Näslund, E., Britton, T., Concha, H., Hassan, M., Rydén, M., Frisén, J., & Arner, P. (2008). Dynamics of fat cell turnover in humans. *Nature*, *453*(7196), 783–787. https://doi.org/10.1038/nature06902

Squillaro, T., Peluso, G., Galderisi, U., & Di Bernardo, G. (2020). Long non-coding RNAs in regulation of adipogenesis and adipose tissue function. *Elife*, *9*. https://doi.org/10.7554/eLife.59053

Stachecka, J., Walczak, A., Kociucka, B., Ruszczycki, B., Wilczyński, G., & Szczerbal, I. (2018). Nuclear organization during in vitro differentiation of porcine mesenchymal stem cells (MSCs) into adipocytes. *Histochem. Cell Biol.*, *149*(2), 113–126. https://doi.org/10.1007/s00418-017-1618-9

Steijger, T., Abril, J. F., Engström, P. G., Kokocinski, F., RGASP Consortium, Hubbard, T. J., Guigó, R., Harrow, J., & Bertone, P. (2013). Assessment of transcript reconstruction methods for RNA-seq. *Nat. Methods*, *10*(12), 1177–1184. https://doi.org/10.1038/nmeth.2714

Stenström, L., Mahdessian, D., Gnann, C., Cesnik, A. J., Ouyang, W., Leonetti, M. D., Uhlén, M., Cuylen-Haering, S., Thul, P. J., & Lundberg, E. (2020). Mapping the nucleolar proteome reveals a spatiotemporal organization related to intrinsic protein disorder. *Mol. Syst. Biol.*, *16*(8), e9469. https://doi.org/10.15252/msb.20209469

Strable, M. S., & Ntambi, J. M. (2010). Genetic control of de novo lipogenesis: role in diet-induced obesity. *Crit. Rev. Biochem. Mol. Biol.*, *45*(3), 199–214. https://doi.org/10.3109/10409231003667500

Stranges, S., Dorn, J. M., Muti, P., Freudenheim, J. L., Farinaro, E., Russell, M., Nochajski, T. H., & Trevisan, M. (2004). Body fat distribution, relative weight, and liver enzyme levels: A population-based study. *Hepatology*, *39*(3), 754–763. https://doi.org/10.1002/hep.20149

Strawford, A., Antelo, F., Christiansen, M., & Hellerstein, M. K. (2004). Adipose tissue triglyceride turnover, de novo lipogenesis, and cell proliferation in humans measured with 2H2O. *Am. J. Physiol. Endocrinol. Metab.*, *286*(4), E577–88. https://doi.org/10.1152/ajpendo.00093.2003

Sun, K., Tordjman, J., Clément, K., & Scherer, P. E. (2013). Fibrosis and adipose tissue dysfunction. *Cell Metab.*, *18*(4), 470–477. https://doi.org/10.1016/j.cmet.2013.06.016

Sun, L., Goff, L. A., Trapnell, C., Alexander, R., Lo, K. A., Hacisuleyman, E., Sauvageau, M., Tazon-Vega, B., Kelley, D. R., Hendrickson, D. G., Yuan, B., Kellis, M., Lodish, H. F.,

& Rinn, J. L. (2013). Long noncoding RNAs regulate adipogenesis. *Proc. Natl. Acad. Sci. U. S. A.*, *110*(9), 3387–3392. https://doi.org/10.1073/pnas.1222643110

Swift, J., Ivanovska, I. L., Buxboim, A., Harada, T., Dingal, P. C. D. P., Pinter, J., Pajerowski, J. D., Spinler, K. R., Shin, J.-W., Tewari, M., Rehfeldt, F., Speicher, D. W., & Discher, D. E. (2013). Nuclear lamin-A scales with tissue stiffness and enhances matrix-directed differentiation. *Science*, *341*(6149), 1240104. https://doi.org/10.1126/science.1240104

Szabo, E., Feng, T., Dziak, E., & Opas, M. (2009). Cell adhesion and spreading affect adipogenesis from embryonic stem cells: the role of calreticulin. *Stem Cells*, *27*(9), 2092–2102. https://doi.org/10.1002/stem.137

Tanaka, T., Yoshida, N., Kishimoto, T., & Akira, S. (1997). Defective adipocyte differentiation in mice lacking the C/EBPbeta and/or C/EBPdelta gene. *EMBO J.*, *16*(24), 7432–7443. https://doi.org/10.1093/emboj/16.24.7432

Tang, Q.-Q., Otto, T. C., & Lane, M. D. (2003). Mitotic clonal expansion: a synchronous process required for adipogenesis. *Proc. Natl. Acad. Sci. U. S. A.*, *100*(1), 44–49. https://doi.org/10.1073/pnas.0137044100

Tardaguila, M., de la Fuente, L., Marti, C., Pereira, C., Pardo-Palacios, F. J., Del Risco, H., Ferrell, M., Mellado, M., Macchietto, M., Verheggen, K., Edelmann, M., Ezkurdia, I., Vazquez, J., Tress, M., Mortazavi, A., Martens, L., Rodriguez-Navarro, S., Moreno-Manzano, V., & Conesa, A. (2018). SQANTI: extensive characterization of long-read transcript sequences for quality control in full-length transcriptome identification and quantification. *Genome Res.* https://doi.org/10.1101/gr.222976.117

Tchkonia, T., Thomou, T., Zhu, Y., Karagiannides, I., Pothoulakis, C., Jensen, M. D., & Kirkland, J. L. (2013). Mechanisms and metabolic implications of regional differences among fat depots. *Cell Metab.*, *17*(5), 644–656. https://doi.org/10.1016/j.cmet.2013.03.008

Tchoukalova, Y. D., Votruba, S. B., Tchkonia, T., Giorgadze, N., Kirkland, J. L., & Jensen, M. D. (2010). Regional differences in cellular mechanisms of adipose tissue gain with overfeeding. *Proc. Natl. Acad. Sci. U. S. A.*, *107*(42), 18226–18231. https://doi.org/10.1073/pnas.1005259107

Tebaldi, T., Re, A., Viero, G., Pegoretti, I., Passerini, A., Blanzieri, E., & Quattrone, A. (2012). Widespread uncoupling between transcriptome and translatome variations after a stimulus in mammalian cells. *BMC Genomics*, *13*, 220. https://doi.org/10.1186/1471-2164-13-220

Tharp, K. M., Kang, M. S., Timblin, G. A., Dempersmier, J., Dempsey, G. E., Zushin, P.-J. H., Benavides, J., Choi, C., Li, C. X., Jha, A. K., Kajimura, S., Healy, K. E., Sul, H. S., Saijo, K., Kumar, S., & Stahl, A. (2018). Actomyosin-Mediated Tension Orchestrates Uncoupled Respiration in Adipose Tissues. *Cell Metab.*, *27*(3), 602–615.e4. https://doi.org/10.1016/j.cmet.2018.02.005

Toivola, D. M., Tao, G.-Z., Habtezion, A., Liao, J., & Omary, M. B. (2005). Cellular integrity plus: organelle-related and protein-targeting functions of intermediate filaments. *Trends Cell Biol.*, *15*(11), 608–617. https://doi.org/10.1016/j.tcb.2005.09.004

Tordjman, J. (2013). Histology of Adipose Tissue. In J.-P. Bastard & B. Fève (Eds.), *Physiology and Physiopathology of Adipose Tissue* (pp. 67–75). Springer Paris. https://doi.org/10.1007/978-2-8178-0343-2_6

Torrino, S., & Bertero, T. (2022). Metabo-reciprocity in cell mechanics: feeling the demands/feeding the demand. *Trends Cell Biol.*, *32*(7), 624–636. https://doi.org/10.1016/j.tcb.2022.01.013

Tsai, M.-C., Manor, O., Wan, Y., Mosammaparast, N., Wang, J. K., Lan, F., Shi, Y., Segal, E., & Chang, H. Y. (2010). Long noncoding RNA as modular scaffold of histone modification complexes. *Science*, *329*(5992), 689–693. https://doi.org/10.1126/science.1192002

Ugarte, F., Sousae, R., Cinquin, B., Martin, E. W., Krietsch, J., Sanchez, G., Inman, M., Tsang, H., Warr, M., Passegué, E., Larabell, C. A., & Forsberg, E. C. (2015). Progressive Chromatin Condensation and H3K9 Methylation Regulate the Differentiation of Embryonic and Hematopoietic Stem Cells. *Stem Cell Reports*, *5*(5), 728–740. https://doi.org/10.1016/j.stemcr.2015.09.009

Ulitsky, I., & Bartel, D. P. (2013). lincRNAs: genomics, evolution, and mechanisms. *Cell*, *154*(1), 26–46. https://doi.org/10.1016/j.cell.2013.06.020

van Mierlo, G., Veenstra, G. J. C., Vermeulen, M., & Marks, H. (2019). The Complexity of PRC2 Subcomplexes. *Trends Cell Biol.*, *29*(8), 660–671. https://doi.org/10.1016/j.tcb.2019.05.004

van Steensel, B., & Belmont, A. S. (2017). Lamina-Associated Domains: Links with Chromosome Architecture, Heterochromatin, and Gene Repression. *Cell*, *169*(5), 780–791. https://doi.org/10.1016/j.cell.2017.04.022

Verstraeten, V. L. R. M., Renes, J., Ramaekers, F. C. S., Kamps, M., Kuijpers, H. J., Verheyen, F., Wabitsch, M., Steijlen, P. M., van Steensel, M. A. M., & Broers, J. L. V. (2011). Reorganization of the nuclear lamina and cytoskeleton in adipogenesis. *Histochem. Cell Biol.*, *135*(3), 251–261. https://doi.org/10.1007/s00418-011-0792-4

Vertii, A., Ou, J., Yu, J., Yan, A., Pagès, H., Liu, H., Zhu, L. J., & Kaufman, P. D. (2019). Two contrasting classes of nucleolus-associated domains in mouse fibroblast heterochromatin. *Genome Res.* https://doi.org/10.1101/gr.247072.118

Wang, W., & Seale, P. (2016). Control of brown and beige fat development. *Nat. Rev. Mol. Cell Biol.*, *17*(11), 691–702. https://doi.org/10.1038/nrm.2016.96

Watanabe-Susaki, K., Takada, H., Enomoto, K., Miwata, K., Ishimine, H., Intoh, A., Ohtaka, M., Nakanishi, M., Sugino, H., Asashima, M., & Kurisaki, A. (2014). Biosynthesis of ribosomal RNA in nucleoli regulates pluripotency and differentiation ability of pluripotent stem cells. *Stem Cells*, *32*(12), 3099–3111. https://doi.org/10.1002/stem.1825

Webster, K. D., Ng, W. P., & Fletcher, D. A. (2014). Tensional homeostasis in single fibroblasts. *Biophys. J.*, *107*(1), 146–155. https://doi.org/10.1016/j.bpj.2014.04.051

Weeks, S. E., Metge, B. J., & Samant, R. S. (2019). The nucleolus: a central response hub for the stressors that drive cancer progression. *Cell. Mol. Life Sci.*, *76*(22), 4511–4524. https://doi.org/10.1007/s00018-019-03231-0

Wei, B., Wei, W., Zhao, B., Guo, X., & Liu, S. (2017). Long non-coding RNA HOTAIR inhibits miR-17-5p to regulate osteogenic differentiation and proliferation in non-traumatic osteonecrosis of femoral head. *PLoS One*, *12*(2), e0169097. https://doi.org/10.1371/journal.pone.0169097

Wei, S., Fan, Q., Yang, L., Zhang, X., Ma, Y., Zong, Z., Hua, X., Su, D., Sun, H., Li, H., & Liu, Z. (2017). Promotion of glycolysis by HOTAIR through GLUT1 upregulation via mTOR signaling. *Oncol. Rep.*, *38*(3), 1902–1908. https://doi.org/10.3892/or.2017.5840

Welsh, G. I., Griffiths, M. R., Webster, K. J., Page, M. J., & Tavaré, J. M. (2004). Proteome analysis of adipogenesis. *Proteomics*, *4*(4), 1042–1051. https://doi.org/10.1002/pmic.200300675

Weyer, C., Foley, J. E., Bogardus, C., Tataranni, P. A., & Pratley, R. E. (2000). Enlarged subcutaneous abdominal adipocyte size, but not obesity itself, predicts type II diabetes independent of insulin resistance. *Diabetologia*, *43*(12), 1498–1506. https://doi.org/10.1007/s001250051560

Willett, M., Brocard, M., Davide, A., & Morley, S. J. (2011). Translation initiation factors and active sites of protein synthesis co-localize at the leading edge of migrating fibroblasts. *Biochem. J*, *438*(1), 217–227. https://doi.org/10.1042/BJ20110435

Wolosewick, J. J., & Porter, K. R. (1976). Stereo high-voltage electron microscopy of whole cells of the human diploid line, WI-38. *Am. J. Anat.*, *147*(3), 303–323. https://doi.org/10.1002/aja.1001470305

Woolnough, J. L., Atwood, B. L., Liu, Z., Zhao, R., & Giles, K. E. (2016). The Regulation of rRNA Gene Transcription during Directed Differentiation of Human Embryonic Stem Cells. *PLoS One*, *11*(6), e0157276. https://doi.org/10.1371/journal.pone.0157276

Wu, L., Murat, P., Matak-Vinkovic, D., Murrell, A., & Balasubramanian, S. (2013). Binding interactions between long noncoding RNA HOTAIR and PRC2 proteins. *Biochemistry*, *52*(52), 9519–9527. https://doi.org/10.1021/bi401085h

Xiang, J.-F., Yin, Q.-F., Chen, T., Zhang, Y., Zhang, X.-O., Wu, Z., Zhang, S., Wang, H.-B., Ge, J., Lu, X., Yang, L., & Chen, L.-L. (2014). Human colorectal cancer-specific CCAT1-L lncRNA regulates long-range chromatin interactions at the MYC locus. *Cell Res.*, *24*(5), 513–531. https://doi.org/10.1038/cr.2014.35

Xu, F., & Zhang, J. (2017). Long non-coding RNA HOTAIR functions as miRNA sponge to promote the epithelial to mesenchymal transition in esophageal cancer. *Biomed. Pharmacother.*, *90*, 888–896. https://doi.org/10.1016/j.biopha.2017.03.103

Yamashita, H., Takenoshita, M., Sakurai, M., Bruick, R. K., Henzel, W. J., Shillinglaw, W., Arnot, D., & Uyeda, K. (2001). A glucose-responsive transcription factor that regulates carbohydrate metabolism in the liver. *Proc. Natl. Acad. Sci. U. S. A.*, *98*(16), 9116–9121. https://doi.org/10.1073/pnas.161284298

Yang, K., Wang, M., Zhao, Y., Sun, X., Yang, Y., Li, X., Zhou, A., Chu, H., Zhou, H., Xu, J., Wu, M., Yang, J., & Yi, J. (2016). A redox mechanism underlying nucleolar stress sensing by nucleophosmin. *Nat. Commun.*, *7*, 13599. https://doi.org/10.1038/ncomms13599

Yang, W., Guo, X., Thein, S., Xu, F., Sugii, S., Baas, P. W., Radda, G. K., & Han, W. (2013). Regulation of adipogenesis by cytoskeleton remodelling is facilitated by acetyltransferase MEC-17-dependent acetylation of α-tubulin. *Biochem. J*, *449*(3), 605–612. https://doi.org/10.1042/BJ20121121

Yang, W., Thein, S., Lim, C.-Y., Ericksen, R. E., Sugii, S., Xu, F., Robinson, R. C., Kim, J. B., & Han, W. (2014). Arp2/3 complex regulates adipogenesis by controlling cortical actin remodelling. *Biochem. J*, *464*(2), 179–192. https://doi.org/10.1042/BJ20140805

Yasuaki Kubo, Sachiko Kaidzu, Ikuyo Nakajima, Kazuaki Takenouchi, & Nakamura, F. (2000). Organization of Extracellular Matrix Components during Differentiation of Adipocytes in Long-Term Culture. *In Vitro Cell. Dev. Biol. Anim.*, *36*(1), 38–44.

Yeh, W. C., Cao, Z., Classon, M., & McKnight, S. L. (1995). Cascade regulation of terminal adipocyte differentiation by three members of the C/EBP family of leucine zipper proteins. *Genes Dev.*, *9*(2), 168–181. https://doi.org/10.1101/gad.9.2.168

Yim, J.-E., Heshka, S., Albu, J. B., Heymsfield, S., & Gallagher, D. (2008). Femoral-gluteal subcutaneous and intermuscular adipose tissues have independent and opposing relationships with CVD risk. *J. Appl. Physiol.*, *104*(3), 700–707. https://doi.org/10.1152/japplphysiol.01035.2007

Yin, Y., Yan, P., Lu, J., Song, G., Zhu, Y., Li, Z., Zhao, Y., Shen, B., Huang, X., Zhu, H., Orkin, S. H., & Shen, X. (2015). Opposing Roles for the lncRNA Haunt and Its Genomic Locus in Regulating HOXA Gene Activation during Embryonic Stem Cell Differentiation. *Cell Stem Cell*, *16*(5), 504–516. https://doi.org/10.1016/j.stem.2015.03.007

Yoon, J.-H., Abdelmohsen, K., Kim, J., Yang, X., Martindale, J. L., Tominaga-Yamanaka, K., White, E. J., Orjalo, A. V., Rinn, J. L., Kreft, S. G., Wilson, G. M., & Gorospe, M. (2013). Scaffold function of long non-coding RNA HOTAIR in protein ubiquitination. *Nat. Commun.*, *4*, 2939. https://doi.org/10.1038/ncomms3939

Zaadstra, B. M., Seidell, J. C., Van Noord, P. A., te Velde, E. R., Habbema, J. D., Vrieswijk, B., & Karbaat, J. (1993). Fat and female fecundity: prospective study of effect of body fat distribution on conception rates. *BMJ*, *306*(6876), 484–487. https://doi.org/10.1136/bmj.306.6876.484

Zha, B. S., & Zhou, H. (2012). ER Stress and Lipid Metabolism in Adipocytes. *Biochem. Res. Int.*, *2012*, 312943. https://doi.org/10.1155/2012/312943

Zhai, N., Xia, Y., Yin, R., Liu, J., & Gao, F. (2016). A negative regulation loop of long noncoding RNA HOTAIR and p53 in non-small-cell lung cancer. *Onco. Targets. Ther.*, *9*, 5713–5720. https://doi.org/10.2147/OTT.S110219

Zhang, Q., Ramlee, M. K., Brunmeir, R., Villanueva, C. J., Halperin, D., & Xu, F. (2012). Dynamic and distinct histone modifications modulate the expression of key adipogenesis regulatory genes. *Cell Cycle*, *11*(23), 4310–4322. https://doi.org/10.4161/cc.22224

Zhang, Z., Zhu, H., Liu, Y., Quan, F., Zhang, X., & Yu, L. (2018). LncRNA HOTAIR mediates TGF-β2-induced cell growth and epithelial-mesenchymal transition in human lens epithelial cells. *Acta Biochim. Biophys. Sin.*, *50*(10), 1028–1037. https://doi.org/10.1093/abbs/gmy101

Zhao, J., Ohsumi, T. K., Kung, J. T., Ogawa, Y., Grau, D. J., Sarma, K., Song, J. J., Kingston, R. E., Borowsky, M., & Lee, J. T. (2010). Genome-wide identification of polycomb-associated RNAs by RIP-seq. *Mol. Cell*, *40*(6), 939–953. https://doi.org/10.1016/j.molcel.2010.12.011

Zheng, P., Xiong, Q., Wu, Y., Chen, Y., Chen, Z., Fleming, J., Gao, D., Bi, L., & Ge, F. (2015). Quantitative Proteomics Analysis Reveals Novel Insights into Mechanisms of Action of Long Noncoding RNA Hox Transcript Antisense Intergenic RNA (HOTAIR) in HeLa Cells. *Mol. Cell. Proteomics*, *14*(6), 1447–1463. https://doi.org/10.1074/mcp.M114.043984

Zhu, Q., Wong, A. K., Krishnan, A., Aure, M. R., Tadych, A., Zhang, R., Corney, D. C., Greene, C. S., Bongo, L. A., Kristensen, V. N., Charikar, M., Li, K., & Troyanskaya, O. G. (2015). Targeted exploration and analysis of large cross-platform human transcriptomic compendia. *Nat. Methods*, *12*(3), 211–4, 3 p following 214. https://doi.org/10.1038/nmeth.3249

Zhuang, Y., Wang, X., Nguyen, H. T., Zhuo, Y., Cui, X., Fewell, C., Flemington, E. K., & Shan, B. (2013). Induction of long intergenic non-coding RNA HOTAIR in lung cancer cells by type I collagen. *J. Hematol. Oncol.*, *6*, 35. https://doi.org/10.1186/1756-8722-6-35

Zwick, R. K., Guerrero-Juarez, C. F., Horsley, V., & Plikus, M. V. (2018). Anatomical, Physiological, and Functional Diversity of Adipose Tissue. *Cell Metab.*, *27*(1), 68–83. https://doi.org/10.1016/j.cmet.2017.12.002

Papers

Paper I

De novo annotation of lncRNA *HOTAIR* transcripts by long-read RNA capture-seq reveals a differentiation-driven isoform switch

I

Evdokiia Potolitsyna*, Sarah Hazell Pickering*, Ave Tooming-Klunderud, Philippe Collas and Nolwenn Briand

De novo annotation of lncRNA *HOTAIR* transcripts by long-read RNA capture-seq reveals a differentiation-driven isoform switch

Evdokiia Potolitsyna[1,§], Sarah Hazell Pickering[1,2,§], Ave Tooming-Klunderud[3], Philippe Collas[1,2,*] and Nolwenn Briand[1,2,*]

[1]Department of Molecular Medicine, Institute of Basic Medical Sciences, Faculty of Medicine, University of Oslo, Oslo, Norway

[2]Department of Immunology and Transfusion Medicine, Oslo University Hospital, Oslo, Norway

[3]Centre for Ecological and Evolutionary Synthesis, Department of Biosciences, University of Oslo, Oslo, Norway

[§]Equal contribution

*Correspondence to: nolwenn.briand@medisin.uio.no (NB); philc@medisin.uio.no (PC)

Evdokiia Potolitsyna: evdokiia.potolitsyna@medisin.uio.no

Sarah Hazell Pickering: s.h.pickering@medisin.uio.no

Ave Tooming-Klunderud: ave.tooming-klunderud@ibv.uio.no

Philippe Collas: philc@medisin.uio.no

Nolwenn Briand: nolwenn.briand@medisin.uio.no

Abstract

Background: LncRNAs are tissue-specific and emerge as important regulators of various biological processes and as disease biomarkers. *HOTAIR* is a well-established pro-oncogenic lncRNA which has been attributed a variety of functions in cancer and native contexts. However, a lack of an exhaustive, cell type-specific annotation questions whether *HOTAIR* functions are supported by the expression of multiple isoforms.

Results: Using a capture long-read sequencing approach, we characterize *HOTAIR* isoforms expressed in human primary adipose stem cells. We find *HOTAIR* isoforms population displays varied splicing patterns, frequently leading to the exclusion or truncation of canonical LSD1 and PRC2 binding domains. We identify a highly cell type-specific *HOTAIR* isoform pool regulated by distinct promoter usage, and uncover a shift in the *HOTAIR* TSS usage that modulates the balance of *HOTAIR* isoforms at differentiation onset.

Conclusion: Our results highlight the complexity and cell type-specificity of *HOTAIR* isoforms and open perspectives on functional implications of these variants and their balance to key cellular processes.

Keywords: ***HOTAIR*; adipose differentiation; adipose stem cells; capture-seq; long-read sequencing; lncRNA isoform**

Background

Long non-coding RNAs (lncRNAs) are increasingly recognized as major regulators of physiological processes and have emerged as biomarkers for disease diagnosis and prognosis [1]. *HOTAIR* (*HOX* Transcript Antisense RNA) is a long antisense transcript of ~500-2200 base pairs (bp) located within, and extending upstream of, the *HOXC11* gene, in the *HOXC* locus on chromosome 12. *HOTAIR* is mostly studied in cancer models where its overexpression promotes cell migration and metastasis by altering gene expression [2–5]. *HOTAIR* is also the most differentially expressed gene between upper- and lower-body adipose tissue, and its expression is induced during adipose differentiation of gluteofemoral adipose stem cells (hereafter referred to as ASCs) [6, 7]. The function of *HOTAIR* in adipose tissue remains, however, unclear. In contrast to its effect in cancer cell lines [8–11], *HOTAIR* overexpression does not affect adipose progenitors' gene expression or proliferation rates [7, 12]. These observations point to different functions and mechanisms of action of *HOTAIR* in cancer vs. mesenchymal progenitor cells.

LncRNAs interact with proteins, DNA and other RNAs to regulate gene expression at multiple levels. *HOTAIR* has been detected in the cytoplasm where it can promote ubiquitin-mediated proteolysis by associating with E3 ubiquitin ligases [13] or function as a microRNA sponge [14]. *HOTAIR* is also found in the nucleus, where it can bind chromatin [13, 15, 16] and act as scaffold for

chromatin-modifying complexes through binding to the Polycomb repressor complex PRC2 subunit EZH2 [17], a histone H3K27 methyltransferase, and to LSD1/KDM1A, the H3K4/K9 demethylase of the REST/CoREST complex [18]. Recent evidence demonstrates that HOTAIR-PRC2 binding can be modulated by changes in *HOTAIR* structure mediated by RNA binding protein (RBP)-RNA-lncRNA interactions [19].

LncRNA folding into secondary and tertiary structures dictates their interactome, making their function dependent on structural conservation[20]. While the full-length *HOTAIR* sequence is poorly evolutionarily conserved, folding prediction has identified two well-conserved structures in the 5' and 3' ends of *HOTAIR [21]*. The currently reported primary structure of the *HOTAIR* gene is complex, with 2 predicted promoters, multiple predicted transcription start sites (TSSs) and potential splice sites leading to several isoforms [22–25]. *HOTAIR* transcripts can harbor small exon length variations [26], or alternative splice site usage that eliminates the PRC2 [18] or RBP [19] binding domains. Therefore, distinct *HOTAIR* splice variants likely have distinct functions, warranting an isoform-specific annotation in relevant tissues.

Current reference annotations for lncRNAs are incomplete due to their overall low expression level, weak evolutionary conservation, and high tissue specificity [27]. Identification of lncRNA isoforms using short-read RNA sequencing (RNA-seq) is challenging because almost every exon can be alternatively spliced [30], and short reads cannot resolve the connectivity between distant exons. Long-read sequencing technologies can address this challenge by covering the entire RNA sequence in a single read, enabling mapping of isoform changes that may impact lncRNA structure and function [28].

Here, we combine long-read Capture-seq and Illumina short-read RNA-seq to resolve changes in the composition of *HOTAIR* isoforms in a well-characterized adipogenic differentiation system [29]. We uncover a temporal shift in the composition of *HOTAIR* isoforms upon induction of differentiation, regulated by distinct promoter usage and hormonal and nutrient-sensing pathways.

Results

HOTAIR is highly expressed in ASCs and regulated during adipogenesis

We first assessed *HOTAIR* expression level in ASCs versus cancer cell lines where *HOTAIR* function has been previously studied [30]. We find that *HOTAIR* expression level in ASCs from two unrelated donors is higher or comparable to that of cancer cell lines (**Fig. 1a**), confirming the relevance of primary ASCs as a model system to assess the relative abundance of *HOTAIR* isoforms.

We examined by short-read RNA-seq the transcriptome of ASCs in the proliferating stage (Pro), after cell cycle arrest (day 0; D0), and after 1, 3 and 9 days of adipogenic induction (D1, D3, D9). Hierarchical clustering of differentially expressed genes across time ($\alpha < 0.01$ between at least two consecutive time points) confirms the upregulation of genes pertaining to the hallmark "Adipogenesis", including the master adipogenic transcription factor *PPARG* (**Additional file 1, Fig. S1**). Moreover, *HOTAIR* displays a diphasic expression profile in this time course, with increased levels upon cell cycle arrest on D0, followed by a progressive downregulation (**Fig. 1b**). *HOTAIR* expression is maintained during osteogenic differentiation (**Fig. 1c**), indicating a lineage-specific mode of regulation.

Identification of main *HOTAIR* isoforms

To identify *HOTAIR* isoforms, we performed PacBio single-molecule, long-read isoform sequencing of captured polyadenylated *HOTAIR* transcripts (PacBio Capture-seq) in proliferating ASCs and during adipose differentiation. Full-length reads were clustered into non-redundant transcripts and aligned to the hg38 genome assembly,

providing excellent coverage over the *HOTAIR* locus with sharp exon boundaries (**Fig. 2a,b**). The Isoseq3 pipeline yielded ~6000 *HOTAIR* isoforms; these were further filtered and merged both across time points and based on internal junctions using Cupcake ToFU [31, 32] or TAMA [33] (**Fig. 2a**), resulting in 34 isoforms (**Fig. 2a,c; Additional file 2, Table S1, Additional file 3**).

To characterize these *HOTAIR* isoforms, we first classified transcripts into four main categories using SQANTI [34]. Out of the 34 aforementioned isoforms, we find (i) 8 full splice matches (FSM) transcripts, (ii) 6 incomplete splice matches (ISM) of an annotated (known) transcript, (iii) 12 novel in catalog (NIC) transcripts containing new combinations of annotated splice sites, and (iv) 8 novel not in catalog (NNC) transcripts using at least one unannotated splice site (**Fig. 2d, Additional file 1, Fig. S2**). Second, we assessed isoform variations at the 5' and 3' ends. Transcripts start sites supported by Cap analysis of gene expression (CAGE) data are distributed evenly across SQANTI categories, with 15 transcripts starting within 15 bp of a CAGE peak summit (**Fig. 2e**). Transcripts with a TSS located more than 250 bp away from a CAGE peak likely represent lowly expressed or highly cell type-specific isoforms of *HOTAIR*, explaining the absence of a dedicated CAGE peak [35, 36]. *HOTAIR* full length transcripts also show variable 3' ends (exon 7; E7) corresponding to the alternative usage of 4 different canonical polyA signals for transcription termination (**Fig. 2f, Additional file 2, Table S2**). Third, we find the highest number of reads for transcripts in FSM, ISM and NIC SQANTI categories (**Fig. 2g**), indicating that most *HOTAIR* transcripts identified here have a known exon and splice junction composition.

To identify the top isoforms expressed across differentiation, we further filtered candidates based on read counts (**Fig. 2h**). Only 23 transcripts accumulate more than 100 reads, and these are also detected in at least 2 samples. These 23 high-confidence isoforms arise from multiple TSS usage, alternative splicing and intron retention events, as well as polyA site usage (**Fig. 2i**). Altogether, our PacBio sequencing analysis identifies with high confidence known and novel uncharacterized *HOTAIR* transcript isoforms in our adipose differentiation system, with notable variation in their TSS and polyA site usage.

HOTAIR splicing affects LSD1 and PRC2 interacting domains

HOTAIR has been described as a scaffold for LSD1 [18] and PRC2 [18], epigenetic modifiers involved in the regulation of adipogenesis [37–39]. The LSD1 binding domain lies in the last 500 bp of *HOTAIR* exon 7 (E7), whereas the PRC2 binding domain spans exons 4 and 5 [40] (**Fig. 3a**).

Inclusion of the LSD1 binding domain in *HOTAIR* isoforms depends on polyA site usage (see **Fig. 3a; Fig. 2f,i**); thus we examined potential changes in exon E7 length during adipogenesis. The proportion of PacBio reads for the long forms of E7, harboring the LSD1 binding domain, does not significantly vary during differentiation (**Fig. 3b**). In agreement, the expression profile of LSD1-containing *HOTAIR* isoforms (E7 long and medium) is similar to that of the total isoform pool (E7 short) (**Fig. 3c,** see **Fig. 1bc**), confirming that alternative polyadenylation pattern of *HOTAIR* is maintained during differentiation (**Fig. 3c**). Hence, variations in *HOTAIR* isoforms during adipogenesis do not in principle impact its LSD1 scaffolding function.

We next investigated alternative splicing events affecting the PRC2 binding domain. Analysis of exon E5 alternative splicing reveals two major alternative splice sites (site 1 and site 3) (**Fig. 3d**). Induction of differentiation promotes splicing at site 3, leading to a slight increase in proportion of the shorter E5 variant (**Fig. 3e**). This splicing event can be readily detected by semi-quantitative RT-PCR analysis of exon E3-E5 expression in ASCs from two independent individuals (**Fig. 3f, Additional file 1, Fig.**

S3a,b,c), emphasizing the robustness of the PacBio approach in capturing relative variations in *HOTAIR* transcript levels during differentiation. Overall, PacBio Capture-seq analysis reveals that *HOTAIR* is expressed as a pool of isoforms with differential ability to bind LSD1 and PRC2. However, adipogenic induction does not significantly affect the proportion of isoforms with LSD1 or PRC2 binding capacity.

Adipogenic induction triggers a switch in *HOTAIR* isoform start sites

One noticeable feature of *HOTAIR* isoform pool is the presence of 9 distinct start sites (**Fig. 4a**, see **Fig. 2i**). To assess TSS usage, we first quantified the total number of reads for each exon start category in PacBio Capture-Seq dataset (**Fig. 4b**). Only transcripts starting from exons E2, E3, E3.1 and E5 cumulated more than 500 reads during differentiation. We next quantified the proportion of each of *HOTAIR* 23 high-confidence isoform at each time point (**Fig. 4c**). Strikingly, while E3.1-starting isoforms contribute to the majority of reads prior to differentiation onset (Pro, D0), adipogenic induction triggers a decrease in the E3.1-starting isoform pool which is compensated by an increase in E3-starting isoform expression (**Fig. 4c,d,e**). Short-read RNA-seq analysis confirms this switch in TSS usage, with exon E3 becoming significantly more expressed than E3.1 upon differentiation onset (D1; **Fig. 4f**). The sharp drop in E3.1 starting isoforms is readily observed by semi-quantitative RT-PCR using primers spanning exons E3.1-E4, while expression of E3-E5 containing isoforms is maintained during early adipogenesis (**Fig. 4g**, left; **Additional file 1, Fig. S3b**). Importantly, osteogenic differentiation of ASCs maintains E3.1 isoforms expression (**Fig. 4g**, right; **Additional file 1, Fig. S3a**), indicating an adipose-specific regulation of *HOTAIR* isoforms. We conclude that adipogenic commitment triggers a switch in *HOTAIR* TSS usage, potentially impacting functional binding domains located in 5' exons [19].

ASCs express a cell type-specific *HOTAIR* isoform

To assess cell type- and tissue-specificity of E3.1 starting *HOTAIR* isoforms, we used Snaptron [41], a search engine for querying splicing patterns in publicly available RNA-seq datasets (**Additional file 2, Table S3**). We found only 24 cell samples with more than 10 reads containing the E3.1-E4 junction, while the E3-E4 junction was detected in 672 samples (**Fig. 5a**; **Additional file 2**, **Table S4**). We confirmed by semi-quantitative RT-PCR the expression of exon E3.1 in cultured primary myoblasts, BJ fibroblasts and HEK 293T cells – albeit to lower levels than in ASCs – and its absence in HeLa cells (**Fig. 5b**).

To gain insight into the regulation of *HOTAIR* isoform expression, we examined the chromatin accessibility landscape of the *HOTAIR* locus in published Assay for Transposable Accessible Chromatin (ATAC)-seq data [42–45] (**Fig. 5c**). We find two regions of accessible ('open') chromatin in ASCs (R3, R4), which our chromatin immunoprecipitation (ChIP)-seq data show are also enriched in H3K4me3 and H3K27ac, histone modifications characterizing active regulatory sites (**Fig. 5c, d**). Region R3 coincides with both activating and repressing regulatory element (REM) annotations by EpiRegio [46], suggesting it constitutes a bivalent regulator for *HOTAIR* or nearby genes expression. Region R4, located immediately upstream of exon E3.1 is also in an 'open' chromatin in myoblasts but not in HeLa cells, which respectively do and do not express E3.1-starting transcripts (**Fig. 5b,c**), and likely represents the active promoter for E3.1-starting isoforms. In contrast, these regions are in a 'closed' configuration in mature adipocytes, consistent with *HOTAIR* downregulation during adipogenesis (see **Fig. 1b**). Thus, *HOTAIR* displays active regulatory sites in ASCs, in line with the expression of specific isoforms. However, *HOTAIR* upregulation upon cell cycle arrest is not accompanied by changes of H3K4me3

and H3K27ac levels, and loss of H3K4me3 at region 4 occurs only at later differentiation time points (D3 and D9). Thus, modulation of *HOTAIR* levels during adipogenesis is not mediated by epigenetic regulation (**Fig. 5d**).

HOTAIR stability increases upon cell cycle arrest

HOTAIR half-life varies according to cell type, from 4 h in HeLa cells [13] to more than 7 h in primary trophoblast cells [47]. We therefore asked whether increased *HOTAIR* levels upon cell cycle arrest (D0; see **Fig. 1b**) could relate to a change in lncRNA stability. Treatment with Flavopiridol to inhibit RNA polymerase II (Pol II) transcription reveals an increase in *HOTAIR* half-life from 3 h in proliferating ASCs to > 4 h in D0 cells (**Fig. 6a**), while cell cycle arrest does not impact the stability of control short-lived *CEBPD* or long-lived *GAPDH* mRNA (**Fig. 6b,c**). Thus, while ATAC-seq data indicate that the *HOTAIR* isoform balance is likely regulated by cell type-specific transcription factors, the global increase in *HOTAIR* levels observed at D0 results at least in part from an increase in its stability.

Discussion

LncRNAs can modulate important biological and pathophysiological processes through their interaction with multiple partners. Our long-read Capture-seq of *HOTAIR* unveils a complex and dynamic pool of isoforms in differentiating ASCs. Adipogenic induction triggers a switch in the expression of main *HOTAIR* isoforms which likely impacts on its structure and interactome. Our results emphasize the importance of robust lncRNA annotation in the tissue of interest prior to functional characterization.

A single lncRNA locus can generate many transcript variants through alternative TSS usage, polyadenylation sites and splicing events [48]. We find that previously undescribed *HOTAIR* variants constitutes the major isoforms in human adipose stem cells, and show that not only lncRNA expression level, but also the isoform pool expressed can be highly cell type-specific, adding another layer of complexity to the regulation of biological processes by lncRNAs.

The chromatin landscape of the *HOTAIR* locus in ASCs is consistent with a promoter upstream of *HOTAIR* exon E3.1, which is in an 'open' and active epigenetic configuration in ASCs and myoblasts, where *HOTAIR* E3.1 starting isoforms are expressed, but not in HeLa cells. However, adipogenic induction results in only mild and delayed changes in active histone modification at this site, suggesting that expression of various *HOTAIR* isoforms is rather regulated by differentiation-stage specific transcription factors. In line, alternative promoter usage is elicited downstream of adipogenic, but not osteogenic, signaling pathways. Additionally, increased *HOTAIR* levels upon cell cycle arrest (D0 cells) also correlates with an increase in its stability. Interestingly, interaction with the RNA-binding protein HuR, a negative regulator of adipogenesis [49], reduces *HOTAIR* stability [13]. Alternatively, increased *HOTAIR* stability could result from its binding to a cell stage-specific protein partner. Collectively, our results indicate a tight, multifactorial regulation of isoform pool during adipogenesis, arguing for a functional importance of the isoform switch.

In cancer cell lines, *HOTAIR* has been reported to scaffold for chromatin regulators with broad effects on gene expression [50–52]. Our long-read sequencing data reveal multiple polyA site usage leading to the exclusion of the LSD1 binding domain at the 3' end, or alternative splicing events affecting the PRC2 minimal binding domain. However, the proportion of *HOTAIR* isoforms containing LSD1 or PRC2 domains does not vary during adipose differentiation, suggesting that *HOTAIR*'s role in adipogenesis is independent from its epigenetic scaffold function. Supporting this idea, *HOTAIR* depletion does not significantly affect PRC2-mediated gene regulation in adipose progenitors [12].

Recent studies have confirmed that a non-protein-coding locus can give rise to functionally distinct transcript isoforms [48, 53–55]. Of note, the switch in *HOTAIR* start site upon differentiation induction leads to the inclusion of *HOTAIR* exon 3 containing a protein binding domain [19], which likely alters *HOTAIR* function. Another intriguing possibility is that short sequence variations at the 5' end impact *HOTAIR*'s secondary structure and thus the folding of functional domains. Observation of *HOTAIR* structure using atomic force microscopy reveals multiple dynamic conformations [56]. It is therefore conceivable that *HOTAIR* functions via conformational changes, induced by or resulting from interactions with protein partners. Hence, variations in isoform composition likely results in cell type specific structures and interactomes, which could account for the divergent roles of *HOTAIR* in primary cells and cancer cell lines.

Conclusions

We generate the first cell type-specific, comprehensive catalog of *HOTAIR* isoforms in a physiological context and describe novel *HOTAIR* isoforms, alternative splicing events, and multiple start site usage. We find that *HOTAIR* splicing in ASCs often leads to the exclusion or truncation of canonical LSD1 and PRC2 binding domains. We uncover a shift in *HOTAIR* TSS usage that controls the balance of *HOTAIR* isoforms during early adipogenesis The variability of *HOTAIR* isoforms opens new perspectives for studies in (patho)physiological contexts.

Methods

All methods were performed in accordance with the guidelines and regulations of the University of Oslo.

Cell culture and differentiation

ASCs from two non-obese donors (ASC-1 and ASC-2) were cultured in DMEM/F12 with 10% fetal calf serum and 20 ng/ml basic fibroblast growth factor (Pro). Upon confluency, growth factor was removed, and cells were cultured for 72 h before induction of differentiation (D0). For adipose differentiation, ASCs were induced with 0.5 µM 1-methyl-3 isobutyl xanthine, 1 µM dexamethasone, 10 µg/ ml insulin and 200 µM indomethacin. For osteogenic differentiation, ASCs were induced with 0.1 µM dexamethasone, 10 mM β-glycerophosphate and 0.05 mM L-ascorbic acid-2 phosphate. Differentiation media was renewed every 3 days, and samples were harvested on D1, D3 and D9 after induction. Differentiation experiments were done in at least biological triplicates. HeLa cells (American Type Culture Collection; CCL-2) were cultured in MEM medium containing Glutamax (Gibco), 1% non-essential amino acids and 10% fetal calf serum. MDA-MB-231 and MCF-7 cells (both from American Type Culture Collection) were cultured in DMEM containing 10% fetal calf serum. Human myoblasts (Lonza) were cultured as described [57]. BJ fibroblasts (American Type Culture Collection) were cultured in DMEM/F12 with 10% fetal calf serum and 20 ng/ml basic fibroblast growth factor. HEK293T (Thermo Scientific) were cultured in DMEM/F12 with 10% fetal calf serum.

RT-qPCR and semi-quantitative PCR

Total RNA was isolated using the RNeasy kit (QIAGEN) and 1 µg was used for cDNA synthesis using the High-Capacity cDNA Reverse Transcription Kit (ThermoFisher). RT-PCR was done using IQ SYBR green (Biorad) with *SF3A1* as a reference gene. PCR conditions were 95°C for 3 min and 40 cycles of 95°C for 30 s, 60°C for 30 s, and 72°C for 20 s. Semi-quantitative PCR was done using a PCR Master Mix (ThermoFisher) with the following conditions: 95°C for 3 min and 30 cycles of 95°C for 30 s, 60°C for 30 s, and 72°C for 30 s. Products were separated in a 2.5% agarose gel with Tris-Borate-EDTA buffer. PCR primers are listed in **Additional file 2 Table S5.** Uncropped gels are presented in **Additional file 4, Fig. S4 to S7**.

Short-read Illumina RNA-sequencing and data analysis

Differentiation time courses from ASC-1 with 5 time points were sequenced in biological triplicates with short (40bp), paired end reads on Illumina NextSeq. Reads were aligned to the hg38 genome (ensembl v95 annotation) using hisat2, and counted with featureCounts (--fraction –M) . To further analyze differentially expressed genes, edgeR and limma packages were used . Low abundance genes were filtered using edgeR's function "filterByExpr". Genes with an adjusted p-value < 0.01 (eBayes method, limma package) between two or more consecutive time points were clustered with DPGP software. FDR adjusted p-value for Adipogenesis cluster was generated by overrepresentation analysis using Hallmark gene sets from MSigDb (v7.4) with all human genes as background. FeatureCounts with strict parameters (-f -g exon_id -p -s 2 -O --fraction -B -C) was used to quantify exon coverage as normalized counts per kilobase of exon sequence.

PacBio Capture-Seq

PacBio Capture-seq was performed on duplicate differentiation time courses from ASC-1. For each differentiation, RNA samples from 5 differentiation time points were used to synthesize full-length barcoded cDNA libraries using the Template Switching RT Enzyme Mix (NEB). Libraries were prepared using Pacific Biosciences protocol for cDNA Sequence Capture Using IDT xGen® Lockdown® probes (https://eu.idtdna.com/site/order/ngs). A pool of 100 probes against all known *HOTAIR* isoform sequences was designed using the IDT web tool. Full-length cDNA was cleaned up using Pronex beads, and 1200 ng was used for each hybridization reactions. Library was sequenced in one 8M SMRT cell on a Sequel II instrument using Sequel II Binding kit 2.1 and Sequencing chemistry v2.0.

Transcript identification from targeted long-read sequencing

CCS sequences were generated for the entire dataset using the Circular Consensus Sequence pipeline (SMRT Tools v 8.0.0.80502) with minimum number of passes 3 and minimum accuracy 0.99. CCS reads were demultiplexed using the Barcoding pipeline (SMRT Tools v7.0.0.63823). Iso-Seq analysis was performed using the Iso-Seq pipeline (SMRT Link v7.0.0.63985) with default settings. Only clustered isoforms with at least 2 subreads, 0.99 quality score and containing a polyA tail of at least 20 base pairs (bp) were used. Isoforms were aligned to the hg38 genome with minimap2 v.2.17 [58]. Primary alignments to the *HOTAIR* locus (chr12: 53,962,308-53,974,956) were selected as target *HOTAIR* transcripts if they had a mapping quality above 20 and less than 50 clipped nucleotides (samclip; https://github.com/tseemann/samclip). Single exon and sense transcripts were also filtered.

HOTAIR transcripts were collapsed with both Cupcake Tofu [31] (https://github.com/Magdoll/cDNA_Cupcake) and TAMA [33] (https://github.com/GenomeRIK/tama). Parameters --dun-merge-5-shorter and –x capped were used for cupcake and TAMA respectively, to prevent shorter transcript models from being merged into longer ones. For TAMA, –z 100 was also set to increase the allowed 3’ variability. To combine transcript lists between timepoints, collapsed transcripts with at least 50 full length reads within one sample were merged using cupcake chain_samples.py or tama_merge.py. Initially this produced ~80 HOTAIR transcripts, with much of the variation in the ends of 3' and 5' exons. To achieve a final transcript list, collapsed transcripts were merged on internal junctions only by increasing the allowed 5' and 3' variability (with TAMA options -a 300 -z 2000) and ranking libraries by the number of polyadenylated *HOTAIR* reads. This resulted in 34 TAMA isoforms.

Final cross-validation was conducted by running SQANTI with unclustered ccs reads as the "novel long read-defined transcriptome" and the top 34 TAMA isoforms as the "reference annotation". This assigned full length reads to their corresponding TAMA isoform and reads annotated as full-splice match were counted for each isoform. SQANTI was used again to classify transcripts against existing reference annotations and to search for polyA motifs near transcript ends from a list of potential human motifs (**Additional file 2, Tables S1, S2**) [34] (https://github.com/ConesaLab/SQANTI). Reference isoforms were collected from four sources: Ensembl (v95), RefSeq, UCSC browser's "lincRNA and TUCP transcripts" and Fantom CAT (Hon 2015), the last of which included isoforms from encode, hubmap and miTranscriptome (**Additional File 1 Fig. S2**). SQANTI categories are defined relative to the reference isoforms as follows (i) FSM: the number of exons and all internal junctions are concordant with the reference isoform. (ii) ISM: the isoform has less 5' exons than the reference, and yet the internal junctions are perfectly consistent. (iii) NIC: all donor and acceptor sites exist in the reference isoform list but their combination in a single isoform is novel. (iv) NNC: at least one of the donor or acceptor sites in the isoform is not found in the reference list. For all categories, the exact length of the 5' and 3' ends of first and last exons, respectively, can differ by any amount.

Snaptron

We searched Snaptron's SRA V2 database [41] , which contains ~49000 public samples, for experiments with reads overlapping *HOTAIR* exon-exon junctions with the web query http://snaptron.cs.jhu.edu/srav2/snaptron?regions=HOTAIR&rfilter=annotated:1 (Additional File 2, Table S3). Sample IDs for experiments with at least 10 exon spanning reads were extracted and cell type information accessed via a matching metadata query. A simplified version of the exon E3.1 metadata table is presented in **Additional file 2, Table S4**.

Chromatin immunoprecipitation

Cells ($2x10^6$/ChIP) were cross-linked with 1% formaldehyde for 10 min and cross-linking was stopped with 125 mM glycine. Cells were lysed for 10 min in ChIP lysis buffer (1% SDS, 10 mM EDTA, 50 mM Tris-HCl, pH 8.0, proteinase inhibitors, 1 mM PMSF, 20 mM Na Butyrate) and sonicated for 30 sec ON/OFF for 10 min in a Bioruptor®Pico (Diagenode) to generate 200-500 bp DNA fragments. After sedimentation at 10,000 g for 10 min, the supernatant was collected and diluted 5 times in RIPA buffer (140 mM NaCl, 10 mM Tris-HCl pH 8.0, 1 mM EDTA, 0.5 mM EGTA, 1% Triton X-100, 0.1% SDS, 0.1% sodium deoxycholate, protease inhibitors, 1 mM PMSF, 20 mM Na Butyrate). After a 100 µL sample was removed (input), diluted chromatin was incubated for 2 h with antibodies (2.5 µg/100 µL) coupled to magnetic Dynabeads Protein A (Invitrogen). ChIP samples were washed 4 times in ice-cold RIPA buffer, crosslinks were reversed and DNA was eluted for 2h at 68ºC in 50 mM NaCl, 20 mM Tris-HCl pH 7.5, 5 mM EDTA, 1% SDS and 50 ng/µl Proteinase K. DNA was purified and dissolved in H_2O. ChIP DNA was used as template for quantitative (q)PCR using SYBR® Green (BioRad), with 95ºC denaturation for 3 min and 40 cycles of 95 ºC for 30 sec, 60 ºC for 30 sec, and 72 ºC for 30 sec. Primers used for ChIP are listed in **Additional file 2**, **Table S5**.

Statistical analyses

Statistics were performed with GraphPad Prism 9.2.0 (https://www.graphpad.com/).

Abbreviations

ASCs, adipose stem cells; ChIP, chromatin immunoprecipitation; GSAT, gluteofemoral subcutaneous adipose tissue; *HOTAIR*, *HOX* Transcript Antisense RNA; LncRN long non-coding RNA; PRC2, polycomb repressor complex 2

Declarations

Ethics approval and consent to participate

The study was approved by the Regional Committee for Research Ethics for Southern Norway (REK 2013/2102 and REK 2018-660), and all subjects gave written informed consent.

Consent for publication

Not applicable.

Availability of data and material

The PacBio dataset supporting the conclusions of this article is available in the SRA repository under accession PRJNA730802 (https://www.ncbi.nlm.nih.gov/bioproject/PRJNA235292) and the filtered transcript list was submitted to GenBank (see accession numbers in **Additional file 1, Table S1**).

Bulk short-read RNA-Seq data has been deposited in the Gene Expression Omnibus (GEO) under accession GSE176020.

ATAC-seq data were obtained from GEO accession GSE118500.

(https://www.ncbi.nlm.nih.gov/geo/query/acc.cgi?acc=GSE118500), GSE139571 (https://www.ncbi.nlm.nih.gov/geo/query/acc.cgi?acc=GSE139571) and GSE157399 (https://www.ncbi.nlm.nih.gov/geo/query/acc.cgi?acc=GSE157399).

CAGE clusters and transcripts from [35] were obtained from FANTOM (https://fantom.gsc.riken.jp/5/suppl/Hon_et_al_2016/data/assembly/lv3_robust/). Other HOTAIR transcripts were downloaded from ensembl v95 [59] (http://jan2019.archive.ensembl.org/index.html) or from the UCSC browser at [60].

Regulatory elements (REMs) [46] associated with the *HOTAIR* locus were queried from the EpiRegio database (https://epiregio.de/geneQuery/; accessed: 23/04/2021).

Competing interests

The authors declare that they have no competing interests.

Funding

This work was funded by South-East Health Norway (grant 40040) and the Research Council of Norway (grant No. 249734 and 313508).

Authors' contributions

EP and NB generated data. SHP performed bioinformatic analysis. ATK performed *HOTAIR* capture and long-read sequencing. EP, SHP and NB interpreted data and made figures. NB supervised the work. EP, SHP, PC and NB wrote or revised the manuscript. All authors read and approved the final manuscript.

Acknowledgements

We thank Anita Løvstad Sørensen for technical assistance and the Norwegian Sequencing Center (Oslo University Hospital) for professional services.

References

1. Cantile M, Di Bonito M, Tracey De Bellis M, Botti G. Functional Interaction among lncRNA HOTAIR and MicroRNAs in Cancer and Other Human Diseases. Cancers . 2021;13.

2. Kogo R, Shimamura T, Mimori K, Kawahara K, Imoto S, Sudo T, et al. Long noncoding RNA HOTAIR regulates polycomb-dependent chromatin modification and is associated with poor prognosis in colorectal cancers. Cancer Res. 2011;71:6320–6.

3. Gupta RA, Shah N, Wang KC, Kim J, Horlings HM, Wong DJ, et al. Long non-coding RNA HOTAIR reprograms chromatin state to promote cancer metastasis. Nature. 2010;464:1071–6.

4. Xue X, Yang YA, Zhang A, Fong K-W, Kim J, Song B, et al. LncRNA HOTAIR enhances ER signaling and confers tamoxifen resistance in breast cancer. Oncogene. 2016;35:2746–55.

5. Milevskiy MJG, Al-Ejeh F, Saunus JM, Northwood KS, Bailey PJ, Betts JA, et al. Long-range regulators of the lncRNA HOTAIR enhance its prognostic potential in breast cancer. Hum Mol Genet. 2016;25:3269–83.

6. Pinnick KE, Nicholson G, Manolopoulos KN, McQuaid SE, Valet P, Frayn KN, et al. Distinct developmental profile of lower-body adipose tissue defines resistance against obesity-associated metabolic complications. Diabetes. 2014;63:3785–97.

7. Divoux A, Karastergiou K, Xie H, Guo W, Perera RJ, Fried SK, et al. Identification of a novel lncRNA in gluteal adipose tissue and evidence for its positive effect on preadipocyte differentiation. Obesity . 2014;22:1781–5.

8. Wu Y, Zhang L, Zhang L, Wang Y, Li H, Ren X, et al. Long non-coding RNA HOTAIR promotes tumor cell invasion and metastasis by recruiting EZH2 and repressing E-cadherin in oral squamous cell carcinoma. Int J Oncol. 2015;46:2586–94.

9. Wu Y, Liu J, Zheng Y, You L, Kuang D, Liu T. Suppressed expression of long non-coding RNA HOTAIR inhibits proliferation and tumourigenicity of renal carcinoma cells. Tumour Biol. 2014;35:11887–94.

10. Ding W, Ren J, Ren H, Wang D. Long Noncoding RNA HOTAIR Modulates MiR-206-mediated Bcl-w Signaling to Facilitate Cell Proliferation in Breast Cancer. Sci Rep. 2017;7:17261.

11. Wu Z-H, Wang X-L, Tang H-M, Jiang T, Chen J, Lu S, et al. Long non-coding RNA HOTAIR is a powerful predictor of metastasis and poor prognosis and is associated with epithelial-mesenchymal transition in colon cancer. Oncol Rep. 2014;32:395–402.

12. Kalwa M, Hänzelmann S, Otto S, Kuo C-C, Franzen J, Joussen S, et al. The lncRNA HOTAIR impacts on mesenchymal stem cells via triple helix formation. Nucleic Acids Res. 2016;44:10631–43.

13. Yoon J-H, Abdelmohsen K, Kim J, Yang X, Martindale JL, Tominaga-Yamanaka K, et al. Scaffold function of long non-coding RNA HOTAIR in protein ubiquitination. Nat Commun. 2013;4:2939.

14. Xu F, Zhang J. Long non-coding RNA HOTAIR functions as miRNA sponge to promote the epithelial to mesenchymal transition in esophageal cancer. Biomed Pharmacother. 2017;90:888–96.

15. Yu G-J, Sun Y, Zhang D-W, Zhang P. Long non-coding RNA HOTAIR functions as a competitive endogenous RNA to regulate PRAF2 expression by sponging miR-326 in cutaneous squamous cell carcinoma. Cancer Cell Int. 2019;19:270.

16. Zhao Y-H, Liu Y-L, Fei K-L, Li P. Long non-coding RNA HOTAIR modulates the progression of preeclampsia through inhibiting miR-106 in an EZH2-dependent manner. Life Sci. 2020;:117668.

17. Rinn JL, Kertesz M, Wang JK, Squazzo SL, Xu X, Brugmann SA, et al. Functional demarcation of active and silent chromatin domains in human HOX loci by noncoding RNAs. Cell. 2007;129:1311–23.

18. Tsai M-C, Manor O, Wan Y, Mosammaparast N, Wang JK, Lan F, et al. Long noncoding RNA as modular scaffold of histone modification complexes. Science. 2010;329:689–93.

19. Balas MM, Hartwick EW, Barrington C, Roberts JT, Wu SK, Bettcher R, et al. Establishing RNA-RNA interactions remodels lncRNA structure and promotes PRC2 activity. Sci Adv. 2021;7.

20. Graf J, Kretz M. From structure to function: Route to understanding lncRNA mechanism. Bioessays. 2020;42:e2000027.

21. He S, Liu S, Zhu H. The sequence, structure and evolutionary features of HOTAIR in mammals. BMC Evol Biol. 2011;11:102.

22. Hajjari M, Rahnama S. HOTAIR Long Non-coding RNA: Characterizing the Locus Features by the In Silico Approaches. Genomics Inform. 2017;15:170–7.

23. Harrow J, Frankish A, Gonzalez JM, Tapanari E, Diekhans M, Kokocinski F, et al. GENCODE: the reference human genome annotation for The ENCODE Project. Genome Res. 2012;22:1760–74.

24. O'Leary NA, Wright MW, Brister JR, Ciufo S, Haddad D, McVeigh R, et al. Reference sequence (RefSeq) database at NCBI: current status, taxonomic expansion, and functional annotation. Nucleic Acids Res. 2016;44:D733–45.

25. Schorderet P, Duboule D. Structural and functional differences in the long non-coding RNA hotair in mouse and human. PLoS Genet. 2011;7:e1002071.

26. Mercer TR, Gerhardt DJ, Dinger ME, Crawford J, Trapnell C, Jeddeloh JA, et al. Targeted RNA sequencing reveals the deep complexity of the human transcriptome. Nat Biotechnol. 2011;30:99–104.

27. Uszczynska-Ratajczak B, Lagarde J, Frankish A, Guigó R, Johnson R. Towards a

complete map of the human long non-coding RNA transcriptome. Nat Rev Genet. 2018;19:535–48.

28. Zampetaki A, Albrecht A, Steinhofel K. Long Non-coding RNA Structure and Function: Is There a Link? Front Physiol. 2018;9:1201.

29. Boquest AC, Collas P. Obtaining freshly isolated and cultured mesenchymal stem cells from human adipose tissue. Methods Mol Biol. 2012;879:269–78.

30. Meredith EK, Balas MM, Sindy K, Haislop K, Johnson AM. An RNA matchmaker protein regulates the activity of the long noncoding RNA HOTAIR. RNA. 2016;22:995–1010.

31. Gordon SP, Tseng E, Salamov A, Zhang J, Meng X, Zhao Z, et al. Widespread Polycistronic Transcripts in Fungi Revealed by Single-Molecule mRNA Sequencing. PLoS One. 2015;10:e0132628.

32. Tseng E. cDNA_Cupcake Wiki. Github.

33. Kuo RI, Cheng Y, Zhang R, Brown JWS, Smith J, Archibald AL, et al. Illuminating the dark side of the human transcriptome with long read transcript sequencing. BMC Genomics. 2020;21:751.

34. Tardaguila M, de la Fuente L, Marti C, Pereira C, Pardo-Palacios FJ, Del Risco H, et al. SQANTI: extensive characterization of long-read transcript sequences for quality control in full-length transcriptome identification and quantification. Genome Res. 2018. https://doi.org/10.1101/gr.222976.117.

35. Hon C-C, Ramilowski JA, Harshbarger J, Bertin N, Rackham OJL, Gough J, et al. An atlas of human long non-coding RNAs with accurate 5' ends. Nature. 2017;543:199–204.

36. Imada EL, Sanchez DF, Collado-Torres L, Wilks C, Matam T, Dinalankara W, et al. Recounting the FANTOM CAGE-Associated Transcriptome. Genome Res. 2020;30:1073–81.

37. Musri MM, Carmona MC, Hanzu FA, Kaliman P, Gomis R, Párrizas M. Histone demethylase LSD1 regulates adipogenesis. J Biol Chem. 2010;285:30034–41.

38. Chen Y, Kim J, Zhang R, Yang X, Zhang Y, Fang J, et al. Histone Demethylase LSD1 Promotes Adipocyte Differentiation through Repressing Wnt Signaling. Cell Chem Biol. 2016;23:1228–40.

39. Wang L, Jin Q, Lee J-E, Su I-H, Ge K. Histone H3K27 methyltransferase Ezh2 represses Wnt genes to facilitate adipogenesis. Proc Natl Acad Sci U S A. 2010;107:7317–22.

40. Wu L, Murat P, Matak-Vinkovic D, Murrell A, Balasubramanian S. Binding interactions between long noncoding RNA HOTAIR and PRC2 proteins. Biochemistry. 2013;52:9519–27.

41. Wilks C, Gaddipati P, Nellore A, Langmead B. Snaptron: querying splicing patterns across tens of thousands of RNA-seq samples. Bioinformatics. 2018;34:114–6.

42. Divoux A, Sandor K, Bojcsuk D, Talukder A, Li X, Balint BL, et al. Differential open chromatin profile and transcriptomic signature define depot-specific human subcutaneous preadipocytes: primary outcomes. Clin Epigenetics. 2018;10:148.

43. Divoux A, Sandor K, Bojcsuk D, Yi F, Hopf ME, Smith JS, et al. Fat Distribution in Women Is Associated With Depot-Specific Transcriptomic Signatures and Chromatin Structure. J Endocr Soc. 2020;4:bvaa042.

44. Martone J, Lisi M, Castagnetti F, Rosa A, Di Carlo V, Blanco E, et al. Trans-generational epigenetic regulation associated with the amelioration of Duchenne Muscular Dystrophy. EMBO Mol Med. 2020;12:e12063.

45. Fraser LCR, Dikdan RJ, Dey S, Singh A, Tyagi S. Reduction in gene expression noise by targeted increase in accessibility at gene loci. Proc Natl Acad Sci U S A. 2021;118:e2018640118.

46. Baumgarten N, Hecker D, Karunanithi S, Schmidt F, List M, Schulz MH. EpiRegio: analysis and retrieval of regulatory elements linked to genes. Nucleic Acids Res. 2020;48:W193–9.

47. Tian F-J, He X-Y, Wang J, Li X, Ma X-L, Wu F, et al. Elevated Tristetraprolin Impairs Trophoblast Invasion in Women with Recurrent Miscarriage by Destabilization of HOTAIR. Mol Ther Nucleic Acids. 2018;12:600–9.

48. Ziegler C, Kretz M. The More the Merrier-Complexity in Long Non-Coding RNA Loci. Front Endocrinol . 2017;8:90.

49. Siang DTC, Lim YC, Kyaw AMM, Win KN, Chia SY, Degirmenci U, et al. The RNA-binding protein HuR is a negative regulator in adipogenesis. Nat Commun. 2020;11:213.

50. Mozdarani H, Ezzatizadeh V, Rahbar Parvaneh R. The emerging role of the long non-coding RNA HOTAIR in breast cancer development and treatment. J Transl Med. 2020;18:152.

51. Hajjari M, Salavaty A. HOTAIR: an oncogenic

long non-coding RNA in different cancers. Cancer Biol Med. 2015;12:1–9.

52. Bhan A, Mandal SS. LncRNA HOTAIR: A master regulator of chromatin dynamics and cancer. Biochim Biophys Acta. 2015;1856:151–64.

53. Guo C-J, Ma X-K, Xing Y-H, Zheng C-C, Xu Y-F, Shan L, et al. Distinct Processing of lncRNAs Contributes to Non-conserved Functions in Stem Cells. Cell. 2020;181:621–36.e22.

54. Yuan J-H, Liu X-N, Wang T-T, Pan W, Tao Q-F, Zhou W-P, et al. The MBNL3 splicing factor promotes hepatocellular carcinoma by increasing PXN expression through the alternative splicing of lncRNA-PXN-AS1. Nat Cell Biol. 2017;19:820–32.

55. Li R, Harvey AR, Hodgetts SI, Fox AH. Functional dissection of NEAT1 using genome editing reveals substantial localization of the NEAT1_1 isoform outside paraspeckles. RNA. 2017;23:872–81.

56. Spokoini-Stern R, Stamov D, Jessel H, Aharoni L, Haschke H, Giron J, et al. Visualizing the structure and motion of the long noncoding RNA HOTAIR. RNA. 2020;26:629–36.

57. Oldenburg AR, Delbarre E, Thiede B, Vigouroux C, Collas P. Deregulation of Fragile X-related protein 1 by the lipodystrophic lamin A p.R482W mutation elicits a myogenic gene expression program in preadipocytes. Hum Mol Genet. 2014;23:1151–62.

58. Li H. Minimap2: pairwise alignment for nucleotide sequences. Bioinformatics. 2018;34:3094–100.

59. Cunningham F, Achuthan P, Akanni W, Allen J, Amode MR, Armean IM, et al. Ensembl 2019. Nucleic Acids Res. 2018;47:D745–51.

60. Schema for lincRNA TUCP - lincRNA and TUCP transcripts. https://genome.ucsc.edu/cgi-bin/hgTables?db=hg38&hgta_group=genes&hgta_track=lincRNAsTranscripts&hgta_table=lincRNAsTranscripts&hgta_doSchema=describe+table+schema. Accessed 28 Sep 2021.

61. Schmidt F, Marx A, Hebel M, Wegner M, Baumgarten N, Kaulich M, et al. Integrative analysis of epigenetics data identifies gene-specific regulatory elements. bioRxiv. 2019;:585125.

Figures

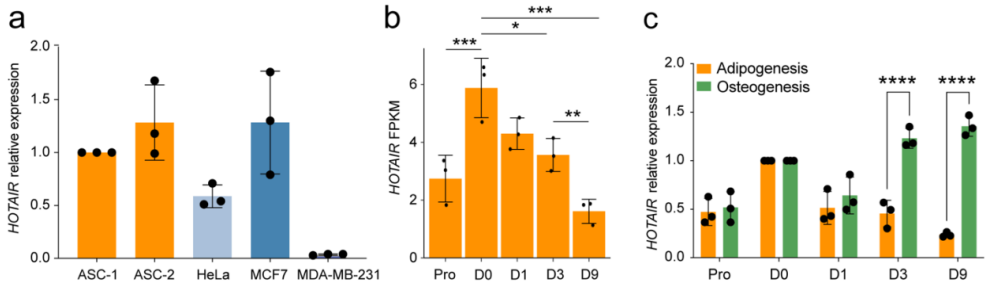

Figure 1. *HOTAIR* expression during adipogenic differentiation. a Quantitative RT-PCR analysis of *HOTAIR* expression in HeLa, MCF7, MDA-MB-231, and ASCs from two independent donors (ASC-1 and ASC-2). **b** Differential expression of *HOTAIR* between differentiation time points analyzed by short-read RNA-seq (mean ± SD; *p < 0.05, **p<0.01, ***p<0.001, limma moderated t-statistic; n = 3). **c** RT-qPCR analysis of *HOTAIR* relative expression, normalized to D0 ASCs, during adipogenic and osteogenic differentiation (mean fold difference ± SD; ****p < 0.0001, two-way ANOVA; n = 3).

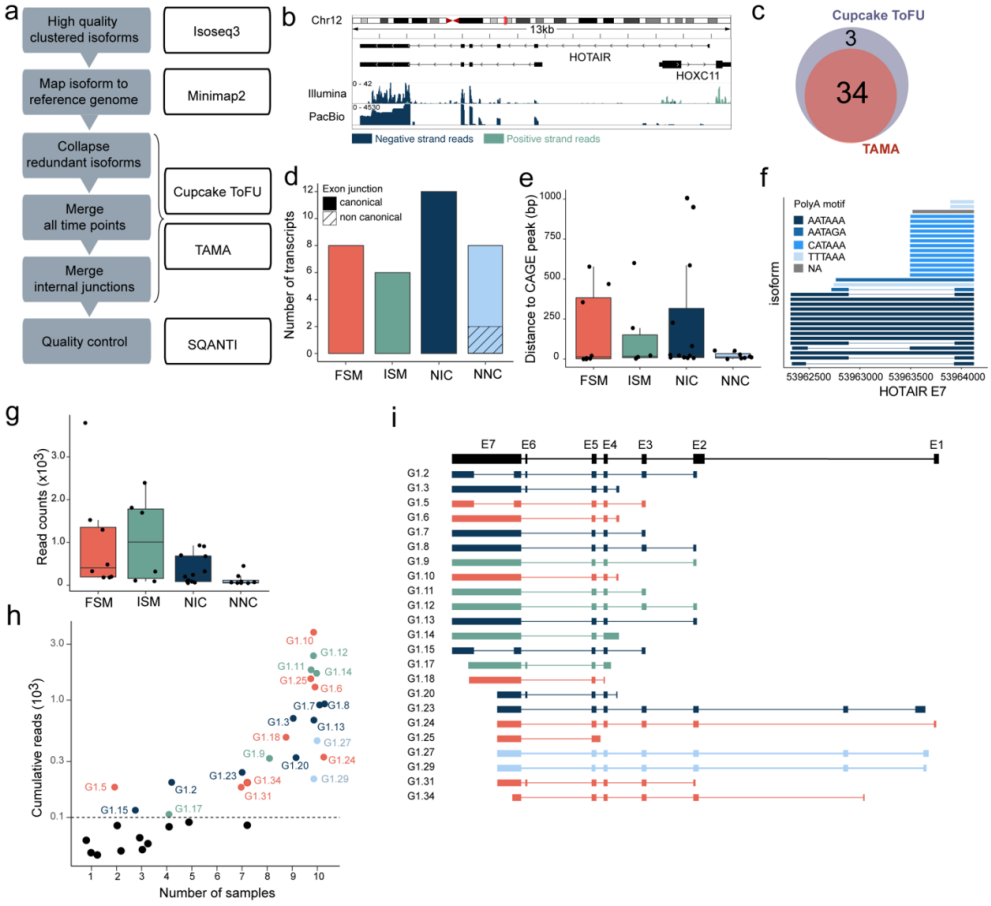

Figure 2. Identification of *HOTAIR* isoforms in differentiating ASCs. **a** Bioinformatic pipeline for identification of HOTAIR isoforms. **b** Representative integrative genomics viewer (IGV) tracks for short-read Illumina RNA-seq (upper) and PacBio capture-seq (lower) coverage tracks on *HOTAIR* (D0). **c** Venn diagram showing the overlap between *HOTAIR* isoforms identified using TAMA and Cupcake ToFU. **d-h** SQANTI characterization of 34 *HOTAIR* transcripts, with: **d** Number of isoforms per SQANTI categories and presence of non-canonical splice sites. **e** Distance in base pairs from the isoform start to the nearest CAGE peak summit from Ref. [34]. **f** HOTAIR exon E7 diagram showing 3' end polyA tails. **g** Cumulative read counts of the isoforms shown by SQANTI categories. **h** Cumulative read number per isoform vs. number of samples in which the isoform was detected (cutoff: 0.1×10^3 reads per isoform). **i** Exon structure of 23 high confidence *HOTAIR* isoforms colored by SQANTI categories. FSM: full splice match; ISM: incomplete splice match; NIC: novel in catalog; NNC: novel not in catalog.

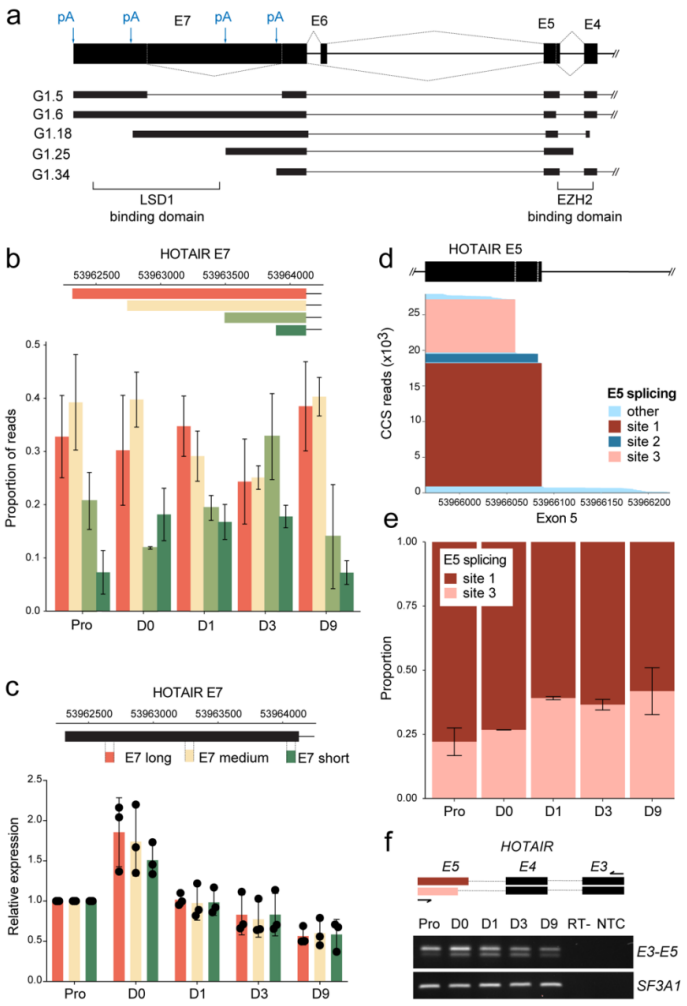

Figure 3. *HOTAIR* splicing across functional domains during adipogenesis. **a** Schematic representation of *HOTAIR* 3' exons (exons E4 to E7) containing LSD1 and PRC2 binding domains. Alternative splicing events and polyA (pA) sites usage detected in 5 representative *HOTAIR* high confidence isoforms are represented. **b** Proportion of long-read Capture-Seq reads for each E7 length across differentiation time points. **c** Schematic representation of RT-qPCR amplicons (upper panel) and qRT-PCR analysis of *HOTAIR* E7 length variation during adipose differentiation (lower panel). **d** PacBio Capture-Seq analysis of HOTAIR exon E5 alternative splice site usage and **e** of the proportion of major exon E5 splice variants during adipogenic differentiation. **f** Schematic representation of PCR amplicons (upper panel) and semi-quantitative RT-PCR analysis of *HOTAIR* expression using primers located in exons E3 and E5 (E3-E5; lower panel). *SF3A1* is shown as a loading control. RT-: no reverse transcriptase control; NTC: no template control. Full-length gels are presented in **Additional file 4, Fig. S4**.

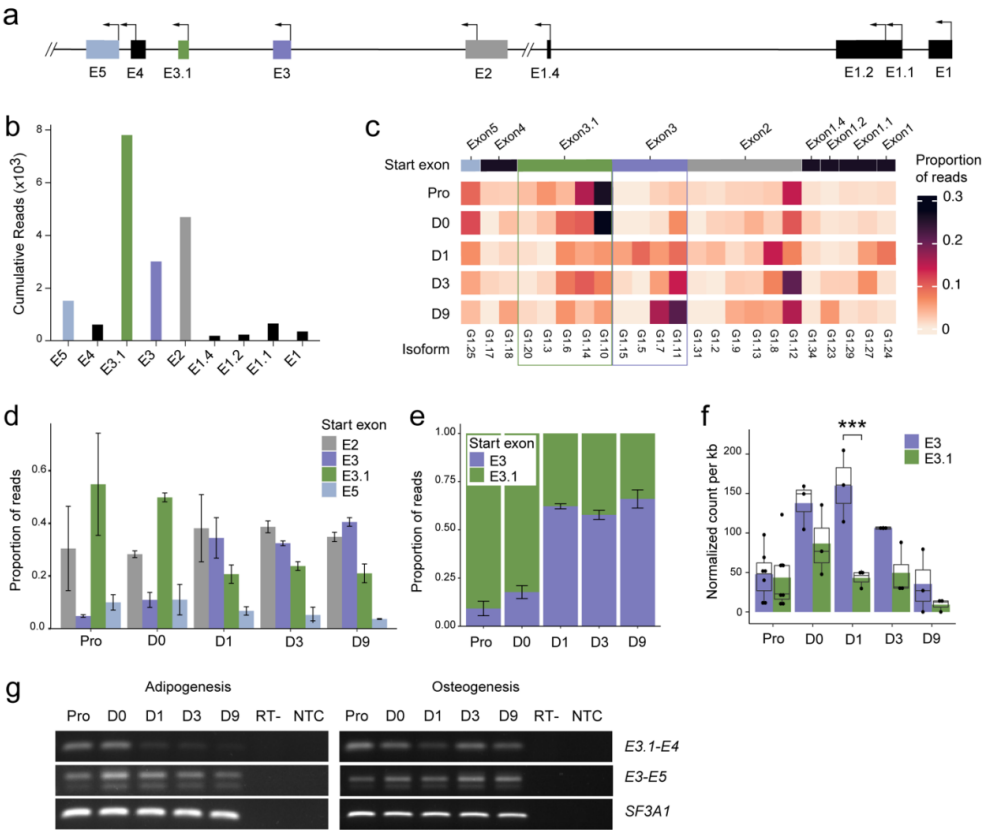

Figure 4. Remodeling of the *HOTAIR* isoform pool during adipogenesis. **a** Schematic representation of *HOTAIR* 5' exons (exons E1 to E5) showing novel *HOTAIR* exons and 9 alternative TSSs detected by PacBio Capture-Seq. **b** Cumulative number of long-reads for each *HOTAIR* starting exon. **c** Heatmap of the proportion of isoforms expressed at each time in the adipogenesis time course. Matching full length reads from PacBio long-read Capture-Seq are compared with each time point. **d,e** Proportion of read coverage for each start exon quantified from long-read data for **d** *HOTAIR* isoforms cumulating > 500 reads over the time course and **e** E3- and E3.1-starting isoforms. **f** Normalized short-read RNA-seq read count per kilobase of exon sequence for E3 and E3.1 exons during differentiation, quantified with featureCounts with strict parameters (-f -g exon_id -p -s 2 -O --fraction -B -C) (n = 3, ***p< 0.001 paired t-test with Benjamini-Hochberg adjusted p value) **g** Semi-quantitative RT-PCR analysis of *HOTAIR* expression using primers located in *HOTAIR* exons E3.1-E4 and E3-E5. *SF3A1* is shown as a loading control. A representative image from one of three independent experiments is shown for adipogenesis (left) and osteogenesis (right); see also **Additional file 1, Fig. S3b,c**. RT-: no reverse transcriptase control; NTC: no template control. Full-length gels are presented in **Additional file 4, Fig. S4,5,6.**

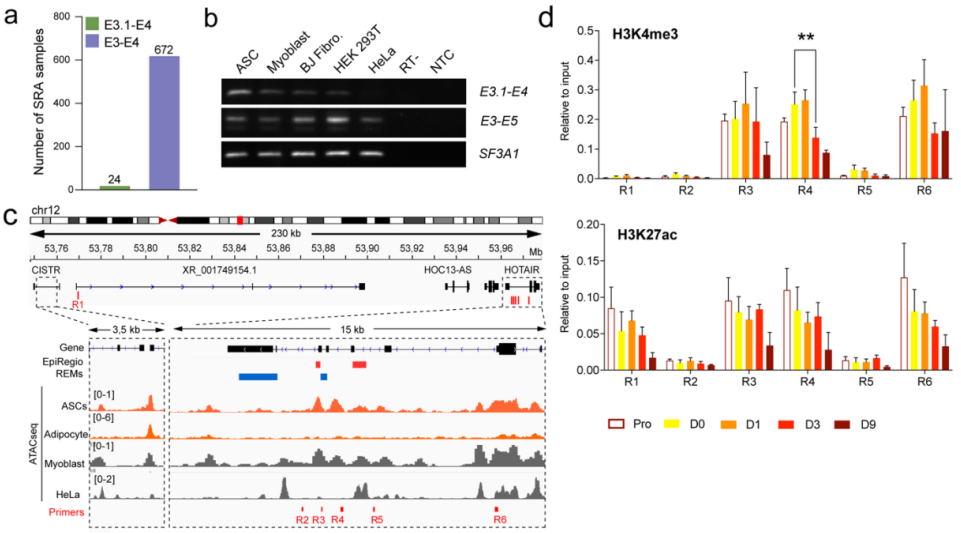

Figure 5. *HOTAIR* isoform expression is highly cell-type specific. a Number of SRA samples with 10 or more junction spanning reads for exons E3.1-E4 and E3-E4. **b** Semi-quantitative RT-PCR analysis of *HOTAIR* expression in ASCs, primary myoblasts, BJ fibroblasts, HEK293T and HeLa cells using primers located in *HOTAIR* exons E3.1-E4 and E3-E5. *SF3A1* is shown as a loading control. Full-length gels are presented in **Additional file 4, Fig.S7. c** IGV tracks over *HOTAIR* locus showing predicted HOTAIR regulatory elements (REMs) from the EpiRegio database [46, 61] (red: activating, blue: repressing), average ATAC-Seq tracks from ASCs [42, 43], Myoblasts [44] and HeLa cells [45], and ChIP primers location. **d** ChIP-qPCR analysis of histone modifications during adipogenesis of ASCs (mean ± SEM of n ≥ 3 independent differentiation experiments; **p < 0.01 Mixed effect analysis).

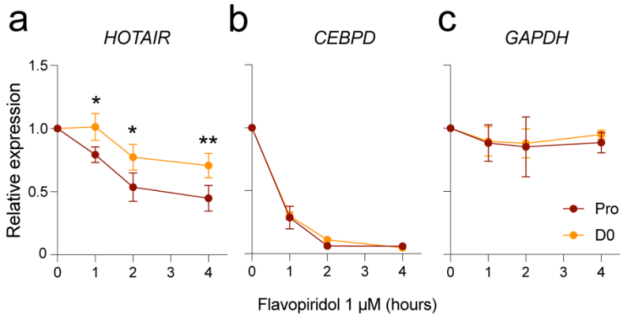

Figure 6. *HOTAIR* stability increases upon growth arrest. RT-qPCR analysis of **a** *HOTAIR*, **b** *CEBPD* and **c** *GAPDH* levels after flavopiridol treatment (mean ± SD; *p < 0.05, **p < 0.01, two-way ANOVA with Šídák's multiple comparisons test; n = 3 independent experiments)**.**

***De novo* annotation of lncRNA *HOTAIR* transcripts by long-read RNA capture-seq reveals a differentiation-driven isoform switch**

Evdokiia Potolitsyna, Sarah Hazell Pickering, Ave Tooming-Klunderud, Philippe Collas and Nolwenn Briand

Supplementary Information

Additional file 1 (pdf)

Figure S1. Validation of adipogenic differentiation efficiency.

Figure S2. Genome browser view of reference *HOTAIR* transcripts for SQANTI characterization

Figure S3. Semi-quantitative RT-PCR replicates.

Additional file 2 (Excel file)

Table S1. SQANTI characterization of *HOTAIR* isoforms identified with TAMA.

Table S2. List of human polyA motifs for SQANTI analysis

Table S3. Snaptron quantification of exon junctions for the HOTAIR locus

Table S4. Snaptron summary of RNA sequencing data containing *HOTAIR E3.1-E4* splice junction.

Table S5. List of primers used in this study.

Additional file 3 (bed file)

BED format file of top 34 HOTAIR isoforms identified in the study. High quality isoforms (black) were further studied while lower quality isoforms (red) were filtered out.

Additional file 4 (pdf)

Figure S4. Uncropped gels for **Fig.3f** and **Additional file 2, FigS3b** left panel

Figure S5. Uncropped gels for **Additional file 2, Fig. S3c**

Figure S6. Uncropped gels for **Fig.4g** and **Additional file 2, Fig. S3b** right panel

Figure S7. Uncropped gels for **Fig.5b**

Additional file 1

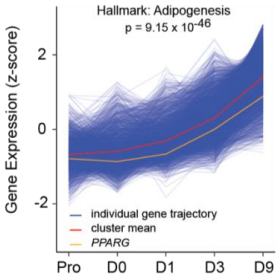

Figure S1. **Validation of adipogenic differentiation efficiency. a** Cluster of differentially expressed genes induced over the adipogenic RNA-seq time-course (n=3, adjusted p-value).

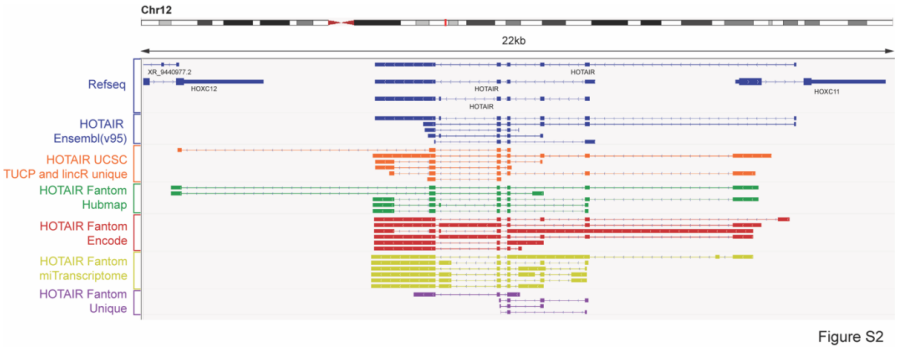

Figure S2. Genome browser view of reference *HOTAIR* transcripts for SQANTI characterization

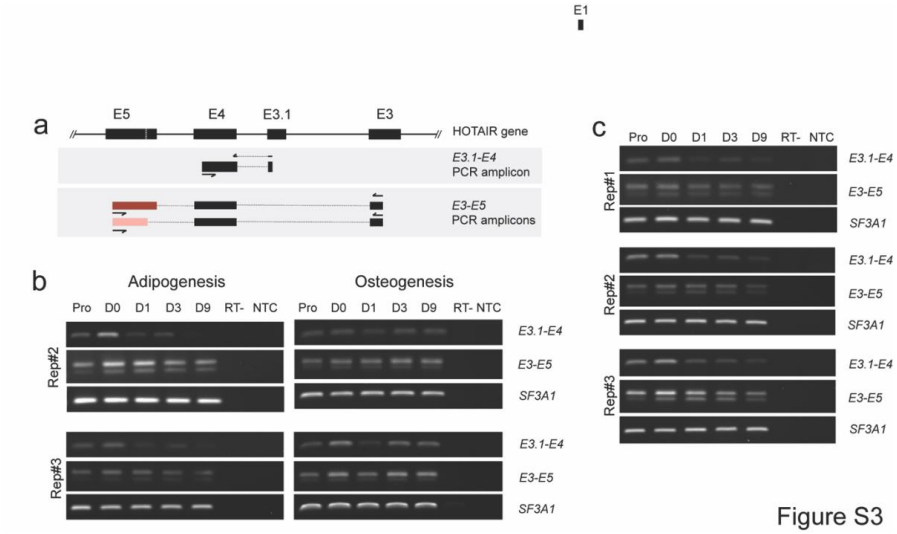

Figure S3. Semi-quantitative RT-PCR replicates. a Schematic representation of *HOTAIR* PCR amplicons using primer pairs located in exons E3.1 and E4 or E3 and E5. **b** Semi-quantitative RT-PCR analysis of *HOTAIR* isoform expression during adipogenic and osteogenic differentiation using primers located in *HOTAIR* exons E3.1-E4 and E3-E5 in ASCs from donor 1 (replicates #2 and #3; Full-length gels are presented in **Additional file 4 Fig.S1** and **S3**) and **c** donor 2 (Full-length gels are presented in **Additional file 4 Fig.S2**) RT-: no reverse transcriptase control; NTC: no template control. SF3A1 is shown as a loading control.

Additional file 4 (pdf)

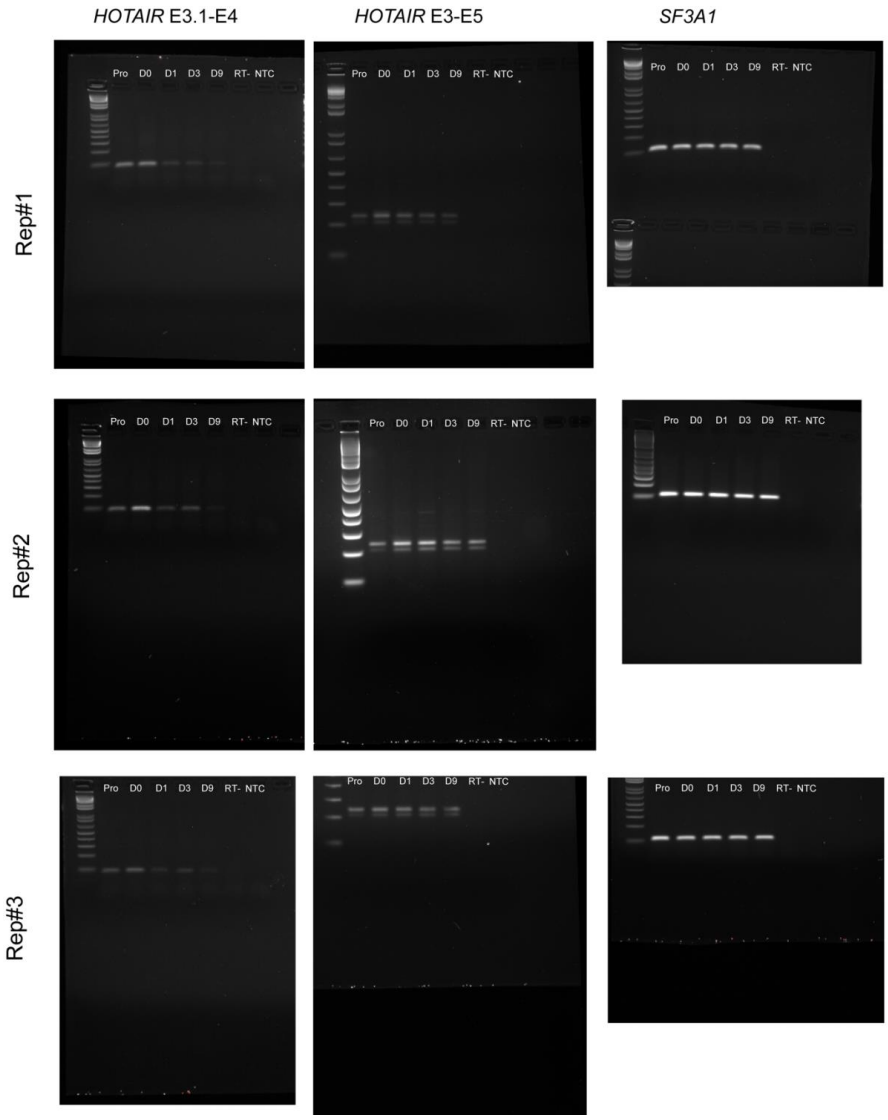

Figure S4. Uncropped gels for **Fig.3f** and **Additional file 1, FigS3b** left panel

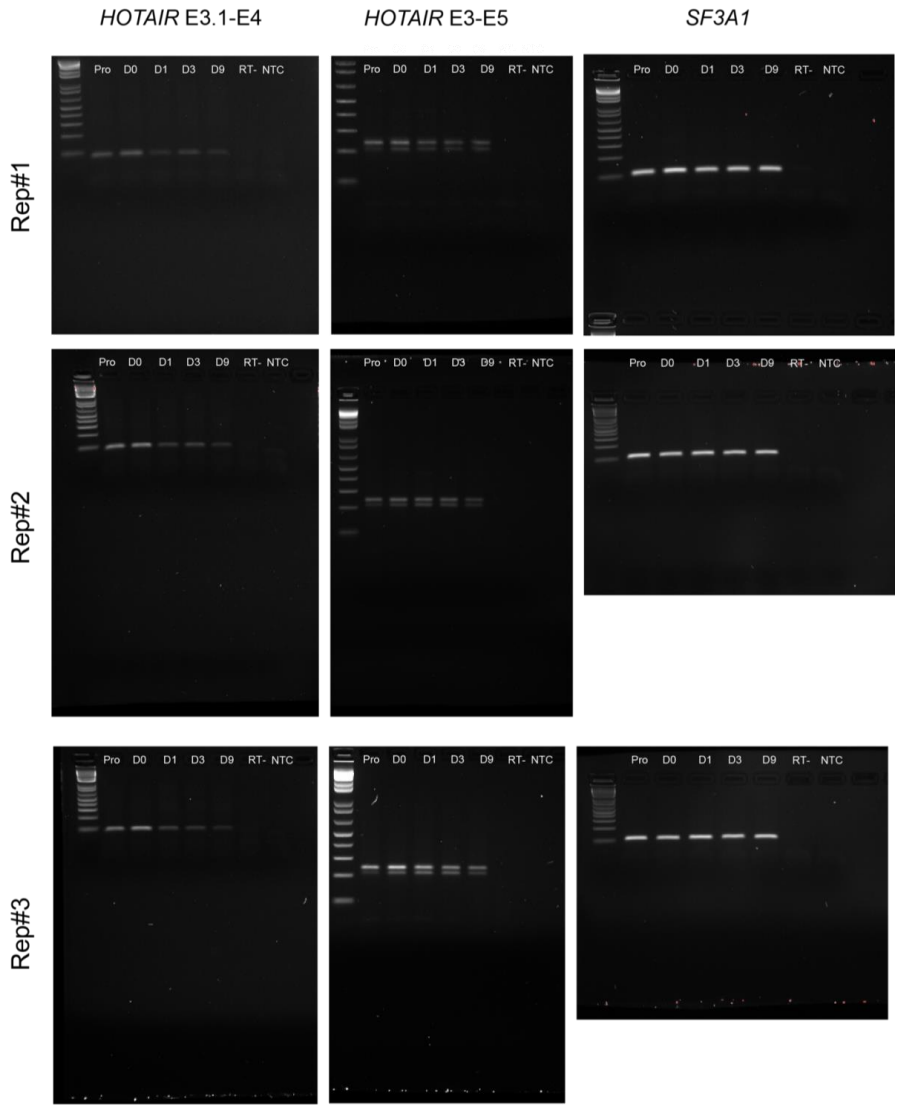

Figure S5. Uncropped gels for **Additional file 1, Fig. S3c**

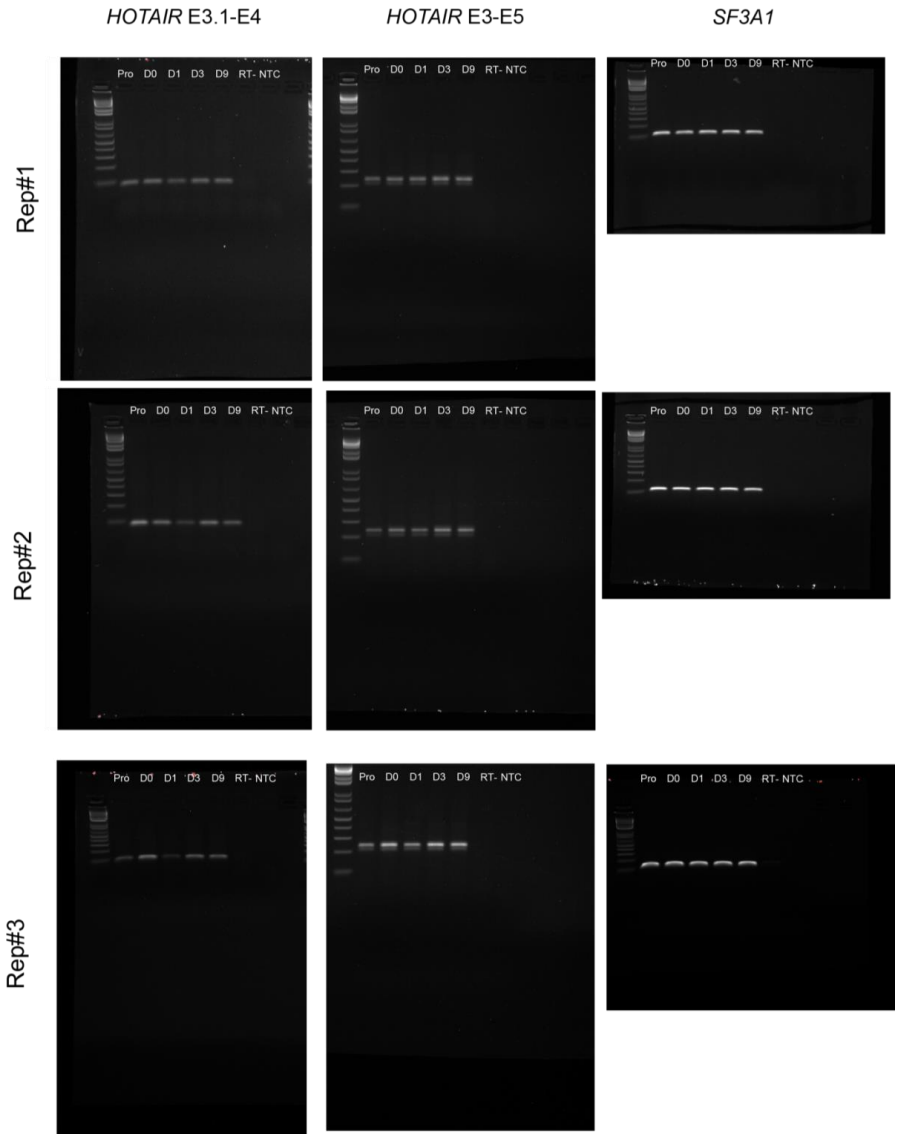

Figure S6. Uncropped gels for **Fig.4g** and **Additional file 1, Fig. S3b** right panel

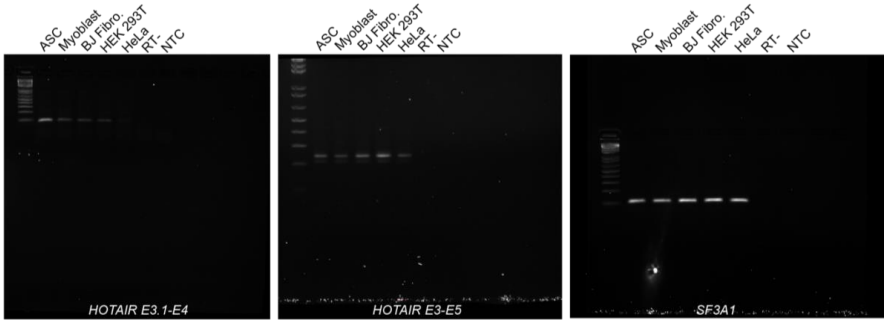

Figure S7. Uncropped gels for **Fig.5b**

Paper II

Long non-coding RNA *HOTAIR* regulates cytoskeleton remodeling and lipid storage capacity during adipogenesis

Evdokiia Potolitsyna, Sarah Hazell Pickering, Thomas Germier, Philippe Collas, Nolwenn Briand

II

scientific reports

Check for updates

OPEN

Long non-coding RNA *HOTAIR* regulates cytoskeleton remodeling and lipid storage capacity during adipogenesis

Evdokiia Potolitsyna[1], Sarah Hazell Pickering[1,2], Thomas Germier[1], Philippe Collas[1,2]✉ & Nolwenn Briand[1,2]✉

The long non-coding RNA *HOTAIR* is the most differentially expressed gene between upper- and lower-body adipose tissue, yet its functional significance in adipogenesis is unclear. We report that *HOTAIR* expression is transiently induced during early adipogenic differentiation of gluteofemoral adipose progenitors and repressed in mature adipocytes. Upon adipogenic commitment, *HOTAIR* regulates protein synthesis pathways and cytoskeleton remodeling with a later impact on mature adipocyte lipid storage capacity. Our results support novel and important functions of *HOTAIR* in the physiological context of adipogenesis.

The distribution of adipose depots in the human body is of high significance for metabolic health[1]. The most differentially expressed gene between upper- and lower-body adipose tissue encodes the gluteofemoral-specific long non-coding RNA (lncRNA) *HOTAIR* (HOX Transcript Antisense RNA)[2,3], within the *HOXC* locus. *HOTAIR* can be found in the nucleus, where it can bind chromatin and act as a scaffold for chromatin-modifying complexes[4], and in the cytoplasm where it can promote ubiquitin-mediated proteolysis[5] or function as a microRNA sponge[6]. The function of *HOTAIR* in adipose tissue, however, remains elusive. *HOTAIR* overexpression has been shown to promote adipogenesis in abdominal adipose stem cells (ASCs)[3] and to prevent adipose differentiation of bone marrow mesenchymal stem cells[7]. In contrast to its effect in cancer cells[8], *HOTAIR* overexpression does not affect ASC proliferation[3,7], suggesting distinct mechanisms of action in adipose progenitors.

Besides the well-characterized adipogenic transcriptional cascade[9], adipogenesis also entails major translational regulation[10] and remodeling of the cytoskeleton[11]. Morphological changes from a fibroblast-like to a round, lipid-filled cell involve the disruption of F-actin stress fibers and the formation of a cortical actin network beneath the plasma membrane[12,13]. In mature adipocytes, lipid overloading induces a drastic remodeling of the actin cytoskeleton[14] and affects the control of ribosomal protein expression downstream of insulin signaling[15]. Although recent evidence points to a functional link between translational regulation and cytoskeleton remodeling[16,17], the molecular determinants coordinating these processes during early adipogenesis remain to be elucidated.

Here, we identify *HOTAIR* as a regulator of translation and of cytoskeleton reorganization during early adipogenesis in human ASCs, and provide evidence of a novel role of *HOTAIR* as a determinant of adipocyte lipid storage capacity.

Results

***HOTAIR* is upregulated during early adipogenesis.** We first determined *HOTAIR* expression profile during adipogenic differentiation of gluteofemoral and abdominal ASCs (respectively G-ASCs and A-ASCs) from two donors, and in mature adipocytes isolated from the same tissues. ASCs from both donors show similar differentiation efficiency, based on induction of expression of the master adipogenic regulator *PPARG2* and of its targets (Fig. 1a; see supplementary Fig. S1a), and we confirm that *HOTAIR* expression is higher in G-ASCs compared to A-ASCs along the 9-day differentiation time course (Fig. 1a). Remarkably, *HOTAIR* expression is strongest in confluent G-ASCs (D0) and until differentiation day 3 (D3); however in contrast to previous find-

[1]Department of Molecular Medicine, Faculty of Medicine, Institute of Basic Medical Sciences, University of Oslo, Blindern, PO Box 1112, 0317 Oslo, Norway. [2]Department of Immunology and Transfusion Medicine, Oslo University Hospital, 0424 Oslo, Norway. ✉email: philippe.collas@medisin.uio.no; nolwenn.briand@medisin.uio.no

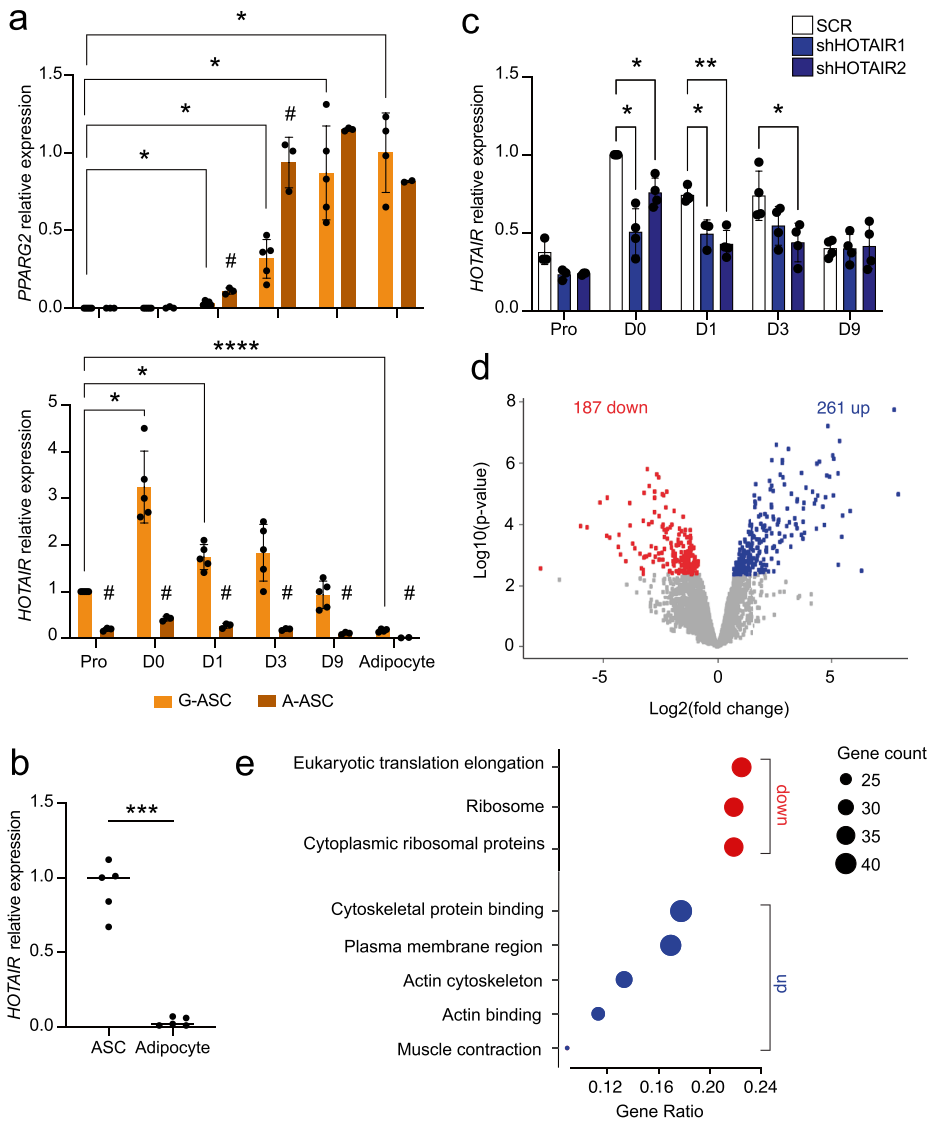

Figure 1. *HOTAIR* is upregulated during early adipogenesis. (**a**) Relative expression in G-ASCs and A-ASCs of *PPARG2,* normalized tomatched mature adipocytes, and of *HOTAIR*, normalized to proliferative G-ASCs (mean fold difference ± SD; $*p<0.05$, $**p<0.005$, $***p<0.001$, mixed effect analysis with Šídák's multiple comparisons test (G-ASC vs A-ASC) or Tukey's multiple comparisons test (time-course); ASCs n ≥ 3; adipocytes n ≥ 2). (**b**) Relative *HOTAIR* expression in proliferative ASCs vs. mature adipocytes from the same tissue (mean fold difference ± SD; $***p<0.001$, two-tailed paired t test; n = 5 adipose tissue depots from 3 independent donors). (**c**) RT-PCR analysis of *HOTAIR* expression in a control (SCR) and two stable *HOTAIR* KD G-ASC lines (shHOTAIR1 and 2) (mean fold difference ± SD; $*p<0.05$, $**p<0.005$, two-way ANOVA with Dunnett's multiple comparisons test; n ≥ 3). (**d**) Differential expression of the top 6000 highly expressed genes between SCR and two shHOTAIR G-ASC lines (adjusted *p*-values < 0.05, limma, n = 3). (**e**) Overrepresentation analysis of downregulated (red) and upregulated (blue) genes from (**d**) using GO, Wikipathways, Reactome and Hallmark gene sets from MSigDb (adjusted p-values $< 1.2 \times 10^{-6}$). The Gene Ratio is the fraction of differentially expressed genes in each gene set.

ings, we find that adipogenesis elicits marked *HOTAIR* downregulation and accordingly, expression is lower in mature adipocytes than in ASCs isolated from the same tissue (Fig. 1a,b; see supplementary Fig. S1b).

LncRNAs are often involved in regulating neighboring protein-coding genes[18]; however, we show by RNA-seq that in differentiating G-ASCs, *HOTAIR* expression does not correlate with that of neighboring *HOXC* genes (see supplementary Fig. S2a, b). To identify genes co-regulated with *HOTAIR*, we performed clustering of differentially expressed genes across time in G-ASCs ($\alpha < 0.01$ between at least two consecutive time points) (see supplementary Fig. S2c). Enriched molecular function GO terms for the gene cluster containing *HOTAIR* relate to "extracellular matrix structural constituent" (GO:0005201) and "cytoskeletal binding protein" (GO:0008092) (see supplementary Fig. S2d).

To get insight into *HOTAIR* function, we stably silenced *HOTAIR* in G-ASCs using two small hairpin (sh) RNAs, both of which prevented *HOTAIR* upregulation at D0 and D1 (Fig. 1c, see supplementary Fig. S2e). Transcriptomic analysis of *HOTAIR*-silenced D0 G-ASCs reveals 187 significantly downregulated and 261 upregulated genes (Fig. 1d, see supplementary Fig. S2e and Table S5). Functional analysis shows that *HOTAIR* depletion results in the downregulation of translation-linked pathways and upregulation of actin cytoskeleton-related pathways, the amplitude of the effect being consistent with the knockdown efficiency (Fig. 1e, see supplementary Fig. S2f, Tables S6 and S7). Of note, genes upregulated in sh*HOTAIR* cell lines are not enriched for PRC2 or *HOTAIR* targets (see supplementary Fig.S2g, h and Table S7), indicating a PRC2-independent function of *HOTAIR* in G-ASCs. Together, these data suggest that *HOTAIR* is involved in the regulation of protein synthesis and actin cytoskeleton processes during early adipogenesis.

***HOTAIR* knockdown alters translation and nucleoli morphology in proliferating G-ASCs.** Because the translation machinery is strongly downregulated upon cell cycle arrest and during early adipogenesis[10], we investigated the effect of *HOTAIR* KD on translation in proliferating G-ASCs. In basal culture conditions, sh*HOTAIR* G-ASCs present with normal cell morphology, and proliferation rates are unchanged (see supplementary Fig. S3a, b, c). Using a SUnSET assay, we find that while translation levels are unaffected in basal culture conditions, resumption of protein synthesis after a fasting and refeeding challenge is significantly impaired in sh*HOTAIR* G-ASCs (Fig. 2a, b). This coincides with a decrease in rDNA transcription in the refed state (Fig. 2c), a significant decrease in nucleolar volumes (see supplementary Fig. S3d–f), and a trend toward reduced nucleoli number (see supplementary Fig. S3g). In addition, phosphorylated P70S6K, a major regulator of protein synthesis in response to growth factors and nutritional cues[19], is significantly decreased upon refeeding (Fig. 2d, e), consistent with the inability of sh*HOTAIR* G-ASCs to resume translation. Importantly, strong but transient downregulation of *HOTAIR* in G-ASCs using two distinct siRNAs (Fig. 2f) leads to a marked nucleoli remodeling, characterized by a morphological change and the redistribution of Nucleolin to the nucleolar periphery and into the nucleoplasm (Fig. 2g), and by a reduction of nucleoli number (Fig. 2h), altogether indicating nucleolar stress. We conclude that *HOTAIR* functions as a regulator of protein synthesis in G-ASCs.

***HOTAIR* KD prevents cytoskeleton remodeling during adipogenesis.** Cytoskeleton remodeling is a key event in the morphological transition from ASCs to mature adipocytes[11,12,17], and our transcriptomic analysis points to a deregulation of actin dynamics in ASCs knocked-down for *HOTAIR* (see Fig. 1e). In agreement, *HOTAIR* KD results in a disorganized F-actin network at D0, measured by a reduction in the orientation coherence of actin filaments (Fig. 3a, b). Upon differentiation (D9), we observe the expected reorganization of the F-actin network in control scrambled shRNA G-ASCs, while actin stress fibers persist in ASCs knocked-down for *HOTAIR* (Fig. 3c). This concurs with the overexpression of the α smooth muscle actin isoform (αSMA; encoded by *ACTA2*) in differentiating *HOTAIR* knocked-down ASCs, both at the mRNA and at protein levels (Fig. 3d–f). Thus, downregulation of *HOTAIR* expression during early adipogenesis impedes cytoskeleton remodeling, resulting in a persistent F-actin network at differentiation endpoint.

***HOTAIR* KD results in impaired adipocyte lipid storage.** Actin cytoskeleton re-organization is required for both adipose differentiation and for the expansion of mature adipocyte lipid storage capacity[12–14]. In agreement, the defective cytoskeleton dynamics in shHOTAIR G-ASCs we observed above is associated with an overall decrease in lipid content at differentiation endpoint (Fig. 4a) and with significantly smaller lipid droplets (Fig. 4b, c). However, expression of the two master regulators of adipogenesis *PPARG2* and *CEBPA* (Fig. 4d), and their target FABP4 protein (Fig. 4e) is unaffected by *HOTAIR* KD. Thus, lipid accumulation or storage, rather than the adipogenic differentiation program per se, are defective after attenuation of *HOTAIR* expression. Accordingly, expression of *SREBF1* and *CHREBPb,* transcription factors mediating de novo lipogenesis gene induction, is significantly reduced by *HOTAIR* KD (Fig. 4d). Further, *HOTAIR* KD leads to reduced gene expression of key regulators of fatty acid availability (*LPL*), de novo fatty acid synthesis (*ACLY*, *ACC*), and triglyceride storage (*PLIN1*) (Fig. 4f, e), and to a blunted lipolytic response to isoproterenol, reflecting the global defect in lipid accumulation (Fig. 4g). Altogether, these results establish that *HOTAIR* functions as an early regulator of adipogenesis with determining effects on mature adipocyte lipid storage capacity.

Discussion

We establish that *HOTAIR* expression is induced in the early phase of adipogenesis but strongly downregulated in mature adipocytes, and that this transient upregulation participates in the regulation of translation and of cytoskeletal remodeling during adipogenic commitment. Importantly, we find that deregulation of these processes later results in a reduced adipocyte lipid storage capacity.

LncRNA molecular function not only depends on their expression pattern and levels but is also determined by their subcellular localization[20]. LncRNA *HOTAIR* can bind DNA and act as an epigenetic scaffold in the nucleus,

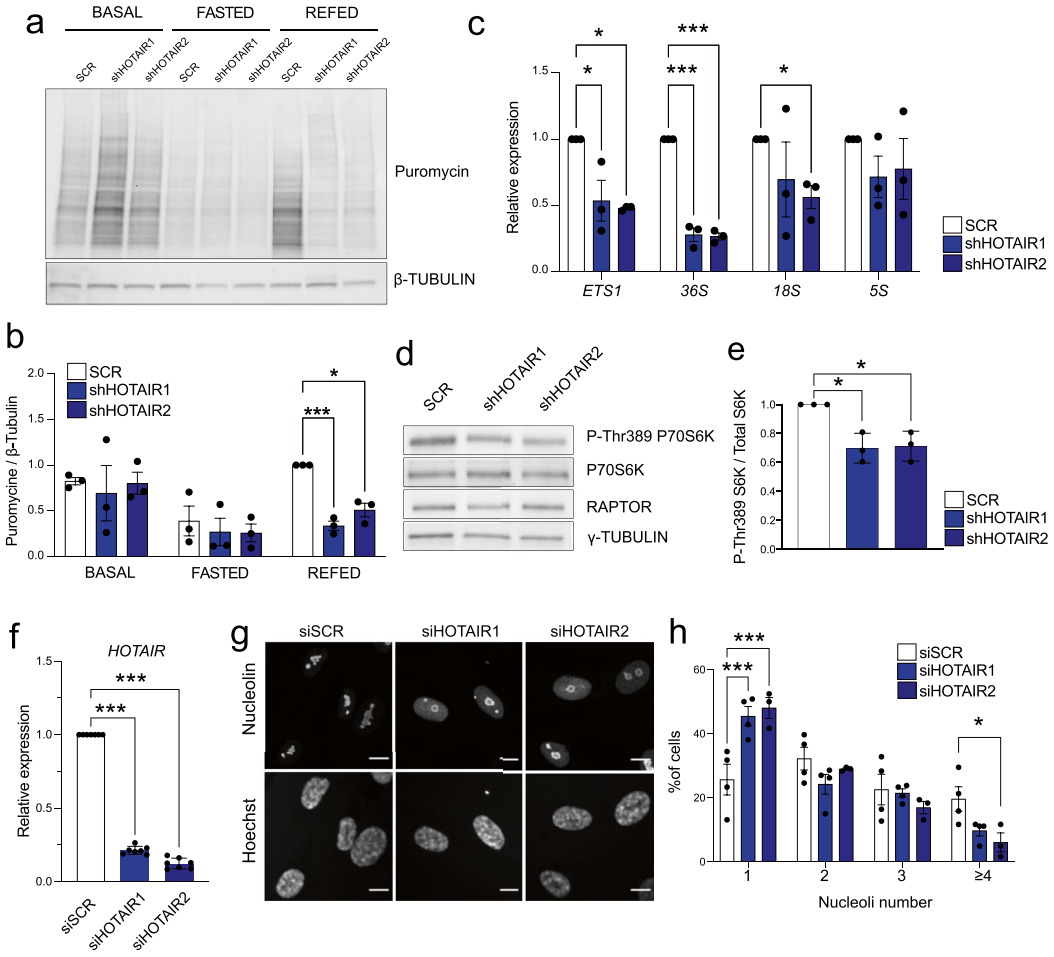

Figure 2. *HOTAIR* KD impairs refeeding-induced protein synthesis in proliferating G-ASCs. (**a**) SUnSET analysis of protein synthesis rates in basal, 24-h fasting (HBSS, 0.2% FFA-free BSA) and 24-h refeeding conditions in SCR, shHOTAIR1 and shHOTAIR2 G-ASCs (see Fig. S5 for original blots). (**b**) SUnSET quantification (*$p < 0.05$, ***$p < 0.001$, two-way ANOVA with Dunnett's multiple comparisons test;; n = 3). (**c**) RT-qPCR analysis of pre-rRNA (ETS1, 36S), 18S and 5S rRNA after 24-h refeeding (*$p < 0.05$, ***$p < 0.001$, two-way ANOVA with Dunnett's multiple comparisons test;; n = 3). (**d**) Western blot analysis of phospho-Thr389 P70S6K, total P70S6K, RAPTOR and γ-Tubulin protein levels after 24-h refeeding (see Fig. S6for original blots). (**e**) Quantification of phospho-Thr389 P70S6K/total P70S6K and RAPTOR/γ-Tubulin (*$p < 0.05$, two-tailed paired T test, n = 3). (**f**) RT-qPCR validation of transient *HOTAIR* KD in proliferating G-ASC (mean ± SD; *** $p < 0.001$, ANOVA with Holm-Sidak's multiple comparisons test; n = 7). (**g**) Immunostaining of Nucleolin in siSCR- and siHOTAIR1- and 2-transfected G-ASCs. Nuclei are stained with Hoechst. Scale bar: 10 µm. (**h**) Number of nucleoli per cell quantified from Nucleolin immunostaining in siSCR- and siHOTAIR1- and 2-transfected G-ASCs (mean ± SD; *$p < 0.05$, ***$p < 0.001$, two-way ANOVA with Dunnett's multiple comparisons test; n = 4 independent transfections; > 20 cells measured per experiment).

and interact with proteins and other RNAs in the cytoplasm. It is conceivable that siRNA-mediated *HOTAIR* silencing differentially affects distinct pools of *HOTAIR,* due to variation in their location, binding partners, or stability[21]. Surprisingly, the transcripts we find deregulated upon *HOTAIR* silencing are not enriched for PRC2 target genes, a well-described *HOTAIR* partner in the nucleus[22]. Instead, we describe a defective cytoskeletal remodeling during early adipogenesis, in line with the recently reported deregulation of the Rho/ROCK-mediated remodeling of actin cytoskeleton in abdominal ASCs upon *HOTAIR* overexpression[23]. Such modulation of

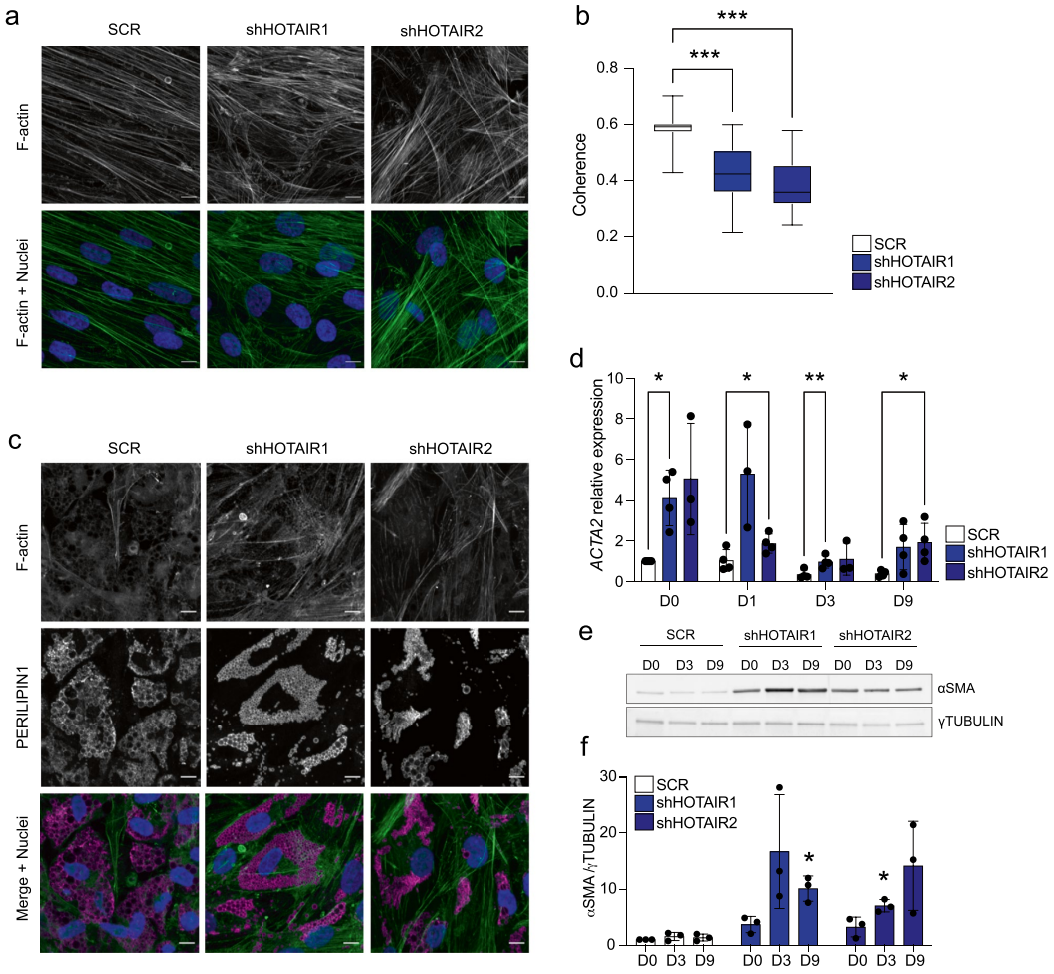

Figure 3. *HOTAIR* KD prevents cytoskeletal remodeling during adipogenesis.(**a**) Phalloidin staining of F-actin in D0 SCR and sh*HOTAIR* G-ASCs. Nuclei are stained with Hoechst. Scale bar: 10 µm. (**b**) Quantification of coherence in F-actin fibers alignment in D0 SCR and sh*HOTAIR* G-ASCs (***$p < 0.0001$, two-way ANOVA with Dunnett's multiple comparisons test; n = 3 experiments, with ≥ 4 fields measured per experiment, 5 measurements per field). (**c**) Phalloidin staining of F-actin (green) and immunostaining of PERILIPIN1 (magenta) in differentiated (D9) SCR and sh*HOTAIR* G-ASCs. Nuclei are stained with Hoechst. Scale bar: 10 µm. (**d**) Relative expression of *ACTA2* in differentiating scrambled control (SCR) and sh*HOTAIR* G-ASCs, normalized to SCR D0 (mean fold difference ± SD; *$p < 0.05$, **$p < 0.005$, two-way ANOVA with Dunnett's multiple comparisons test; n ≥ 3). (**e**) Western blot analysis (see Fig. S7for original blots) and (**f**) quantification of αSMA protein levels in differentiating SCR and sh*HOTAIR* G-ASCs (mean fold difference ± SD; *$p < 0.05$, two-way ANOVA with Tukey's multiple comparisons test; n = 3). γ-Tubulin is shown as a loading control.

Rho GTPases signaling, plausibly through *HOTAIR* cytoplasmic miRNA-sponge function[24], could account for the downstream transcriptomic defects observed upon HOTAIR silencing.

HOTAIR knockdown in proliferating ASCs affects nucleolus morphology and results in an inability to resume translation upon nutrient availability, which correlates with a decrease in mTORC1 signaling. Regulation of mTOR signaling by *HOTAIR* has been reported[25,26], although the mechanistic basis for this regulation remains unknown. Interestingly, mTORC1 activation by nutrients is supported by its association with focal adhesions and with the actin cytoskeleton[27], suggesting that cytoskeletal alterations might underlie the mTORC1 signaling defect we detect after attenuation of *HOTAIR* expression in ASCs.

An active cytoskeleton remodeling during adipogenesis is necessary to regulate adipocyte formation and accommodate lipid droplet expansion[12–14]. We find that preventing *HOTAIR* transient upregulation upon

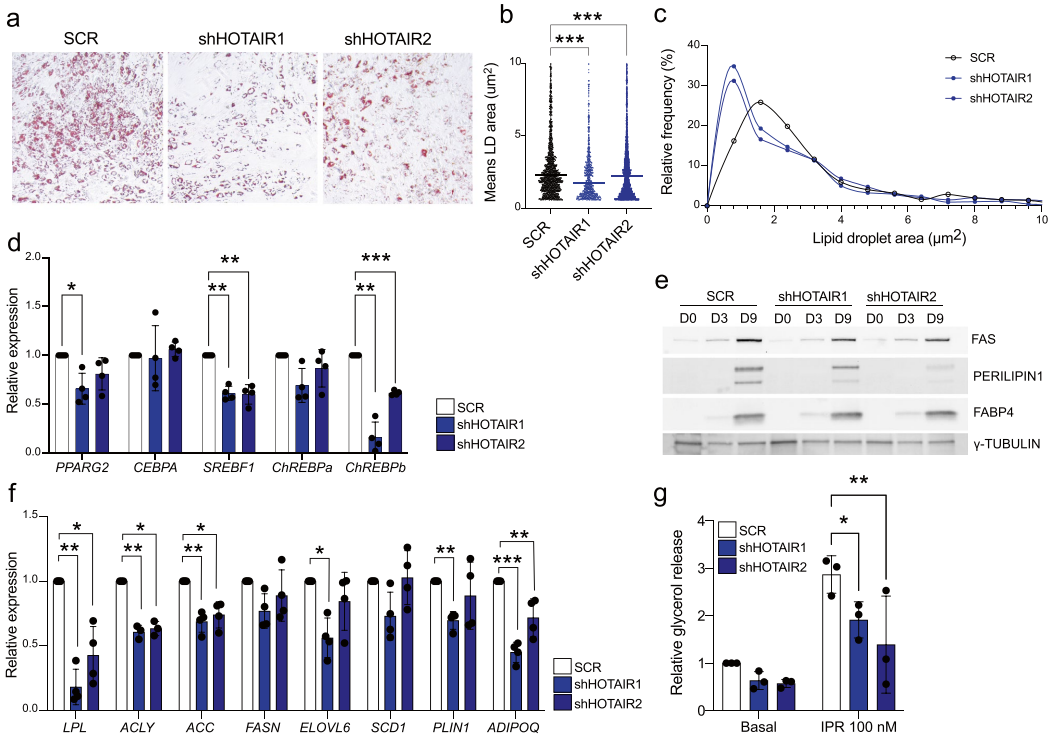

Figure 4. *HOTAIR* KD impairs lipid storage in mature adipocytes.(**a**) Oil red O staining (20X) of differentiated (D9) SCR and sh*HOTAIR* G-ASCs. LipidL droplet area analysis from PERILIPIN immunostainings of differentiated (D9) SCR and *HOTAIR* KD G-ASCs presented as (**b**) individual data scatter plot and mean (***$p < 0.0001$, two-way ANOVA with Dunnett's multiple comparisons test;; n = 3 experiments, with ≥ 3 fields measured per experiment) and (**c**) distribution frequency. (**d**) RT-qPCR analysis of adipogenic transcription factor gene expression at D9 (mean fold difference ± SD; *$p < 0.05$, **$p < 0.005$, ***$p < 0.001$, two-way ANOVA with Dunnett's multiple comparisons test; n = 4). (**e**) Western blot analysis of fatty acid synthase (FAS), PERILIPIN1, and FABP4 in differentiating SCR and shHOTAIR G-ASCs (representative blot from n = 3; see Fig. SS7for original blots). γ-Tubulin is shown as a loading control. (**f**) RT-qPCR analysis of glucose- and lipid uptake-related genes, de novo lipogenesis genes and mature adipocyte markers in differentiated (D9) SCR and shHOTAIR G-ASCs (mean fold difference ± SD; *$p < 0.05$, **$p < 0.005$, two-way ANOVA with Dunnett's multiple comparisons test; n = 4). (**g**) Fold induction of glycerol release in response to 100 nM isoproterenol stimulation for 2 h in differentiated (D9) SCR and shHOTAIR G-ASCs (mean fold difference ± SD; *$p < 0.05$, **$p < 0.005$, two-way ANOVA with Dunnett's multiple comparisons test; n = 3).

adipogenic commitment results in a defective actin cytoskeleton reorganization. This phenotype persists at later differentiation stages and is accompanied by a drastic reduction of lipid droplet size, and altered de novo lipogenesis downstream of SREBP1 and ChREBPβ. While *SREBF1* downregulation could result from compromised mTOR signaling[19,28], altered dynamics of the actin cytoskeleton and increased mechanical constraints could also directly account for a reduction of SREBP1 activity[29].

Adipose tissue depots differ by their mechanisms of expansion, with lower-body adipose tissue having the capacity to rapidly increase in mass through ASC differentiation, rather than adipocyte hypertrophy[30]. ASCs commitment towards the adipogenic lineage is controlled by both the niche and intrinsic cellular mechanical properties[31]. Therefore, depot-specific remodeling mechanisms might be linked to distinct macro-architecture[32] and cellular structure[33,34]. In gluteofemoral ASCs, *HOTAIR*-mediated regulation of the cytoskeletal tensional state might preserve ASC differentiation capacity, thereby promoting healthy lower-body adipose tissue expansion.

HOTAIR downregulation in ASCs results in the downregulation of translation-related genes, and in the upregulation of cytoskeletal genes, a phenotype that strikingly mirrors that of *Zc3h10* silenced preadipocytes[17]. In both models, deregulation of these coordinated cellular processes upon adipogenic commitment leads to an altered lipid storage capacity in differentiated adipocytes. Deregulation of the translation machinery and of the cytoskeleton occurs in both lipoatrophy[12,35] and obesity[14,15], highlighting the importance of these processes in the pathophysiology of adipose tissue.

Methods

Primary cells isolation. This study was approved by and conducted in agreement with the guidelines and regulations of the Regional Committee for Research Ethics for Southern Norway. ASCs were isolated from liposuction material from subcutaneous gluteal or abdominal adipose tissue from five healthy women (age 28–50; BMI 22–27 kg/m^2) after informed consent was given. After washing in Hank's balanced salt solution (HBSS), tissues were dissociated for 50 min at 37 °C with 1% collagenase (Worthington #LS004204). Adipocytes were separated from stromal vascular (SV) cells after sedimentation at 300 × *g* for 10 min and lysed in TRIzol (Invitrogen) before RNA isolation. ASCs were further selected by differential plating.

Cell culture and differentiation. ASCs were cultured in DMEM/F12 (17.5 mM glucose) with 10% fetal calf serum and 20 ng/ml basic fibroblast growth factor (Pro). Upon confluency, growth factor was removed and cells were cultured for 72 h before induction of differentiation (D0). For adipose differentiation, ASCs were induced with a cocktail of 0.5 µM 1-methyl-3 isobutyl xanthine, 1 µM dexamethasone, 10 µg/ ml insulin and 200 µM indomethacin. Differentiation media was renewed every 3 days, and samples harvested 1, 3, and 9 days after induction. Cells were stained with Oil Red-O on D9. All differentiation experiments were done in at least three biological replicates between passage 4 and 9.

HOTAIR knockdown. For transient *HOTAIR* knockdown (KD), gluteofemoral ASCs were electroporated with 30 nM of one of the two siRNAs (siHOTAIR 1: N272221 or siHOTAIR 2: N272230; Ambion). Lonza Nucleofector device was used with a human MSC nucleofection kit (VVPE-1001; Lonza) according to manufacturer instructions. After electroporation, cells were cultured for 72 h before harvesting RNA. Stable *HOTAIR* KD was achieved by expression of two shRNAs (Table S1) cloned into a pLV-hU6-EF1a-bsd vector (Biosettia). Second generation lentiviral packaging system (plasmids psPAX2 #12,260 and pCMV-VSV-G #8454; Addgene) was used to produce virus in LentiX cells (632,180; Takara Bio). Media containing viral particles was filtered with a 0.45 µm filter and equal volumes of this media were used to infect ASC together with 8 µg/ml Polybrene (TR-1003-G, Merck). Infected cells were selected for 7 days in 10 µg/ml Blasticidin (ant-bl-05, Invivogen).

Gene expression. RNA was isolated using RNeasy kit (QIAGEN) and 1 µg was used for cDNA synthesis using High-Capacity cDNA Reverse Transcription Kit (ThermoFisher). RT-PCR was done using IQ SYBR green (Bio-Rad Laboratories) with *SF3A1* as a reference gene. PCR conditions were 95 °C for 3 min and 40 cycles of 95 °C for 30 s, 60 °C for 30 s, and 72 °C for 20 s followed by a melting curve. PCR primers are listed in Table S2.

Protein expression. Proteins were resolved by gradient 4–20% SDS–PAGE, transferred onto Immobilon-FL (Millipore) or nitrocellulosis 0.45 µm (Biorad) membranes and blocked with Odyssey blocking buffer (LI-COR). Membranes were cut horizontally to allow for multiple parallel hybridizations. Membranes were incubated with antibodies overnight at 4 °C (Table S3). Proteins were visualized using IRDye-800-, IRDye-680-, or HRP-coupled secondary antibodies. Bands were quantified by densitometry (Image Lab; BioRad).

RNA sequencing analysis. Paired-end Illumina RNA sequencing (RNA-seq) was done in biological triplicates for 2 independent donors. Reads were filtered with fastp, aligned to the hg38 genome (ensembl v95 annotation) with hisat2, counted using featureCounts (–fraction -M), and differential gene expression was analyzed using limma[36] (Table S4). Genes differentially expressed between SCR and both shHOTAIR G-ASC lines with a FDR adjusted p-value < 0.05 are shown in Table S5. Differentially expressed genes with high average expression (within the top 6000 genes) were tested for overrepresentation against GO, KEGG, Wikipathways, Reactome and Hallmark gene sets from MSigDb and terms with a FDR adjusted p-value < 0.01 are presented in Tables S6 and S7. DPGP[37] was used to cluster genes with differential expression (FDR adjusted p-value < 0.01) across adipogenesis in native G-ASCs (Fig. S2c).

Lipolysis and SUnSET assays. To assess lipolysis, G-ASCs on D9 were serum-deprived overnight. Glycerol release in response to 100 nM isoproterenol was measured in the medium (GY105; Randox) and normalized to well protein content. SUnSET assay was done by labeling newly synthesized proteins with 1 µM Puromycin for 1 h followed by Western blotting using anti-Puromycin antibodies (Table S3).

Imaging. For immunofluorescence, cells were fixed in 4% paraformaldehyde, permeabilized in PBS/0.1% Triton X-100/0.01% Tween 20/2% BSA, incubated with relevant antibodies and stains (Table S3) and mounted (DAKO S3023, Agilent). Fluorescence images were taken on a Dragonfly microscope (Oxford Instruments; 60 × 1.4 NA objective; 4-µm stack with 0.3-µm steps).

Image analysis. Nucleolar volumes and numbers were measured using Nemo software with the nucleolin channel used as a nucleolar marker. The number of nucleoli was corrected manually in the transient KD analysis due to major redistribution of nucleolin to the nucleoplasm preventing correct segmentation of nucleoli in some cases. Morphological Segmentation plugin from MorphoLibJ collection of plugins in ImageJ was used to define lipid droplets from perilipin-1 immunostaining, "border object" and connectivity of 8 settings were used (https://imagej.net/plugins/morpholibj). Lipid droplet area was then measured with the "Analyse particles" function with a threshold on circularity and size. Actin cytoskeleton coherence was measured from phalloidin staining with the OrientationJ plugin (http://bigwww.epfl.ch/demo/orientation/). Cell size and confluency were measured from phase-contrast images with Morphological Segmentation and PHANTAST plugins. Raw

unmodified images were used for all the analyses except for phase-contrast images which were adjusted for contrast and Gaussian blur was used to enhance the segmentation quality.

Data availability

RNA-seq data are available from Gene Expression Omnibus (GEO) accession GSE176020.

Received: 28 March 2022; Accepted: 3 June 2022
Published online: 16 June 2022

References

1. Karpe, F. & Pinnick, K. E. Biology of upper-body and lower-body adipose tissue–link to whole-body phenotypes. *Nat. Rev. Endocrinol.* **11**, 90–100 (2015).
2. Pinnick, K. E. *et al.* Distinct developmental profile of lower-body adipose tissue defines resistance against obesity-associated metabolic complications. *Diabetes* **63**, 3785–3797 (2014).
3. Divoux, A. *et al.* Identification of a novel lncRNA in gluteal adipose tissue and evidence for its positive effect on preadipocyte differentiation. *Obesity* **22**, 1781–1785 (2014).
4. Tsai, M.-C. *et al.* Long noncoding RNA as modular scaffold of histone modification complexes. *Science* **329**, 689–693 (2010).
5. Yoon, J.-H. *et al.* Scaffold function of long non-coding RNA HOTAIR in protein ubiquitination. *Nat. Commun.* **4**, 2939 (2013).
6. Xu, F. & Zhang, J. Long non-coding RNA HOTAIR functions as miRNA sponge to promote the epithelial to mesenchymal transition in esophageal cancer. *Biomed. Pharmacother.* **90**, 888–896 (2017).
7. Kalwa, M. *et al.* The lncRNA HOTAIR impacts on mesenchymal stem cells via triple helix formation. *Nucleic Acids Res.* **44**, 10631–10643 (2016).
8. Ding, W., Ren, J., Ren, H. & Wang, D. Long noncoding RNA HOTAIR modulates MiR-206-mediated Bcl-w signaling to facilitate cell proliferation in breast cancer. *Sci. Rep.* **7**, 17261 (2017).
9. Rosen, E. D., Walkey, C. J., Puigserver, P. & Spiegelman, B. M. Transcriptional regulation of adipogenesis. *Genes Dev.* **14**, 1293–1307 (2000).
10. Marcon, B. H. *et al.* Downregulation of the protein synthesis machinery is a major regulatory event during early adipogenic differentiation of human adipose-derived stromal cells. *Stem Cell Res.* **25**, 191–201 (2017).
11. Spiegelman, B. M. & Farmer, S. R. Decreases in tubulin and actin gene expression prior to morphological differentiation of 3T3 adipocytes. *Cell* **29**, 53–60 (1982).
12. Yang, W. *et al.* BSCL2/seipin regulates adipogenesis through actin cytoskeleton remodelling. *Hum. Mol. Genet.* **23**, 502–513 (2014).
13. Nobusue, H. *et al.* Regulation of MKL1 via actin cytoskeleton dynamics drives adipocyte differentiation. *Nat. Commun.* **5**, 1–12 (2014).
14. Hansson, B. *et al.* Adipose cell size changes are associated with a drastic actin remodeling. *Sci. Rep.* **9**, 12941 (2019).
15. Mileti, E. *et al.* Human white adipose tissue displays selective insulin resistance in the obese state. *Diabetes* **70**, 1486–1497 (2021).
16. Keen, A. N. *et al.* Eukaryotic initiation factor 6 regulates mechanical responses in endothelial cells. *J. Cell Biol.* https://doi.org/10.1083/jcb.202005213 (2022).
17. Audano, M. *et al.* Zc3h10 regulates adipogenesis by controlling translation and F-actin/mitochondria interaction. *J. Cell Biol.* https://doi.org/10.1083/jcb.202003173 (2021).
18. Vance, K. W. & Ponting, C. P. Transcriptional regulatory functions of nuclear long noncoding RNAs. *Trends Genet.* **30**, 348–355 (2014).
19. Chakrabarti, P., English, T., Shi, J., Smas, C. M. & Kandror, K. V. Mammalian target of rapamycin complex 1 suppresses lipolysis, stimulates lipogenesis, and promotes fat storage. *Diabetes* **59**, 775–781 (2010).
20. Carlevaro-Fita, J. & Johnson, R. Global positioning system: understanding long noncoding RNAs through subcellular localization. *Mol. Cell* **73**, 869–883 (2019).
21. Lennox, K. A. & Behlke, M. A. Mini-review on current strategies to knockdown long non-coding RNAs. *J. Rare Dis. Res. Treat.* **1**(3), 66–70 (2016).
22. Rinn, J. L. *et al.* Functional demarcation of active and silent chromatin domains in human HOX loci by noncoding RNAs. *Cell* **129**, 1311–1323 (2007).
23. Kuo, F.-C. *et al.* Aberrant overexpression of HOTAIR inhibits abdominal adipogenesis through remodelling of genome-wide DNA methylation and transcription. *Mol. Metab.* **60**, 101473 (2022).
24. Ghafouri-Fard, S., Noroozi, R., Abak, A., Taheri, M. & Salimi, A. Emerging role of lncRNAs in the regulation of Rho GTPase pathway. *Biomed. Pharmacother.* **140**, 111731 (2021).
25. Wei, S. *et al.* Promotion of glycolysis by HOTAIR through GLUT1 upregulation via mTOR signaling. *Oncol. Rep.* **38**, 1902–1908 (2017).
26. Li, Z., Qian, J., Li, J. & Zhu, C. Knockdown of lncRNA-HOTAIR downregulates the drug-resistance of breast cancer cells to doxorubicin via the PI3K/AKT/mTOR signaling pathway. *Exp. Ther. Med.* **18**, 435–442 (2019).
27. Rabanal-Ruiz, Y. *et al.* mTORC1 activity is supported by spatial association with focal adhesions. *J. Cell Biol.* https://doi.org/10.1083/jcb.202004010 (2021).
28. Tang, Y. *et al.* Adipose tissue mTORC2 regulates ChREBP-driven de novo lipogenesis and hepatic glucose metabolism. *Nat. Commun.* **7**, 11365 (2016).
29. Bertolio, R. *et al.* Sterol regulatory element binding protein 1 couples mechanical cues and lipid metabolism. *Nat. Commun.* **10**, 1–11 (2019).
30. Tchoukalova, Y. D. *et al.* Regional differences in cellular mechanisms of adipose tissue gain with overfeeding. *Proc. Natl. Acad. Sci. U. S. A.* **107**, 18226–18231 (2010).
31. González-Cruz, R. D., Fonseca, V. C. & Darling, E. M. Cellular mechanical properties reflect the differentiation potential of adipose-derived mesenchymal stem cells. *Proc. Natl. Acad. Sci. U. S. A.* **109**, E1523–E1529 (2012).
32. Estève, D. *et al.* Lobular architecture of human adipose tissue defines the niche and fate of progenitor cells. *Nat. Commun.* **10**, 2549 (2019).
33. Vogel, M. A. A. *et al.* A comparison between the abdominal and femoral adipose tissue proteome of overweight and obese women. *Sci. Rep.* **9**, 4202 (2019).
34. Divoux, A. *et al.* Differential open chromatin profile and transcriptomic signature define depot-specific human subcutaneous preadipocytes: primary outcomes. *Clin. Epigenet.* **10**, 148 (2018).
35. Liu, L. & Pilch, P. F. PTRF/Cavin-1 promotes efficient ribosomal RNA transcription in response to metabolic challenges. *Elife* https://doi.org/10.7554/eLife.17508 (2016).
36. Law, C. W. *et al.* RNA-seq analysis is easy as 1-2-3 with limma Glimma and edgeR. *F1000Res.* **5**, 1408 (2016).

37. McDowell, I. C. *et al.* Clustering gene expression time series data using an infinite Gaussian process mixture model. *PLoS Comput. Biol.* **14**, e1005896 (2018).

Acknowledgements
We thank Tommy Karlsen for ASCs and reagents and the Norwegian Sequencing Center (Oslo University Hospital) for professional services.

Author contributions
E.P. and N.B. designed the study, performed experiments and analyzed data. S.H.P. did bioinformatics analysis. T.G. contributed to microscopy. E.P., S.H.P. and N.B. made figures. E.P., S.H.P., P.C. and N.B. wrote the manuscript. N.B. is supervisor and guarantor of this work.

Funding
This work was funded by South-East Health Norway (grant 40040) and the Research Council of Norway (grants 249734 and 313508).

Competing interests
The authors declare no competing interests.

Additional information
Supplementary Information The online version contains supplementary material available at https://doi.org/10.1038/s41598-022-14296-6.

Correspondence and requests for materials should be addressed to P.C. or N.B.

Reprints and permissions information is available at www.nature.com/reprints.

Publisher's note Springer Nature remains neutral with regard to jurisdictional claims in published maps and institutional affiliations.